Radio Properties and Optical Identification of Two Samples of Milli-Jansky Radio Sources at 1.4 GHz

Nanyao Y. Lu

Infrared Processing and Analysis Center

Jet Propulsion Laboratory

MS 100-22

California Institute of Technology

Pasadena, CA 91125

Email: lu@ipac.caltech.edu

G. Lyle Hoffman

Physics Department, Lafayette College, Easton, PA 18042

Email: hoffmang@astro.phys.lafayette.edu

Edwin E. Salpeter and James R. Houck

Space Sciences Building, Cornell University, Ithaca, NY 14853

Emails: tomion@astrosun.tn.cornell.edu, jrhouck@nasamail.nasa.gov

ABSTRACT

From the 1.4 GHz radio survey of Condon, Dickey, & Salpeter (1990) in a region much devoid of rich galaxy clusters at redshifts $z \lesssim 0.4$, we selected a "distant" sample of 57 radio sources complete to a 1.4 GHz flux density of 35 mJy and a "nearby" sample of 36 mostly weaker radio sources which are optically brighter than $B \sim 19$ msg. Our ultimate goals are (1) to study the radio, optical and near-IR properties of those high-redshift ($z \sim 1$), moderate-power radio sources in the distant sample and to compare them with that of more powerful radio sources, and (2) to make a comparison of primarily non-cluster radio sources in the nearby sample with a companion survey of radio sources in a pair of rich superclusters at $z \sim 0.1$. In this first paper of a series, we report our new C-array VLA continuum snapshots at 4.86 GHz and optical R-band CCD imaging photometry for these two samples and tabulate the observational results on individual sources.

Some direct sample statistical properties are also discussed in the paper and summarized as follows: (1) The distant sample: (a) The sample median flux density at 1,4 GHz is about 65 mJy. (b) The majority (80%) of the sample sources have a steep spectrum between 1.4 and 4.86 GHz with a spectral index around 0.9. Nineteen (90%) of the 21 sources that are *fully* resolved at 4.86 GHz (i.e., angular sizes $\theta \gtrsim 11$") have a radio morphology of Fanaroff-Riley (FR) II type. (c) 'Thirty-seven (88%) of the 42 optically imaged sample sources were optically identified to a limiting R-band magnitude of $R \sim 23.5$ mag. About 15% of the identified radio sources appear to be point sources and the others are extended galaxies with an appearance similar to nearby elliptical galaxies. (d) 'Twenty-eight (76%) of the optically identified sources have R >20 mag, suggesting that these are probably distant ($z \gtrsim 0.8$), with a redshift distribution

peaking at $z \sim 1$ where their radio luminosities are about 10 times the break power between the FR I and II classes. (e) We found no strong evidence for the radio and optical axes of the resolved radio sources (i.e., O $\gtrsim$ 5") to be correlated or anti-correlated, nor any evidence for strong clustering around sample radio sources on average. (2) The nearby sample: Except for $R \lesssim 15$, the sample is dominated by elliptical galaxies with $16 \lesssim R <18.5$ mag and a spectral index distribution similar to that of the distant sample. Based on the radial distribution of optical objects around each radio source, we found that the average radio source environment becomes richer from that characteristic of galaxy groups for $R <17$ mag ($z \lesssim 0.2$) to that of galaxy groups to clusters at R $\gtrsim$ 18 mag ($z \gtrsim 0.3$).

Subject headings: cosmology — galaxies: photometry --- galaxies: distances and redshifts — galaxies: clustering — radio continuum: galaxies --- surveys

1. Introduction

A recent survey using 56 contiguous Very Large Array (VLA)[1] D-array fields (Condon, Dickey,& Salpeter 1990; hereafter CDS90) has yielded a uniform catalog of 354 radio-continuum sources with radio flux densities at 1.4 GHz, $S_{1.4}$, down to about 1.5 mJy in a 12 square degree area at high Galactic latitudes. The area is known to be much devoid of rich Abell clusters below a redshift $z \sim 0.4$ (Gunn, Hoessel & Oke 1986). As explained below, this geometry has several advantages.

Firstly, the general deficiency of galaxies at low redshifts increases the chance for selecting distant radio sources. We are particularly interested in a sample of CDS90 sources complete to $S_{1.4}$ = 35 mJy (hereafter referred to as the "distant" sample or 1) S). The break power ($\sim 10^{25}$ W Hz^{-1} at 1.4 GHz) between the high-power, Fanaroff-Riley type 11 (FR II-type; Fanaroff & Riley 1974) and low-power, FR 1-type radio sources corresponds to $S_{1.4} \approx$ 10 mJy at $z \sim 1$. The above distant sample, at $z \sim 1$, explores moderate-power, typical FR II-type radio sources; and therefore it extends the extensively studied 3CR radio catalog ($\gtrsim$ 1500 mJy at 1.4 GHz; Spinrad et al. 1985) and the so--called 1-Jy sample ($\gtrsim$ 400 mJy at 1.4 GHz; Allington-Smith 1982). One motivation in constructing such a mJy radio sample is to address the fundamental question of how the dramatic optical, near-IR and radio evolution of radio galaxies from the present to $z \sim 1$ (e.g., Lilly & Longair 1984; McCarthy et al. 1987; Le Fevre & Hammer 1988; Eisenhardt & Chokshi 1990; Rigler et al. 1992; McCarthy 1993 and references therein) depends on radio power and redshift. This question arises because the most detailed studies, including those cited above, were based primarily on the powerful 3CR radio sources which show a strong correlation between radio

[1] The Very Large Array (VLA) is a facility of the National Radio Astronomy Observatory operated by Associated Universities, Inc., under cooperative agreement with the National Science Foundation.

luminosity and redshift (McCarthy 1988). Some recent studies on fainter radio sources at high redshifts (Dunlop & Peacock 1993; Owen & Keel 1995) have shown some indications of a radio-luminosity dependence of radio source evolution between $z \sim 1$ and the present. The distant sample studied in this paper is about 45 times fainter than the 3CR, and with appropriate redshift and photometric data it is ideal for addressing; the above question.

Using $S_\nu \propto \nu^{-0.9}$ to compare intensities at different frequencies, our distant sample is $\sim$ 8 times fainter than the l-Jy sample of Allington-Smith (1982) or the similarly bright, but less completely identified 4C sample (Pilkington & Scott 1965), MRC/1-J y survey (McCarthy et al. 1990) and Parkes Survey (Wright, Savage, & Bolton 1977). The existing samples comparable to ours in flux are the B3 survey (Ficarra, Grueff, & Tomassetti 1985) and the Texas surveys (Bozyan 1992). However, their optical identifications arc quite incomplete yet. The deeper 5C 12 sample @enn et al. 1982) and sub-mill lijansky sample of Windhorst et al. (1984, 1985) are far from completely identified and contain many low-power FR I radio sources even for $z \gtrsim 1$.

Our second interest lies in the fact that most of the CDS90 radio sources at redshifts below $z \sim 0.4$ arc of FR l-type and in non-cluster environments. By scanning a Palomar Observatory Sky Survey (POSS) plate, CDS90 generated a catalog of optical galaxies down to $B \sim 19$ msg. This led to optical identifications of most of the radio sources with $z \lesssim 0.3$ (i.e., Table IV of CDS90). Using the same optical catalog of galaxies, CDS90 found some evidence for clustering over small scales (of that of galaxy groups or 100SC clusters) around these radio sources. Although it has been known that FR I-type radio sources apparently tend to live in rich clusters (e.g., Longair & Seldner 1979), an interesting question is whether the current radio activities depend more on their immediate environments (say, over scales of galaxy groups), than on environments over a much 1 arger scale (say, over scales of galaxy clusters or superclusters). One approach to this question is to study the local environments

of radio sources of similar powers, but in quite different environments over a much larger scale. In a future paper we will describe our companion radio survey, similar to CDS90, but in a direction towards two of the richest superclusters (R.A.$\sim 15^h20^m$, decl.$\sim$ 29°; $z \sim 0.1$; see Bahcall & Soneira 1984a, and Batuski & Burns 1985) in the local universe and will make a comparison between it and the sample of nearby CDS90 radio sources. in the current paper wc study a sample of nearby radio sources from Cl)S90 with $B \lesssim 19$ mag (hereafter, referred to as the "nearby" sample or NS).

Spectroscopic redshift data on most NS sources and some DS sources have been obtained and will be given in subsequent papers, together with some optical color data, In this first paper, we report our new C-array VLA continuum snapshots at 4.86 GHz and optical R-band CC]) imaging photometry on the above two samples. The remainder of this paper is organized as follows: We describe our sample selection in §2, VLA radio observations at 4.86 GHz and their results in §3, and optical CCD imaging photometry and radio source identification in §4. Some direct statistics of the distant and nearby samples are discussed in §5 and §6, respectively. Finally, a summary is given in §7.

2. Samples of Radio Sources

The 1.4 GHz radio catalog of CDS90 is confined to the area bounded roughly by $9^h36^m < \alpha < 9^h55^m$ and 46°<6<48°30' (centered at about 47° in Galactic latitude) and is fairly complete to a flux density of 3 mJy at 1.4 GHz. The two radio samples in the current paper arc selected from their catalog as follows:

After excluding two sources with a primary VLA beam correction greater than 5 (R001 and R002 in their Table 11), the remaining 56 radio sources with an integrated flux density at 1.4 GHz, $S_{1.4}$, greater than 35 mJy in CDS90 constitute our distant sample. Fig. 1

shows the integral distribution of the DS sources as a function of $S_{1.4}$, illustrating a good completeness down to $S_{1.4} = 35$ mJy. The median value of $S_{1.4}$ for this sample is about 65 mJy.

Using a catalog of optical galaxies down to $B \sim 19$ mag that was generated by scanning the appropriate 1'0SS plate, CDS90 optically identified 58 of their radio sources with $\delta\theta \leq 15$", where SO is the separation between the 1.4 GHz position of the radio source and the optical counterpart, defined to be the nearest object in their optical galaxy catalog. These are primarily nearby ($z \lesssim 0.3$), low-power radio sources and are listed in their Tables IV(a) and IV(b). Our nearby radio sample (or NS) contains those 36 sources with $\delta\theta \lesssim 10''$, including two (R133 and IWO]) that have a large enough radio flux to also be in the distant sample.

We also managed to obtain VLA C-array snapshots at 4,86 G] lz and some optical CC]) imaging photometry for 8 additional radio sources of which R195 and R231, together with the other three (R082, R] 91, and R252) that are already in our nearby sample, lie within 40" on the sky of some Abell-like clusters (likely at $z \gtrsim 0.4$) in Gunn et al. (1986). The CCD fields of these sources arc used in §5 and §6 as references to study the environments of our DS and NS radio sources. All of the forenamed radio sources arc listed in 'J'able 2, to be explained in the next section.

3. VLA Continuum Snapshots at 4.86 GHz and Compilation of Radio Data

3.1. VLA Snapshots, Data Reduction and Results

In order to obtain better positions, radio spectral indices and morphological data, radio-continuum snapshots at 4.86 Gllz ($\lambda \approx 6$ cm) were obtained for all but two sources (R262 and R353) in the distant sample, 18 sources in the nearby sample and all the

additional radio sources described in §2. The snapshots, centered on the 1.4 GHz positions from CDS90, were taken in a single 8 hour session on 1990 December 1 with the VLA in its C configuration. Each source was observed for 5 minutes with a 50 M Hz bandpass. Phase calibration was performed using the source 0920+446 (J2000) from the standard VLA calibrator list, and fluxes were calibrated against both 3C 48 and 3C 286. The resulting synthesized (FWHM) beam is about 4".2. The data were "CLEA Ned" and corrected for primary beam response using standard routines in the AIPS software package of National Radio Astronomy Observatory. Cleaning reached the expected radiometer noise of 0.15 mJy/beam or so for all but the brightest 2 to 3 sources. Source parameters were measured using the AIPs task IMFIT to fit Gaussian functions to the individual components of each source.

The 4.86GHz contour maps arc shown in Fig. 2. We give in Table 1 some derived parameters for each radio 'signal" detected on these radio maps, organized in column (1) by the source names taken from CDS90. In the fields of R147 and R202, the detected signals appear to contain two independent radio sources: in addition to a well defined, bright FR II-type radio source near the 1.4 GHz position, there is a weaker radio signal away from the map center. For these cases, the brighter source was taken to be our radio source while the weaker onc is noted by suffixing a letter "n" (for '(near") to its name in Table 1. The remaining columns of 'l'able 1 are as follows: Columns (2) and (3) arc, respectively, the right ascension and declination (in the format of "hmmss.ss" and "ddmmss.s", respectively; equinox 1950) for each detected signal. These are the peak position of the best-fit Gaussian profile to each signal. The typical rms positional error is of < 0".3 for unresolved signals and is somewhat larger for resolved sources. Colu nns (4) and (5) give, respect ively, the peak and integrated flux densities in mJy. Columns (6) and (7) arc, respectively, the estimated major and minor axes of each detected source in units of arcseconds if these arc obtainable. Finally, column (8) gives the position angle (north to cast of the major axis) in degrees.

The numbers appearing in parentheses in columns (4) to (8) are the estimated rms errors,

3.2. Compilation of the Radio Data

Table 2 is a complete list of the radio sources in tile two samples plus the few additional sources. We tabulated here the following integral parameters by combining 'l'able 1 in this paper and the 1.4 GHz radio survey of CDS90: Column (2) indicates to which sample a radio source belongs to, where "DS" and "NS" represent the distant and nearby samples, respectively, and 'a" denotes an additional source. Columns (3) and (4) arc the right ascension and declination (equinox 1950) of the adopted center of each radio source. Unless a source was not observed at 4.86 GHz in this paper for which the 1.4 GHz position taken from CDS90 was quoted, the position was determined from the 4.86GHz C-array radio map using the following rule: for a radio source showing only one component, this position is the peak position from the Gaussian fitting, i.e., that given in columns (2) and (3) of Table 1; for a double-lobed source with a detected core, the core peak position is used; for a double-lobed source without a detected core, the mean position of the two radio lobes is usually used; and for a source of more than 3 cornponcnts, the average position of all the components is usually given here. Columns (5) and (6) list the integrated flux densities in mJy at 1.4 and 4.86 GHz, respectively. Column (7) gives the spectral index, α, between the frequencies 1.4 and 4.86 GHz. This was derived from the flux densities in the previous two columns assuming $S_\nu \propto \nu^{-\alpha}$. Column (8) gives θ, the (maximum) angular size in units of arcseconds from the 4.86GHz radio map. For unresolved and single-cornponcnt sources, this is simply the major axis (or its upper limit) given in column (6) of Table 1; for double-lobed sources, this was taken to be the separation between the peaks of the two radio lobes; and for a fcw sources with more than 3 components, this is the estimated maximum angular extent of the source. Column (9) gives the position angle (north to east) in degrees

of the major axis for single-component sources or of the axis connecting the two radio lobes for double-lobed sources. Finally, in column (10) we give a very brief morphological description, where FR 1 and FR II morphology, assigned only to *fully* resolved sources (i.e., $\theta \gtrsim 11" \approx 2.5$ times the VLA beam), was determined as in Fanaroff & Riley (1974); namely, the ratio of the separation between the peaks in the brightness distribution of each lobe to that between the outermost contours on opposite sides of the source is measured. FR I or FR 11 is assigned if this ratio is less or greater than 0.5.

Two DS sources (R] 82 and R307) and one NS source (R203) likely contain two independent radio sources each, based on their radio morphology and probable optical identifications (see the next section). Wc have simply divided the total 1.4 GHz flux density between the two independent components in proportion to their 4.86 GHz flux densities and identified each of thcm in Table 2 by a suffix of "A" or "B" to its namc. As a result R307A from the DS now has $S_{1.4}$ <35 mJy and R203B was not optically identified (see 'I'able 3). The above two sources were left out of their respective samples. For the remainder of this paper and in Table 2, our DS consists of 57 sources (including RI 82A, R182B and R307B, but excluding R307A) and our NS still consists of 36 sources (including R203A, but excluding R203B).

4. Optical CCD Imaging Photometry and Radio Source Identification

4.1. Optical Observations and Data Reduction

Optical CCD images in broad R-band, centered on the 1.4 GHz radio positions, were obtained for a total of 59 radio sources, including 42 from the DS, 16 from the NS (including 2 that overlap with the DS) and some additional sources.

The observations were carried out with the 200 inch (5.08m) telescope equipped with

the four-shooter CCD cameras (see Gunn et al. 1987 for a description of this instrument) at Palomar Observatory[2] during nights of (UT) 1990 February 24, 26, and 27 and April 27 and 28 and of 1991 January 18 to 20 in 1991. The final CCD images have a field of about 4.2' x 4.2' and a scale of 0".336 per pixel. For our primary imaging it-band, we used a Gunn r filter that centers at $\lambda_0 \sim 6650$Å and that mimics the Cousins-R filter (Cousins 1976). The integration time per field was 600 seconds per source except for R042. Additional V- and I-band images were also obtained for a large fraction of the sources observed in R and the resulting colors will be present in a subsequent paper. During each observing night, a few standard stars from Landolt (1983) and/or stars in the field of M67 (Schild 1983) were observed over a wide range of air masses for the purpose of flux calibration. The weather condition was not quite photometric for part of the nights of (UT) 1990 February 24 and 1991 January 17. The seeing varied (1".2 to greater than 2") over the course of our run. Therefore, wc give in 'l'able 3 (to be explained below), for each image, its date of observation and optical seeing.

Each CCD image was reduced in the conventional way: The zero-level bias was determined by fitting a polynomial to an overscan exposure and was subsequently removed from the whole CCD frame. The flattening was done using a skyflat generated by median-filtering a number of '(sky" exposures, The resulting background is flat within about 0.5% for most frames.

---

[2]Observations at the Palomar Observatory were made as part of a cent inuing co]] aborat ive agreement. between the California Institute of Technology and Cornell University.

4.2. Detections, Catalogs and Photometry of Optical Objects

Objects on each CCD image were detected and their various photometric parameters were evaluated using the Faint Object Classification and Analysis System (hereafter referred to as FOCAS; Valdes 1982, see also Jarvis & Tyson 1981) provided by National Optical Astronomy Observatories. The procedure is described briefly below:

Object detection: The FOCAS detected any object whose area, $A_{\rm iso}$, is larger than a predetermined minimum area $A_{\rm min}$, where $A_{\rm iso}$ is made of the contiguous pixels whose values are more than k times the rms sky noise (σ) above the local sky level. We used k = 2.5 as recommended by Valdes (1982). The optimal value of $A_{\rm min}$ depends on the optical seeing. We used a conservative value of $A_{\rm min} = 10$ pixel^2 (or 1.1 arcsec^2). However, below $A \lesssim 20$ pixels^2, a significant fraction of detections were found to be spurious. We also used in our detection process the FOCAS built-in filter of 5 x 5 pixels (Valdes 1982) that increases the S/N ratio.

Photometry: For a detected object, the FOCAS further elaborated the local sky value by analyzing the pixels around that object, and an isophotal magnitude, $R_{\rm iso}$, was evaluated by summing up the sky-subtracted pixels within the area $A_{\rm iso}$. $R_{\rm iso}$ was found to be, on average, equivalent to the isophotal magnitude at a surface brightness of $\mu_R \sim 30$ mag arcsec^{-2}. At this faint isophote, $R_{\rm iso}$ essentially measures the total magnitude and the effect of varying optical seeings on the value of $R_{\rm iso}$ is small. A second magnitude, $R_{\rm tot}$, was also evaluated by summing up the pixels within an aperture whose area is $2A_{\rm iso}$. We will use this aperture magnitude below to define, in a consistent way, the isophotal magnitudes of overlapped objects.

Geometry: The pixels within the area $A_{\rm iso}$ were also used to obtain various simple and luminosity-weighted moments which we used to determine the diameters, ellipticity and position angle of an object.

Overlapped Objects: Overlapped objects were separated as follows: First, FOCAS raised the intensity threshold for detection by 0.2 times the sky sigma, then it ran the same detector for detecting objects with areas larger than A_{min}. If two or more objects were detected, the original object (parent) was split into individual objects (daughters) and each of the daughter objects was subject to further splitting if the level of this splitting loop was less than N_s, a predetermined quantity. For each split object, the total magnitude was not evaluated directly. Instead the total luminosity of the parent object was divided between daughter objects in proportion to their isophotal luminosities. To avoid a large number of spurious splits around bright objects, we used N_s = 5. This usually gave satisfactory results except for highly overlapped binaries or galaxies in very crowded regions. We found that such a splitting usually increases the number of objects by 5%0 to 15% for R $\lesssim$ 24 msg.

For a split object, we defined its isophotal magnitude and area in the following self-consistent way:

$$R^i_{iso} = R^p_{iso} + (R^i_{tot} - R^p_{tot}), \quad (1)$$

and

$$A^i_{iso} = A^p_{iso}(A^i_{iso} / \sum_j A^j_{iso}), \quad (2)$$

where the superscript "i" stands for the i^{th} daughter object, the superscript '(p" stands for its parent object, and the sum in eq. (2) was evaluated over all the daughter objects of the same parent. The input isophotal parameters on the right-hand side of eq. (2) are those given by the FOCAS. For multiple-level splits, eqs. (1) and (2) were calculated from the top, single parent object down to each final split object.

Statistics of a typical optical catalog are illustrated in Fig. 3 using the representative CCD field of R035 with an optical seeing of $\sim$ 1 ".5 (FWHM). Fig. 3a shows the distribution of the isophotal magnitudes of 545 originally detected objects (the solid squares). No attempt has been made in Fig. 3 to separate galaxies from stars. We plot by the dashed

curve the expected counts for our CCD field from field galaxies and Galactic stars. This curve was built using the R-band galaxy counts of Tyson (1988) and the V-band star counts of Bahcall & Soneira (1984b) that were converted to the R-band by assuming $(V - R)$ = 0.4 msg. Since the radio source field is at high Galactic latitude ($b \sim 470$), no latitude correction was applied in converting the star counts of Bahcall & Soneira (towards the northern Galactic pole) to our CCD fields. It is gratifying to see that up to $R_{\rm iso} \sim 24$ mag the data points follow the curve fairly well, suggesting that our optical catalogs are complete to about $R_{\rm iso} \gtrsim 23.5$ msg. Fig. 3b plots $R_{\rm iso}$ versus $R_{\rm tot}$ for all the detected objects. It shows that the average systematic difference between $R_{\rm iso}$ and $R_{\rm tot}$ is always smaller than 0.3 mag for $R \lesssim 24$ msg. The measurement errors of $R_{\rm iso}$ are dominated by the uncertainty of the sky value. A comparison between the magnitudes obtained with a local sky value and those obtained using a global sky value indicates that the measurement errors are on the order of 0.3 mag for $R \sim 24$ msg. We therefore believe that $R_{\rm iso}$ measures the total magnitude within an accuracy of 0.5 mag at $R \sim 24$ msg. The mean isophotal area, $A_{\rm iso}$ is about 35 pixels^2 (or 4 arcsec^2) at $R_{\rm iso} \approx 24$ as shown in Fig. 3c which plots the isophotal area in units of square pixels (1 pixel = 0".336) versus $R_{\rm iso}$ for the originally detected objects. Fig. 3 changed little if the objects after FOCAS splitting with $N_s = 5$ were used instead. In the remainder of this paper, we shall use $R_{\rm iso}$ only (and leave out its subscript for simplicity), truncate each optical catalog at $R \sim 23.5$ mag, and refer the number of objects (with $R \lesssim 23.5$ mag) in an optical catalog as $N^{23.5}_{\rm opt}$.

Both optical seeing and weather conditions could have some effect on the completeness of an optical catalog. This is illustrated in Fig. 4, a plot of $N^{23.5}_{\rm opt}$ as a function of the FWHM of the optical seeing. We have used circles for the DS sources and squares for the NS and additional sources. The 5 sources that are close to some known galaxy clusters (cf. §1) have their square symbols darkened (one of them, R082, with $N^{23.5}_{\rm opt} = 453$ and an optical seeing of 1".6, is off the scale), as do the 5 DS sources that are not optically

identified in this paper (see §4.3 below). The figure indicates that the optical seeing starts to affect the completeness of an optical catalog when it becomes greater than $\sim 2''$. Although the CCD fields of the 5 DS sources that are not optically identified in this paper have a moderate optical seeing (1".4 to 2".4), all but one (RI 47) have relatively low values of $N^{23.5}_{\rm opt}$. The majority of the CCD fields with $N^{23.5}_{\rm opt} \lesssim 150$ were obtained on the night of UT 24 February 1990 or 18 January 199], both of which had periods of unstable weather. It is, therefore, plausible that at least some of the optically unidentified DS sources may actually be brighter than our detection limit. Those CCD fields with $N^{23.5}_{\rm opt} \lesssim 150$ will not be used in our statistical analysis in §5 and §6.

4.3. Optical Identification of Radio Sources

4.3.1. Astrometry

Astrometry was done using two kinds of position calibrators: (1) the Hubble Space Telescope (11 S'1') Guide Star Catalog (G SC; see Lasker et al. 1990 and references therein) and (2) a catalog of fainter stars (down to about $B \sim 19$ mag), generated from scanning the Palomar Sky Survey plate in CDS90. The former has an overall rms positional error of about 0".5 (Russell et al. 1990), but contains only relatively bright stars which are sparse over our relatively small CC]) fields; while the latter usually provides about 5 to a dozen stars in each CCD field, but has somewhat larger positional errors (see CDS90 or Dickey, Keller, & Bennington 1987). Using the stars common to these two catalogs, we found a systematic offset of $\lesssim 2''$ in both R.A. and decl. between these two catalogs. Since a higher rate of radio source identifications was obtained using astrometry based on the GSC positions than on the stellar positions of CDS90, we have tied the coordinate system of CDS90 to that of the GSC by statistically correcting, in the Appendix, the above systematic offsets. The final rms positional difference between the CGS system and the converted

CDS90 system is about 0".9 in either RA or Dec, in agreement with the statistical errors of these two catalogs. Taking into consideration the external errors of the GSC, we simply adopted a value of 1".0 for the total rms positional error for each calibrator from CDS90.

4.3.2. Definition of Error Ellipses

An optical object detected by the FOCAS as described in §4.2 was regarded to be an identification of the radio source under consideration if the optical object is within the error (or searching) ellipse of the radio source (except for a few sources identified with an optically bright, extended galaxy as noted in Table 3). For a single-component radio source (including the unresolved ones) or a double-lobed source with a detected radio core, this error ellipse reduces to a circle centered at the position of the radio source (or its core) with a radius given by

$$r_s = 3\sqrt{\sigma_{\rm radio}^2 + \frac{\sigma_{\rm star}^2}{N_{\rm star}}}, \qquad (3)$$

where $\sigma_{\rm radio}$ is the rms positional error in our 4.86 GHz radio data, $\sigma_{\rm star}$ is the rms positional error for the calibrating stars, and $N_{\rm star}$ is the number of stars used in astrometry. We have adopted the following values: $\sigma_{\rm radio} \approx$ 0."3 and 0".6 for unresolved and clearly resolved radio sources, respectively; and $\sigma_{\rm star} \approx$ 1".0 as discussed in §4.3.1.

For a double-lobed radio source without a detected core, the most probable position of its optical counterpart is within an ellipse centered at the middle point between the peaks of the two radio lobes and being elongated along the radio axis as shown by Laing, Riley & Longair (1983). Following their results, we placed the center of the error ellipse at this middle point (given in Table 2) and adopted the following semi-major and semi-minor axes:

$$\begin{cases} a = 0.20 + r_s, \\ b = 0.10 + r_s, \end{cases} \qquad (4)$$

where, on the right-hand side of eq. (4), θ is the angular separation between the two radio lobes, given in Table 2; and r_s, given in cq. (3), is usually much smaller than the first term. Finally, for R230, which was not detected at 4.86 GHz, we simply used a large searching radius of 15″.

4.4. The Results

Optical identification was carried out on all the R-band CCD images. The results are summarized in Table 3 which contains, for each source, the following data columns:

Columns (2) to (4) arc data related to the whole CCD image, where column (2) identifies the date of observation (UT); column (3) gives the FWHM of the optical seeing in units of arcscconds; and column (4) gives $N^{23.5}_{opt}$, the number of the detected optical objects with R < 23.5 msg. Note that $N^{23.5}_{opt}$ is not given for three CCD fields that contain "bleeded" images of brig] ıt stars.

Astrometric data are given in columns (5) to (8) of Table 3. The semi-major and semi-rninor axes of the adopted error ellipse are given in units of seconds of arc in column (5) while its position angle (north to east) in degrees is in column (6). Columns (7) and (8) are the positional offsets in the R.A. and decl. directions, respectively, measured in units of seconds of arc from the radio position to the position of an optical identification.

For faint optical identifications, we give in columns (9) to (1 O) the offsets in units of arcscconds in the R.A. and decl. directions from a nearby bright star to the optical identification. The approximate R magnitude of this offsetting star is given in column (11).

Columns (12) to (16) of Table 3 arc photometric data on each optical counterpart. Column (12) differentiates between a point source (Q SO) and an extended source (Gal) based on the point spread function in the CCD field. Column (13) is the I~OCAS-measured

isophotal magnitude. For a split object, this magnitude is given by eq. (1). If there are multiple identifications, the brightest one is usually taken to be the most probable optical identification and is listed first in Table 3. Column (14) is the isophotal area in units of arcsec^2, determined by eq. (2). For each optical identification, its major and minor diameters in units of arcscc.ends arc given in column (15) and its position angle (north to cast) in degrees in column (16). These were derived from the following parameters:

$$\tan(2\beta) = \frac{2 < xy >}{< x^2 > - < y^2 >}, \tag{5a}$$

$$r_p^2 = < x^2 > \cos^2\beta + < y^2 > \sin^2\beta + \sin(2\beta) < xy >, \tag{5b}$$

and

$$r_m^2 = < x^2 > \sin^2\beta + < y^2 > \cos^2\beta - \sin(2\beta) < xy >. \tag{5c}$$

in the above formula, $< x^2 >$, $< y^2 >$ and $< xy >$ are the (unweighted) 2nd moments evaluated within the FOCAS isophotal area; β and r_p^2 are, respectively, the angle of the major or minor axis with respect to the x-axis and the second moment evaluated along this axis; and r_m^2 is the second moment evaluated along the other axis. For an isolated object, its major and minor diameters were given, respectively, by

$$2a = max(2\sqrt{r_p^2}, 2\sqrt{r_m^2}) \tag{6a}$$

and

$$215 = min(2\sqrt{r_p^2}, 2\sqrt{r_m^2}), \tag{6b}$$

and finally its position angle was determined. For a split object, the diameters given by eqs. (6) were multiplied further by $(A^c_{\rm iso}/A^{focas}_{\rm iso})^{1/2}$ to *derive* the *fills]* diameters listed in I'able 3, where $A^c_{\rm iso}$ and $A^{focas}_{\rm iso}$ arc, respectively, the "corrected" (by eq. [2]) and 1~'OCAS-measured isophotal areas.

Of the 42 optically observed DS sources, 37 (88%) were optically identified. These include (i) 34 sources with unique optical identifications and (ii) 3 sources (1{014, R080,

and R276) with two optical objects within their searching ellipses. For group (i), the optical counterparts arc mostly within 2" of the radio positions. Based on the average surface density of the detected objects in our CCD fields and a Poisson fluctuation, the chance for an unrelated background object of $R \lesssim 24$ mag to be within 1 ".5 of the radio source position is about 3%. This suggests that one out of the 34 optical identifications may be false. Since many of the optical counterparts are much brighter than $R = 24$ mag, the number of false identification is probably much less than one. The same arguments led us to believe that a few radio sources, as already specified in §2, actually consist of two independent sources each with an identified optical counterpart. For group (ii), the optical] y brighter onc was taken to be the most probable optical counterpart and used in the statistical analysis below. The chance for a false identification is still quite low here, except for R080, which has two possible faint optical counterparts.

For the observed NS sources, one source (R139) turned out to be a galaxy of $R \gtrsim 20$ msg. The remaining NS sources all have an identification of $15.5 < R < 18.5$ mag, in agreement with CDS90 identification.

We display the it-band CCD images of the observed radio fields in Fig. 5. In each image wc have marked each optical counterpart if the radio source was identified or the radio position if it was unidentified. For optically faint radio sources, the offsetting stars given in Table 3 for positional offsets are also marked in Fig. 5.

5. Statistical Properties: 'I'he Distant Sample

5.1. Radio Angular Sizes and Spectral Indices

Radio data at 4.86 GHz were obtained for all DS sources but two (R262 and R353). The distribution of the (maximum) angular sizes at 4.86 GHz, θ, for the DS sources is

shown in Fig. 6 (unhatched histogram), where in addition, the hatched histogram represents the subset of sources with $\theta \gtrsim 11$" and FR II radio morphology (including two with FR 1/11). It is clear that the majority of these fully resolved DS sources have FR II radio morphology. Together with the sample characteristic flux density, this suggests that most of these sources are likely at high redshifts.

The distribution of the radio spectral indices, α, is shown in Fig. 7 for two subsamples divided by O $\approx$ 5". All but one DS sources with O $\gtrsim$ 5" are '(steep spectrum" sources with $\alpha > 0.55$ and their Gaussian-like distribution of α has a mean of 0.95 and a standard deviation of 0.20. In contrast, about 40% (1 O in number) of the sources with O $\lesssim$ 5" (all arc unresolved) arc "flat-spectrum" sources with $\alpha < 0.55$. The fact that all these flat-spectrum sources are unresolved implies that their physical sizes must be relatively compact. Overall, our distant radio sample contains roughly 80% steep-spectrum, extended sources and 20% flat-spectrum, compact sources.

5.2, Optical Characteristics

The majority of optical counterparts appear to be extended galaxies with elliptical isophotes, consistent with existing findings in samples at similar flux levels (e.g., Windhorst et al. 1985). As noted in Table 3, five of the 37 optically identified DS sources arc possibly QSOS with a point-source like image. If none of them are Galactic stars, this suggests a QSO fraction of 14% $\pm$ 6% in the distant sample. This rate is slightly lower than the average QSO fractions of 20% to 25% found in the 3CR catalog (Laing et al. 1983), the 1-Jy sample (Allington-Smith et al. 1982), and a radio sample that is even fainter than our 1)S (Kron, Koo, & Windhorst 1985). A revised estimate of this QSO fraction will be given when we have optical colors or spectra.

The unhatched histogram in Fig. 8a shows the R magnitude distribution for all the 37 identified DS sources, while the hatched part of the histogram represents the 5 possible QSOs. The flat-spectrum sources all have R <21 mag, brighter on average than those with steeper radio spectra.

Of the 5 unidentified DS sources, one (R] 47) is probably fainter than our detection limit. The CCD images of the remaining 4 sources have a value of $N^{23.5}_{\rm opt}$ that is, on average, 100 counts less than that of a CCD field taken under a good weather (see Fig. 4). Together with Fig. 3a, this suggests that these sources should be at least fainter than about 21.5 mag in R.

5.3. On Redshifts and Radio Luminosities

Spectroscopic redshift data for most DS sources arc not yet available at the time of writing this paper. But some order-of-magnitude estimates could bc made on the basis of their optical morphology and R magnitudes. Fig. 8b plots redshifts versus R magnitudes for the 3CR (Spinrad et al. 1985) and 1-Jy radio sources (Allington-Smith 1984; Allington-Smith, Lilly & Longair 1985; Lilly 1989) with spectroscopic redshifts, represented by triangles and circles, respectively. The symbols for known QSOs arc darkened in the figure in order to bc differentiated from radio galaxies. For the 3CR sources, their R magnitudes were derived from the available V magnitudes in Spinrad et al. (1 985) by simply assuming $(V- R)=1$ mag, a rough average color as implicitly suggested by the colors tabulated in Laing et al. (1 983). The same average $(V - R)$ color was assumed for some 1-Jy sources whose V magnitudes are given in Lilly (1989).]n spite of the fact that the optical magnitudes used here arc quite nonuniform and of various accurac.its, the two plotted parameters show a fairly good correlation for radio galaxies. A comparison between Figures 8a and 8b would imply that most of the optically identified 1)S sources with $R \gtrsim 20$

mag should have $0.8 \lesssim z < 4$ if the correlation in Fig. 8b is largely independent of radio powers. The above upper limit in redshift is very 100SC given the uncertainties in, e.g., the K-correction, and inevitable evolution effect. On the other hand, most of the optical luminosity of a radio galaxy could be triggered by radio activities at high redshifts, $z \gtrsim 1$ (e.g., Chambers & Chariot 1990). In this case the R-band optical luminosity could scale as $P_{1.4}{}^{0.6}$, where $P_{1.4}$ is the radio power at 1.4 GHz (Chokshi & Eisenhardt 1991; see also Auriemma et al. 1977 for earlier work on the bivariate radio-optical luminosity function). Being 45 times weaker than the 3CR sources in radio, our DS sources would be about 2 magnitude fainter in the R-band than the 3CR sources at a given high redshift and would only reach up to $z \sim 1.5$ or so. Of course, the reality could well be somewhere between these two extremes. Nevertheless, a significant fraction of the DS sources should have $z \sim 1$ or $P_{1.4} \sim 1026$ W Hz^{-1}, making them typical FR I]-type radio sources.

5.4. Alignment between Optical and Radio Images

Most powerful radio galaxies at $z \sim 1$ show some tendency for their radio axes to be aligned with the optical or near-]lt major axes of the underlying galaxies (e.g., McCarthy et al. 1987; Eisenhardt & Chokshi 1990; Rigler et al. 1992). However, whether such optical-radio alignment phenomenon depends strongly on radio power has to be tested by using samples of lower-power radio galaxies at high redshifts. Insignificant or much weaker optical-radio alignment was found for some weaker radio galaxies at high redshifts by Dunlop & Peacock (1993) using the Parkes survey and by Thompson et al. (1994) using the B3 survey.

For 24 optically identified radio sources that are partially or fully resolved at 4.86GHz (i.e., $\theta \gtrsim 5$"), we plot in Fig. 9 the distribution of the angles, $\delta(PA)$, between the optical and radio major axes of each source. 'I'here is an apparent tendency for the two axes to be

within about 20° of either parallel or perpendicular to each other, but only at a significance of $\lesssim 2\,\sigma$ (assuming Poisson statistics). The significance for $\delta(PA)$ to be within 20° of zero is only about 1 u. Wc therefore conclude that our data do not show any evidence for a tendency of the optical and radio axes to be aligned with each other.

5.5. Radio Source Environments

The environments of radio galaxies in the local universe (e.g., $z \lesssim 0.2$) are correlated with radio powers, in the sense that low-power, FR I sources tend to be in rich clusters while the powerful, FR II radio sources usually lie in the field or in galaxy groups (e.g., Longair & Seldner 1979; Prestage & Peacock 1988). Clustering analysis has been recently extended to radio galaxies around $z \sim 0.5$ by Yates, Miller, & Peacock (1989) using 3CR radio galaxies of Cygnus A type and by Hill & Lilly (1991) using radio galaxies of both FR types. Both studies found positive evidence for z $\sim$ 0.5 radio galaxies to have at least an equal probability to be found in clusters as in the field. However, the least well sampled part of the radio luminosity function at z $\sim$ 0.5 in the above two studies is around a radio power of $P_{1.4} \sim 10^{26}$ W Hz^{-1} where most nearby FR 11 radio galaxies (mostly from the 3CR) lie.

Even without spectroscopic redshift data, wc have some statistical inferences on the average environments of our DS radio sources. To extract an optically uniform subsample for this purpose, wc have selected only those DS sources that satisfy (1) 18< $R \lesssim$ 21.5 mag, (2) the optical seeing <2“, and (3) $N^{23.5}_{\rm opt} > 150$. For each selected source, wc calculated the following quantity:

$$\Delta N(R_1, R_2, r_1, r_2) \equiv N_{\rm opt}(R_1 < R < R_2;\ r < r_1) - N_{\rm opt}(R_1 < R < R_2;\ r_1 < r < r_2), \quad (7)$$

where $N_{\rm opt}(R_1 < R < R_2; r_1 < r < r_2)$ is the number of the detected optical objects (including the radio source itself if geometrically appropriate) that have an R-band

magnitude between R_1 and R_2 and lie between radii of r_1 and r_2 of the center of the CCD field (near which the radio source lies). Thus, ΔN in eq. (7) measures the magnitude-limited excess of number counts within the inner radius r_1 over that in the annulus delimited by radii r_1 and r_2.

We note that the angular size of a given metric length does not vary much between $z \sim 1$ and 2 (e.g., Weedman 1986, p. 66). We further divided the above selected sources into two subsamples in terms of the estimated redshifts from Fig. 8: a subsample of 11 sources with $20 < R \lesssim 21.5$ mag (or likely to have $0.8 \lesssim z \lesssim 1.5$) and a subsample of 4 sources with $18 < R < 20$ mag (or roughly $0.3 \lesssim z \lesssim 0.8$). We shall refer to these two subsamples as DS1 and DS2, respectively. For simplicity, we assigned a redshift of unity to every DS1 source and a redshift of 0.5 to every DS2 source. Furthermore, we chose $r_1 = 75$" and $r_2 = 106$" for the DS1 sources, and $r_1 = 90$" and $r_2 = 127$" for the DS2 sources. Assuming $q_0 = 0.5$ and $H_0 = 75$ km $s^{-1}Mpc^{-1}$, for a given metric length, the ratio of its angular size at $z = 0.5$ to that at a redshift between 1 and 2 is about 1.2 and an angular size of 75" corresponds to 0.43Mpc at $z \sim 1.0$ (e.g., Weedman 1986, p. 66). Thus, the above choice of r_1 and r_2 implies that we are sampling roughly the same metric area for both subsamples, and that the linear size of r_1 corresponds to about 2.5 cluster core radii at which the projected galaxy density of a typical cluster falls to $\sim 8\%$ of the central peak density (e.g., Bahcall 1975).

As we will show in the next section, at least three of the five radio sources, which lie within 40" of the nominal center of some galaxy clusters in Gunn et al. (1 986), are very likely to be the first ranked cluster galaxies. These clusters have a spectroscopic or estimated redshift around $z \sim 0.5$ (Gunn et al. 1986; Dressler & Gunn 1992) and have richnesses ranging from being very rich (i.e., Abell 851 around R082) to an Abell richness 1 or so. Having $18 < R < 20$ mag and passing the same selection criteria as the DS1 and DS2, these 5 sources constitute a third subsample (hereafter, referred to as NSal),

for which we also used $z = 0.5$, $r_1 = 90$" and $r_2 = 127$". Table 4 lists all the three subsamples with the following parameters: Column (2) lists the sources in each subsample. Column (3) gives the (sub) sample median or mean and the range of R-band magnitudes in each subsample. Columns (4) and (5) have similar formats as Column (3), but for $S_{1.4}$ and $\log P_{1.4}$, respectively. The *rest-frame* radio power at 1.4 GHz, $P_{1.4}$, was calculated using the assumed redshift for each subsample, $H_0 = 75$ km s^{-1} Mpc^{-1}, $q_0 = 0.5$ and a spectral index of $\alpha = 0.9$. We used medians for DS1 but means for the other two subsamples of smaller sizes. It is clear that the median power of the DS1 is around 10^{26} W Hz^{-1}, the typical power of nearby FR II-type radio galaxies in the 3CR catalog.

Fig. 10 shows the distribution of ΔN of each subsample in Table 4, where the hatched histogram represents $\Delta N(R_{\rm radio}, R_{\rm radio} + 2, r_1, r_2)$ and the unhatched, thick solid histogram represents $\Delta N(R_{\rm radio} -]\ ,\ R_{\rm radio} +],\ r_1, r_2)$, with $R_{\rm radio}$ being the optical R magnitude of the radio source under consideration. Note that $R_{\rm radio} + 2 < 23.5$, the limiting magnitude for our optical CCD catalogs. Recent CCD surface photometry of nearby radio galaxies indicated that on average, the host galaxies of FR 1 radio sources are probably 1 mag brighter than the host galaxies of FR II radio sources (Owen & White 1991). If this is also the case at high redshifts, the unhatched histograms of the DS1 and DS2, which contains mainly FR II sources, should be compared with the hatched histogram of the FR I-type radio sources in the NSal.

The sample mean value of $\Delta N(R_{\rm radio}, R_{\rm radio} + 2, r_1, r_2)$ and its standard deviation, derived from the sample mean value of $N_{\rm opt}(R_{\rm radio} < R < R_{\rm radio} + 2;\ r < r_1)$ using Poisson statistics, are given in column (6) of Table 4. For the NSal sources, the value of ΔN is clearly correlated with the richness of the cluster: from a value of 3 to 4 for R191 and R252 which may or may not be physically in clusters (see §6), to around 15 for the richest cluster around R082. The sample mean of A AT is 8 ± 2.9. On the other hand, as shown in Table 4,

the mean of AN for the DS 1 sources using either the hatched or unhat chcd histogram is essentially zero, suggesting either that there is no significant clustering (i.e., much less than Abell richness 1) around these sources on average or that most DS1 sources are primarily on the outer parts of a cluster (i.e., $\gtrsim 3$ cluster core radii). The situation of the DS2 sources are intermediate with an mean of $\Delta N \lesssim 3 \pm$ '2.4.

6. Statistical Properties: The Nearby Sample

Of the 36 NS sources, seventeen were included in both our 4 .86GHz VLA snapshot and R-band CCD imaging observations. One (R139) turned out to have R $\approx$ 20.3 mag which is much fainter than the limiting magnitude of the NS. We shall not discuss this galaxy further here. Fig. 11 plots the CCD R magnitude as a function of log $D^r_{65\%}$, the logarithmic diameter measured on the red POSS plate at 65% plate transmission in CDS90 (roughly at a surface brightness of 24 mag arcscc^{-2} in red), for all the NS sources with CCD images except for R160 (a quasar) and R201 for which its close, equally-bright companion makes $D^r_{65\%}$ uncertain. While deferring a detailed photometric calibration on POSS galaxies (both the optical counterparts of the NS radio sources and other optical galaxies) to a future paper in which wc will compare our NS radio sources with a sample of radio sources in rich superclusters of galaxies at $z \sim 0.1$, we derive here a crude photometric calibration for the NS sources without CCD measurements. We have simply fitted two linear relations to the points in Fig. 11 and adopted the following fit:

$$R = \begin{cases} (27 - 5 \log D^r_{65\%}) & \text{if } \log D^r_{65\%} \geq 2, \\ 17 + 0.6[(27 - 5 \log D^r_{65\%}) - 17] & \text{otherwise.} \end{cases} \quad (8)$$

The fit results in an rms residual of ~ 0.3 msg. Eq. (8) was used to show, in Fig. (12), the magnitude distribution for all our NS sources. The hatched histogram in Fig. (12) singles out the subset of 16 sources with CCD magnitudes. The two optically brightest sources are

nearby spiral galaxies: R043 (UGC 05157; R $\sim$ 12,9 mag and z $\approx$ 0.016) and R213 (UGC 05263; $R \sim$ 13.7 mag). Thus, wc start to sample low-radio power spiral galaxies at $R \lesssim 15$. For $R > 15.5$, all the sources with CCD images appear to be normal elliptical galaxies except for R133 and R160. R133 has an impressive point source-like nucleus surrounded by vigorous spiral arms and, therefore, resembles the so-called N-galaxy. R160 has been confirmed to be a QSO based on our spectroscopic observations (Huchra et al. 1995). Fig. 12 also shows that the subsample of the 16 NS sources included in our VLA and optical CCD observations is fairly representative of the total NS sample for $R \gtrsim 15.5$ msg. Consequently, wc only discuss the statistical properties of this subsample below.

The spectra] indices of the NS sources range from O to 1.2 and have a mean around 0.7. The distribution of the 4.86GHz radio sizes span up to $\sim$ 20", with 53% of the sources being unresolved (i.e., $\theta \lesssim 5$").

While our particular sample selection on the sky implies that most of the NS sources arc not in clusters, wc found that most of them have close companions. Except for R160 (QSO), R247 and R281, all of the remaining NS sources have, within a radius of 15", a companion with a magnitude neither brighter nor more than 3 mag fainter than the radio source. This separation corresponds to a linear size of $\lesssim 50$ kpc even at $z \sim 0.5$ ($H_0 \sim 75$ km s^{-1}Mpc^{-1}). We show in Fig. 13 the variations of the surface density of the detected optical objects (excluding the radio source itself) as a function of the radial distance from the radio source. Only optical objects with an R magnitude between $R_{\rm radio}$ and ($R_{\rm radio}$ + 4) were used. Shown in Fig. 13 arc three sets of radio sources: (a) the 5 sources with 18< R <19.5 mag that are near some known clusters, of which three (R082, R191 and 1{.252) arc NS sources; (b) five NS sources with 17 < R < 18.5 mag, not including any NS source in (a); and (c) six NS sources with 15.5 < R < 17 mag. Three of the 5 sources in (a) including the NS source R082 and two additional NS sources, R212 and R239,

in (b) have similar radial profiles that fall slowly eve] our sampled radii, making them all characteristic of cluster sources. On the other hand, the other two NS sources in (a), R191 and R252, may not be physically associated with clusters at all as their curves, like those of the NS sources with $15.5 < R < 17$ mag, have negligible slopes beyond a radial distance of 40" to 60". We summarize our findings as follows: Most of the NS radio sources with R <17 mag (or roughly $z \lesssim 0.2$) have excess companions only within a radius of ~ 50", making their environments typical of galaxy groups; for $17 < R \lesssim 19$ mag (or roughly $0.2 < z \lesssim 0.5$), about 40% of the NS sources are in clusters, 50% arc in groups, and 10% are in the field.

7. Summary

From the 1.4 GHz radio survey of Condon, Dickey, & Salpeter (1990) in a region much evoid of rich galaxy clusters at $z \lesssim 0.4$, we selected two subsamples: (1) a "distant" sample, DS (or "optically faint"), namely, all the 57 radio sources which have 1.4 GHz flux density of 35 mJy or more, irrespective of optical magnitudes; and (2) a "nearby sample)', NS (or "optically bright"), namely all the radio sources in the original survey, irrespective of radio flux, which arc optically brighter than $B \sim 19$ mag. These include two sources in common. Our ultimate goals arc (a) to study the radio, optical and near-IR properties of those high-redshift ($z \sim 1$), moderate-power radio sources in the distant sample and to compare thcm with that of more powerful radio sources, and (b) to make a comparison of primarily non-cluster radio sources in the nearby sample with a companion survey of radio sources in a pair of rich superclusters at $z \sim 0.1$. in this first paper, we report our ncw C-array VLA continuum snapshots at 4.86 GHz and optical R-band CCD imaging photometry for these two samples and tabulate the observational results on individual sources.

We hope to collect more redshift data for our sources, which will be needed for

unambiguous interpretations. However, we have almost complete optical identifications for our two samples (i.e., apparent magnitudes) and radio spectral indices, so some statistical properties are already known. These can be summarized as follows. (1) The distant sample: (a) The majority (80%) of the sample sources have a steep spectrum between 1.4 and 4.86GHz with a spectral index around 0.9. Nineteen (90%) of the 21 sources that are fully resolved at 4.86 GHz (i.e., angular sizes O $\gtrsim$ 11") have a radio morphology of Fanaroff-Riley (FR) II type. (b) Thirty-seven (88%) of the 42 optically imaged sample sources were identified to a limiting R-band magnitude of $R \sim 23.5$ mag. About 15% of the identified radio sources appear to be point sources and the others are extended galaxies with an appearance similar to nearby elliptical galaxies. (c) 'I'wenty-eight (76%) of the optically identified sources have R >20 mag, suggesting that these are probably distant ($z \gtrsim 0.8$), with a redshift distribution peaking at $z \sim 1$ where their radio luminosities are about 10 times the break power between the FR I and 1 I classes. (d) We found no strong evidence for the radio and optical axes of the resolved radio sources (i.e., O $\gtrsim$ 5") to be correlated or anti-correlated, nor any evidence for strong clustering around sample radio sources on average. (c) The median 1.4 GHz flux density for the distant sample as a whole is about 65 mJy and the median red apparent magnitude is about 21.0 mag, compared with about 2820 mJy and 17.5 mag for the 3CR sample (see Spinrad et al. 1985) and about 490 mJy and 20.2 mag for the "1-Jy" sample of Allington-Smith (1982). (2) The nearby sample: Except for $R \lesssim 15$, the sample is dominated by elliptical galaxies with $16 \lesssim$ R <18.5 mag and a spectral index distribution similar to that of the distant sample. Based on the radial distribution of optical objects around each radio source, we found that the average radio source environment becomes richer from that characteristic of galaxy groups for $R < 17$ mag (roughly $z \lesssim 0.2$) to that of galaxy groups to clusters at $R \gtrsim 18$ mag (roughly $z \gtrsim 0.3$).

We are grateful to the staffs of both Palomar Observatory and VLA for their help in our

observations, to N. Rowlands for helping us with some of the CCD imaging observations, to J. Dickey for providing us with a catalog of stars generated from Minnesota Automatic Plate Scanner, to F. Valdes for helps on installing and running the FOCAS, to M. Dickinson for providing us with a machine-readable 3CR catalog, to K. Zadorozny for making the radio contour plots, to P. Eisenhardt for many enlightening discussions, to J. Condon, J. Huchra, O. Liivak, P. McCarthy, R. Windhorst for helpful conversations, and to the referee of this paper. This work was supported in part by the Jet Propulsion laboratory, California Institute of Technology, under a contract with the National Aeronautics and Space Administration, by NSF grants AST91- 19475 at Cornell University, by NSF grants AST-90151 81 and AST-9316213 at Lafayette College, and by the National Radio Astronomy Observatory which is operated by the Associated University Inc. under a cooperative agreement with the National Scicn cc Foun dati on.

A. Conversion of CDS90 Positions to the 11ST Guide Star Catalog (GSC) System

We found a total of 53 stars in common between the CDS90 and GSC catalogs, and show in Fig. 14 the R.A. and decl. differences between these two systems. It is evident that $\Delta(\alpha)$, which $\equiv \alpha(\text{CDS90}) - \alpha(\text{GSC})$, has a dependence on δ; and $\Delta(\delta)$, which $\equiv \delta(\text{CDS90}) - \delta(\text{GSC})$, depends on both α and δ. For simplicity, we have least-squares fit $\Delta(\alpha)$ to a linear function of δ and A(6) to a linear combination of α and δ. The results are

$$\Delta(\alpha) = 1.47(\delta - 47.4^\circ) + 0.23 \tag{9}$$

and

$$\Delta(\delta) = 7.24(\alpha - 9.75^h) + 0.83(\delta - 47.4^\circ) - 1.44, \tag{lo}$$

where α and δ are in units of hours and degrees, respectively; and $\Delta(\alpha)$ and A(6) are in units of arcseconds. These fits are sufficient in the sense that they take away almost all the observed correlations in Fig. 14. After converting the CDS90 positions to the GSC scale using eqs. (9) and (1 O), the rms values for $\Delta(\alpha)$ and A (δ) are, respectively, 0".88 and 0".94, in agreement with the random error estimates.

REFERENCES

Allington-Smith, J. R. 1982, MNRAS, 199, 611

Allington-Smith, J. R., Perryman, M. A. C., Longair, M. S., Gunn, J. E., & Westphal, J. A. 1982, MNRAS, 201, 331

Allington-Smith, J. R. 1984, MNRAS, 209, 665

Allington-Smith, J. R., Lilly, S. J., & Longair, M. S. 1985, MNRAS, 213, 243

Auriemma, C. Perola, G., Ekers, R., Fanti, R., Lari, C., Jaffe, W. J., Ulrich, M. H. 1977, A&A, 57, 41

Benn, C. R., Grueff, G., Vigotti, M., & Wall, J. V. 1982, MNRAS, 200, 747

Bahcall, J. N. 1975, ApJ, 1{]8,249

Bahcall, J. N., & Soneira, R. M. 1984a, ApJ, 277, 27

Bahcall, J. N., & Soneira, R. M. 1984b, ApJS, 55, 67

Batuski, D. J., & Burns, J. O. 1985, AJ, 90, 1413

Bozyan, E. 1'.1992, ApJS, 82, 1

Chambers, K. C., & Chariot, S. 1990, ApJ, 348, L1

Chokshi, A., & Eisenhardt, P. 1991, Comments Astrophysics, 15, 343

Condon, J. J., Dickey, J. M., & Salpeter, E. E. 1990, AJ, 99, 1071 (CDS90)

Cousins, A. W. J. 1976, *Mem. RAS, 81, 25*

Dickey, J., Keller, D. T., & Bennington, R.. 1987, AJ, 93, 788

Dressler, A., & Gunn, J. E. 1992, ApJS, 78, 1

Dunlop, J. S., & Peacock, J. A. 1993, MNRAS, 263, 936

Eisenhardt, 1'., & Chokshi, A. 1990, ApJ, 351, L9

Fanaroff, B. L. & Riley, J. M. 1974, MNRAS, 167, 31

Ficarra, A., Grueff, G., Tomassetti, G. 1985, A&A, 59, 255

Gunn, J. E., et al. 1987, *Optical Engineering,* 26, *779*

Gunn, J. E., Hoessel, J. G., & Oke, J. B. 1986, ApJ, 306, 30

Hill, G. J., & Lilly, S. J. 1991, ApJ, 367, 1

Huchra, J. P., et al. 1995 (in preparation)

Jarvis, J. F., & Tyson, J. A. 1981, AJ, 86, 476

Kron, R. G., Koo, D. C., & Windhorst, R. A. 1985, A&A, 146, 38

Laing, R. A., Riley, J. M., & Longair, M. S. 1983, MNRAS, 204, 151

Landolt, A. U. 1983, AJ, 88, 439

Lasker, B. M., Sturch, C. R., McLean, B. J., Russell, J. L., Jenkner, H., & Shara, M. M. 1990, AJ, 99, 2019

Le Fevre, O., & Hammer, F. 1988, ApJ, 333, 1,37

Lilly, S. J. 1989, ApJ, 340, 77

Lilly, S. J., & Longair, M. S. 1984, MNRAS, 211, 833

Longair, M. S., & Seldner, M 1979, MNRAS, 189, 433

McCarthy, P. J, 1988, Ph.]). thesis, University of California, Berkeley

McCarthy, P. J. 1993, ARA&A, 31, 639

McCarthy, P. J., Kapahi, V. K., van Breugel, W. J. hf., & Subrahmanya, C. R., 1990, AJ, 100, 1014

McCarthy, 1'. J., van Breugel, W. J. M., Spinrad, H., & Djorgovski, S. G. 1987, ApJ, 321, 1,29

Owen, F. N., & Keel, W. C. 1995, AJ, 109, 486

Owen, F. N., & White, R. A. 1991, MNRAS, 249, 164

Pilkington, J. D. 11., & Scott, P. 1'.1965, *MmRAS*, 69, *183*

Prestage, R. M., & Peacock, J. A. 1988, MNRAS, 230, 131

Rigler, M. A., Lilly, S. J., Stockton, A., Hammer, F., & Le Fevre, O. 1992, ApJ, 385, 61

Russell J. I,., l.asker, B. hi., McLean, B. J., Sturch, C. R., & Jenkner, 11.1990, AJ, 99,2059

Schild, R. E. 1983, PASP, 95, 1021

Spinrad, 11., Djorgovski, S., Marr, J., & Aguilar, 1,.1985, PAS]', 97, 932

Thompson, D., Djorgovski, S., Vigotti, M., & Grueff, G. 1994, AJ, 108, 828

Tyson, J. A. 1988, AJ, 96, 1

Valdes, F. 1982, The FOCAS User's Manual (Tucson: NOAO)

Weedman, D. W. 1986, Quasar Astronomy (Cambridge: Cambridge Univ. Press)

Windhorst, R. A., van Heerde, G. M., Katgert, P. 1984, A&AS, 58, 1

Windhorst, R. A., Miley, G. K., Owen, F. N., Kron, R. G., & Koo, D. C. 1985, ApJ, 289, 494

Wright, A. E., Savage, A., & Bolton, J. A. 1977, Australian *J. Phs. Astrophys. Suppl.*, *41*, 1

Yates, M. G., Miller, L., & Peacock, J. A. 1989, MNRAS, 240, 129

This manuscript was prepared with the A AS LaTeX macros v4 ,0.

Figure Captions

Fig. 1,--- Integral distribution of the DS sample sources in terms of radio flux density, $S_{1.4}$, at 1.4 GHz. The error bars represent 1σ (Poisson) and the dashed line with a slope of $-\frac{3}{2}$ for $S_{1.4}$>35 mJy is a nominal fit to the data points except the two with the largest flux densities.

Fig. 2.-- Radio continuum contour plots from the VLA C-array snapshots at 4.86GHz. North is at the top and cast is to the left. Shown in the lower right corner of each plot is the 4".2 VLA synthesized beam which also serves as a rough indicator of the size of the plot. The contour levels arc marked at the lower left corner of each plot as follows: a general notation '5 x 2" means that the lowest contour is 5 mJy beam^{-1} and that the others follow in multiples of 2 (i.e., 5, 10, 20, etc.); but for some cases we used a notation such as "5, 8, 13" to indicate the actual contour levels in mJy beam-l.

Fig. 3.— Plots of FOCAS originally detected objects from a typical R-band CCD image (R035 in this case with an optical seeing of $\sim$ 1".5): (a) distribution of the isophotal magnitudes, R_{iso}, where the error bar represents 1σ and the dashed curve is the expected number counts from field galaxies (from Tyson 1988) and stars (from Bahcall & Soneira 1984b; see the text for more explanation); (b) plot of tile total magnitude, R_{tot}, as a function of R_{iso}, where the diagonal line indicates where $R_{tot} = R_{iso}$; (c) same as (b), but the ordinate is now the logarithmic isophotal area A_{iso}. *These* plots change only a little if objects obtained after FOCAS splitting procedure arc used instead.

Fig. 4.-- Plot of the number of the detected optical objects with R <23.5 mag in a CCD field as a function of the FWHM of the optical seeing when that CC]) image was taken. The circles arc for the DS sources and squares are for the NS and additional sources. The 5 sources that arc close to some known galaxy clusters have their square symbols filled (one

of them, R082, with $N_{opt} = 453$ and an optical seeing of 1 ".6, is off the scale), as do the 5 DS sources that are not optically identified in this paper.

Fig. 5.-- R-band CCD images of the observed radio sources. Each CCD field covers an area of about 4'.2 x 4'.2. North is at the top and cast to the left. The two solid lines bisect the optical identification of the radio source or the radio source position in the case where no optical counterpart was identified. The single solid line points to the offset star listed in Table 3. Additional "blow-up" images of 30" x 30" are shown for R124, R212, R216, R239 and R304 which all have close objects.

Fig. 6--- The unhatched histogram represents the distribution of the (maximum) angular sizes, θ, for all the 1)S sources, while the hatched histogram is for the subset of sources with $\theta \gtrsim 11$" that show a FR II radio morphology on our VLA snapshots at 4.86GHz.

Fig. 7.-- Distributions of the spectral indices, α, between 1.4 and 4.86 GHz for two DS subsamples: (a) 24 sources with a (maximum) angular size, θ, less than about 5", and (b) the remaining 31 1)S sources with $\theta > 5$".

Fig. 8.— (a) The unhatched histogram shows the R magnitude distribution for all 37 DS sources that have been optically identified in this paper. The part of the histogram for the 5 possible QSOS is hatched. (b) Plot of spectroscopic redshifts vs. R magnitudes for the 3CR (triangles) and 1-Jy radio sources (circles). The symbols for known QSOS arc filled.

Fig. 9.— Distribution of the position-angle differences (limited to between 0° and 90°) between the radio sources and their optical counterparts for the 24 optically identified 1)S sources that arc at least partially resolved (i.e., with a maximum angular size $\gtrsim 5$") on our 4.86GHz snapshots. The dashed line shows the expected mean from a random distribution.

Fig. 10--- Histogram distributions of AN, defined in eq. (7) in the text, for three subsamples: (a) DS1 -11 DS radio sources with $20 < R \lesssim 21.5$ mag, (b) DS2 --4 DS radio sources with $18 < R < 20$ mag, and (c) NSal -- the five radio sources near some known galaxy clusters. The hatched histograms arc for $\Delta N(R_{\rm radio}, R_{\rm radio} + 2, r1, r2)$ and the unhatched, thick solid histograms arc for $\Delta N(R_{\rm radio} -], R_{\rm radio} +], r1, r2)$, Where $R_{\rm radio}$ is the R magnitude of the radio source under consideration, r_1 = 75" (90") and r_2 = 106" (1 27") for DS1 (1)S2 and NSal) sources. The value of AN measures the magnitude-limited excess of number counts within the inner radius r_1 over that in the annulus delimited by radii r_1 and r_2.

Fig. 11---- Plot of CCD R magnitudes vs. $(27 - 5 \log D^r_{65\%})$ for the 14 NS sources with available CCD magnitudes. $D^r_{65\%}$ is the diameter, in units of microns, measured on the red POSS plate at 65% plate transmission in CDS90 (roughly at the 24th mag arcscc^{-2} in red). The solid lines represent cq. (8), a simplified least-squares fit to the data.

Fig. 12.—- R-band magnitude distribution of all the NS sources. The hatched part represents those with available CCD magnitudes. The magnitudes of sources without CCD magnitudes were estimated using cq. (8).

Fig. 13.-— Variations of the surface density of optical objects (excluding the radio source itself) as a function of the radial distance from the radio source for three data sets: (a) the 5 sources with $18 < R < 19.5$ mag that are near some known clusters, including 3 NS sources; (b) five NS sources with $17 < R < 18.5$ mag, not including any NS source in (a); and (c) six NS sources with $15.5 < R < 17$ msg. Only optical objects with an R magnitude between $R_{\rm radio}$ and $R_{\rm radio} + 4$ were used, where $R_{\rm radio}$ is the magnitude of the radio source.

Fig. 14.- Positional differences in Equatorial Coordinates between the CDS90 and the 11ST GSC systems for 53 stars in common: (a) α(CDS90) – α(GSC) vs. α, (b) α(CDS90) -- α(GSC) vs. δ, (c) δ(CDS90) – δ(GSC) vs. α, and (d) δ(CDS90) – δ(GSC) vs. δ.

TABLE 1

RESULTS FROM THE RADIO-CONTINUUM SNAPSHOT OBSERVATIONS AT 4.86 GHz

Source (1)	α (2)	δ (3)	S_{max} (4)	S_{int} (5)	$2a$ (6)	$2b$ (7)	P.A. (8)
Ro 13	93615.54	464258,1	9.99(0.15)	10.59(0.46)	<2.5	...	...
	93615.26	464245.3	2.37(0.05)	2.50(0.16)	<2.6	...	...
R014	93619.38	470024.2	2.57(0.10)	10.16(0.29)	12.2(0.3)	8.6(0.4)	107(5)
	93617.67	470122.6	0.89(0.07)	7.83(0.21)	24.5(1.6)	11.0(0.7)	140(4)
R016	93633.94	475605.6	14.46(0.08)	14.94(0.25)	<1.7	...	...
R019	93641.36	480420.6	14.90(0.07)	14.97(0.22)	<1.0	...	...
Ro20	93645.32	475141.6	8.89(0.16)	14.65(0.48)	7.9(0.2)	<7.9	...
R035	93722.04	470439.2	3.18(0.17)	3.63(0.52)	2.5(0.6)	2.0(0.7)	106(27)
	93723.28	470500.6	5.90(0.19)	12.88(0.58)	8.4(0.3)	4.7(0.3)	40(4)
	93720.14	470416.9	5.04(0.12)	6.81(0.38)	4.4(0.2)	2.6(0.3)	63(7)
R042	93737.68	470323.2	28.83(0.08)	29.61(0,24)	1.0(0.1)	1.0(0.1)	94(1)
R050	93755.34	475628.6	33.63(0.25)	46.52(0.80)	5.6(0.1)	1.0(0.2)	5(1)
Ro57	93816.28	460718.8	11.74(0.07)	12.36(0.21)	1.7(0.1)	1.0(0.2)	95(8)
R071[a]	93910.98	473420.4	0.76(0.08)	0.98(0.30)	5,6(1 .3)	<5.6	134(16)
R077	93928.33	474125.1	3.60(0.06)	3.78(0.19)	2.2(0.1)	<2.2	89(14)
R080	93937.51	460507.5	31.43(0.66)	43.56(1.98)	5.5(0.2)	1 .3(0.4)	145(2)
	93938.54	460453.5	13.53(0,39)	19.08(1.19)	5.3(0.3)	2.1(0.4)	144(4)
R082	93942.82	471233.8	3.24(0.06)	2.74(0.19)	<2.7	...	...
R084	93948.48	475521.8	6.29(0.07)	6,93(0.20)	2.2(0.1)	1.6(0.2)	108(10)
	93947.68	475508.0	2.79(0.06)	3.24(0.19)	3.2(0.2)	0.2(0.4)	53(8)
R091	94003.27	462214.7	4.12(0.08)	6.61 (0.24)	6.2(0.2)	3.0(0.2)	178(2)
	94003.01	462244.7	2.53(0.09)	4.38(0.27)	7.0(0.3)	3.1(0.4)	4(3)
R093	94020.12	464717.7	58.06(0.07)	58.44(0.21)	0.6(0.1)	0.4(0.1)	60(22)
R109	94120.89	480240.2	1.63(0.10)	3.87(0.32)	8.7(0.2)	5.4(0.1)	42(4)
	94120.54	480237.2	1.18(0.08)	9.00(0.31)	27.0(2.5)	7.9(0.6)	46(4)
	94118.33	480222.6	0.95(0.04)	3.18(0.13)	11.8(0.5)	6.8(0.4)	36(4)
	94117.90	480212.9	0.71(0.03)	2.20(0.12)	9.4(0.6)	8.0(0.5)	77(17)
R110	94123.71	465237.4	74.28(0.09)	74.62(0.26)	<0.7	...	...
R118	94147.46	475833.3	29.35(0.08)	29.24(0.25)	<0.9	...	...
R121	94203.48	473227.1	3.86(0.11)	1O.98(O.33)	9.2(0.2)	7.1(0.3)	93(6)
	94204.24	473158.7	2.42(0.10)	4.35(0.32)	6.1(0.5)	4.6(0.4)	19(15)
RI 24	94218.10	474331.2	1.11(0.07)	1,41(0.72)	4.4(0.6)	1.3(0.5)	173(19)
R130	94228.69	465041.5	413.30(0.50)	416.20(1.50)	<0.9	...	...
R133	94244.25	463311.0	31.92(0.08)	32.81 (0.25)	1.2(0.1)	0.7(0.1)	179(7)
R137	94249.81	474902.0	6.00(0.08)	6.07(0.23)	2.1(0.1)	<2.1	...
R138	94302.89	475113.0	1.91(0.07)	2.48(0.?0)	4.2(0.3)	2.2(0.5)	12(8)
R139	94253.91	465411.5	3.12(0.08)	4.1 O(O.X3)	3.7(0.3)	3.0(0.3)	156(19)
R140	94257.14	464739,4	5.60(0.25)	11.17(0.75)	9.2(0.4)	2.5(0.5)	125(3)
R145	94312.95	462427.5	7.17(0.13)	8.56(0.39)	3.5(0.2)	1.4(0.4)	67(5)
	94311.55	462415.7	4.26(0.06)	5.02(0.18)	2.8(0.2)	2.3(0.2)	21(15)
R147	94314.39	475133.8	6.86(0.07)	7.70(0.20)	2.5(0.1)	1.6(0.2)	6(7)
	94314.40	475148.1	1.42(0.09)	1.38(0.27)	1.5(0.4)	<1.5	134(34)
	94314.34	475206.6	1 .77(0 .06)	2.45(0.20)	5.6(0.2)	0.7(0.3)	84(5)
R147n	94310.92	475209.8	1.53(0.09)	1.60(0.28)	2.1(0.4)	<2.1	8(41)
R148	94314.34	473757.0	15.88(0.28)	30.31 (0.86)	8.9(0.2)	2,2(0.2)	5(1)
R151	94316.68	462606.7	11.60(0.14)	21.91(0.46)	9.0(0.2)	1.9(0.2)	18(1)
R152	94318.90	461103.1	6.91(0.11)	16.57(0.34)	9.8(0.2)	4.5(0.1)	53(1)
R160	94350.45	473537.1	0.94(0.06)	0.61(0.21)	<4.4		...

TABLE 1 -- Continued

Source (1)	α (2)	δ (3)	s (4)	S_{int} (5)	$2a$ (6)	$2b$ (7)	P.A. (8)
R171	94428.24	460552.1	8.34(0.05)	10.24(0.10)	3.2(0.1)	2.4(0.1)	20(4)
	94427.35	460515.2	1.78(0.06)	2.87(0.18)	5.0(0.3)	4.4(0.3)	59(23)
R174	94443.65	462156.0	29.63(0.08)	29.58(0.25)	<0.6	...	...
R176	94449.43	473229.4	6.53(0.06)	6.73(0.18)	1.5(0.1)	0.1(0.1)	22(15)
	94448.27	473153.6	1.95(0.06)	1.88(0.19)	1.6(0.2)	<1.6	136(16)
R180	94508.32	455815.2	7.04(0.09)	7.42(0.27)	2.1(0.1)	<2.1	125(10)
RI 82	94508.60	474632.2	25.51(0.07)	28.02(0.21)	2.6(0.1)	0.8(0.1)	64(1)
	94502.34	474757.5	29.71(0.08)	30.12(0.24)	1.0(0.1)	<1.0	145(8)
R191[b]	94530.79	470041.4	0.58(0.06)	0.94(0.23)	8.0(0.6)	<8.0	91(11)
	94528.68	470051.3	0.31(0.04)	3.95(0.13)	29.7(3.2)	14.0(1.6)	32(14)
RI 94	94543.53	463142.6	17.43(0.06)	17.39(0.20)	<0.9	...	...
R195	94545.26	462456.2	8.84(0.18)	11 .82(0.57)	4.7(0.2)	2.0(0.4)	59(4)
R201	94607,15	482643.6	9.54(0.26)	33,10(0.86)	11.8(0.3)	7.2(0.3)	103(3)
R202	94609.97	463722.1	1.56(0.08)	6.77(0.23)	16.5(0.6)	6.5(0.4)	57(3)
	94608.09	463702.8	0.85(0.06)	1,40(0.20)	7.1(0.4)	2.3(0.7)	62(10)
	94606.80	463651.4	1.23(0.08)	4.05(0.24)	13.8(0.8)	5.1(0.6)	53(4)
R202n	94610.93	463635.9	1,06(0.09)	0.49(0.24)	<4.8	...	...
R203[c]	94609.81	481605.7	0.87(0.06)	2.82(0.20)	11.7(0.5)	6.5(1.0)	92(7)
	94617.77	481639.6	0.77(0.06)	1.63(0.18)	8.2(0.7)	4.6(0.7)	6(9)
R212	94644.10	472434.4	2.59(0.16)	7.16(0.55)	12.9(0.3)	3.6(1 .2)	81(3)
R216	94700.54	460721.8	27.97(0.17)	29.88(0.51)	1.7(0.1)	1.4(0.1)	14(13)
R226	94745.83	481809.5	5.04(0.13)	6.59(0.38)	4.6(0.2)	1 .7(0.5)	121(5)
	94748.59	481745.4	1.47(0.05)	3.01(0.15)	8.8(0.3)	3.4(0.3)	134(3)
	94747.34	481757.6	0.68(0.07)	1.12(0.24)	18.4(3.1)	<9.2	144(7)
R230[d]	...	...	<0.55	<1.70	...	...	...
R231	94753.32	475812.6	0.52(0.07)	1.36(0.22)	17.2(2.2)	<8.6	127(7)
R233	94804.93	482723.7	8.49(0.07)	8.28(0.23)	<1.4	...	...
R239	94845.93	461953.3	0.79(0.07)	1.51(0.23)	7.4(0.8)	4.0(0.9)	21(12)
R247	94904.37	480454.5	3.18(0.08)	3.55(0.23)	<3.3	...	...
R249	94913.05	472034.8	6.75(0.40)	25.45(1.36)	12.5(0.3)	4.9(0.8)	66(3)
R251	94916.02	464324.3	15.88(0.08)	15.67(0.25)	<1.2	...	...
R.252	94919.66	462728.5	1.09(0.08)	2.38(0.25)	10.8(0.7)	2.1(0.5)	128(6)
R254	94922.94	480553.7	7.16(0.07)	7.37(0.22)	1.3(0.2)	0.6(0.1)	58(25)
R276	95023.66	463932.4	17.80(0.41)	24.87(1.24)	5.1(0.2)	2.2(0.3)	144(3)
	95024.20	463918.6	15.20(0.46)	22.48(1.38)	6.0(0.3)	1.8(0.4)	151(3)
R277	95025.02	473820.0	14.32(0.09)	14.21(0.27)	<1.0	...	...
R281	95043.29	480200.7	3.16(0.09)	2.86(0.27)	<2,4	...	...
R285	95048.30	480011.4	2.85(0.08)	2.83(0.25)	<2.5	...	...
R295	95103.35	460222.4	17.01(0.11)	22.14(0.33)	4.9(0.1)	0.9(0.2)	93(1)
R297	95107.57	472012.4	9.44(0<34)	12.80(0.11)	5.5(0.3)	<5.5	124(6)
R303	95129.53	460013.4	65.16(0.14)	66.19(0.41)	0.8(0.1)	0.7(0.1)	132(30)
R304	95130.65	475042.5	46.18(0.24)	62.04(0.72)	5.](0.1)	1.3(0.1)	122(1)
R305	95130.48	462220.0	5.55(0.29)	15.56(0.95)	11.5(0.3)	5.0(0.8)	80(4)
	95131.58	462224.1	4.51(0.21)	12.58(0.64)	10.3(0.5)	5.9(0.4)	59(5)
R307	95141.25	472946.2	15.26(0.26)	25.94(0.81)	7.6(0.2)	2.0(0.2)	136(1)
	95139.45	472953.8	2.57(0.07)	2.39(0.21)	<2.7	...	...
R31o	95153.35	463517.3	6.77(0.09)	7.39(0.27)	2.5(0.2)	0.6(0.2)	11(8)
R313	95156.21	455744.8	5.56(0.14)	6.72(0.44)	3.3(0.2)	2.1(0.4)	66(12)

TABLE 1-- *Continued*

Source (1)	α (2)	δ (3)	S_{max} (4)	S_{int} (5)	$2a$ (6)	$2b$ (7)	P.A. (8)
	95157.32	455'748.4	2.34(0.14)	3.35(0.44)	5.6(0.4)	1.8(0.5)	67(11)
R319	95207.42	472306.0	45.85(0,12)	46.49(0.34)	0.9(0.1)	0.5(0.1)	92(9)
	95206.84	472254.6	4.70(0.06)	4.77(0.18)	<1.6	...	...
R324	95228.43	473608.9	39.42(0.13)	40.62(0.42)	1.2(0.1)	0.9(0.1)	107(13)
R326	95240.70	470413.4	24.53(0.10)	24.75(0.29)	<1.2	...	
R329	95251.29	455946.6	13.21(0.14)	15,32(0.42)	3.0(0.1)	1,7(0.2)	44(5)
	95252.65	455946.4	2.82(0.09)	4.42(0.28)	5.6(0.2)	3.4(0.4)	95(6)
R337	95354.64	470738.6	21.27(0.43)	35.81(1.29)	7.7(0.2)	1.7(0.3)	10(2)
X338	95355.80	461958.0	10.14(0.09)	10.10(0.26)	<1.1	...	...
R349	95505.76	462808.8	9.85(0.09)	9.96(0.27)	<1.3	...	...
R350	95508.04	462259.6	4.36(0.29)	7.67(0.88)	8.5(0.6)	1.1(0.4)	144(7)
	95507.56	462304.6	3.57(0.24)	10.85(0.75)	13.4(0.8)	4.4(0.6)	122(4)
	95509.79	462246.0	4.50(0.07)	4.74(0.20)	2.4(0.1)	<2.4	106(8)
R351	95508.52	473928.3	872.70(1 .30)	887.70 (3.{10)	1.0(0.1)	0.5(0.1)	142(6)

[a]Radio signals arc weak.

[b]Radio signals are weak. Only the two largest components are listed, i .e., the one on the most left and the onc in the middle of the radio contour plot in Figure 2.

[c]Radio signals arc weak. The two components of R203 arc shown separatedly in Figure 2 as R203A and R203B. The objects arc at the center of each plot.

[d]Not detected. Uppers limits are 3σ.

TABLE 2

RADIO PROPERTIES OF SAMPLE SOURCES AT 1.4 AND 4.86 GHz

Source (1)	Sample (2)	R.A. (3)	Declination (4)	$S_{1.4}$ (5)	$S_{4.86}$ (6)	α (7)	θ (8)	P.A. (9)	Morphology (lo)
Ro13	DS	93615.40	464251.7	50.5	13.35	1.07	13.1	13	FR 11
R014	DS	93618.45	470056.2	76.1	23.00	0.96	69.4	162	FR 11
R016	1)S	93633.94	475605.6	41.5	14.94	0.82	<1.7	...	Unresolved
R019	DS	93641.36	480420.6	38.7	14.97	0.76	<1.0	...	Unresolved
Ro20	DS	93645.32	475141.6	54.4	14.65	1.05	<7.9	75	Unresolved
R035	DS	93722.04	470439.2	86.2	31.19	0.82	59.2	33	FR 11
R042	DS	93737.68	470323.2	135.4	29.61	1.22	1.0	94	Unresolved
R043[a]	NS	93742.1	475052	7.5	...	...	...	...	...
R046[a]	NS	93744.6	463753	3.0	...	...	...	...	...
R050	DS	93755.34	475628.6	166.8	46.52	1.03	5.6	5	Unresolved
R052[a]	NS	93800.6	470735	4.4	...	...	...	...	...
R057	DS	93816.28	460718.8	37.9	12.36	0.90	1.7	95	Unresolved
R071	NS	93910.98	473420.4	1.7	0.98	0.44	5.6	134	Unresolved
R077	NS	93928.33	474125.1	5.3	3.78	0.27	2.2	89	Unresolved
R080	DS	93938.00	460500.5	198.9	64.27	0.91	11.3	145	FR 11
R082	NS	93942.82	471233.8	3.1	3.24	-0.04	<2.7	...	Unresolved
R084	a	93948.08	475514.9	32.0	10.61	0.89	16.8	35	FR II
R087[a]	NS	93953.1	471045	3.2	...	...	...	...	...
R091	DS	94003.10	462229.7	36.3	11.99	0.89	31.1	175	FR 11
R093	DS	94020.12	464717.7	76.7	58.44	0.22	0.6	60	Unresolved
R096[a]	NS	94022.6	472454	0.4	...	...	...	...	...
R109	DS	94119.40	480228.2	36.7	24.30	0.33	66.0	43	FR 11?
R110	DS	94123.71	465237.4	92.7	74.62	0.17	<0.7	...	Unresolved
R116[a]	NS	94137.6	475354	1.3	...	...	...	...	...
R118	DS	94147.46	475833,3	105.0	29.24	1,03	<0.9	...	Unresolved
R121	DS	94203.90	473212.9	62.4	18.59	0.97	29.4	165	FR 11
R124	NS	94218.10	474331.2	3.8	1,41	0.80	4.4	173	Unresolved
R130	DS	94228.69	465041.5	470.8	416.20	0.10	<0.9		Unresolved
R133	DS/NS	94244.25	463311.0	42.8	32.81	0.21	1.2	179	Unresolved
R137	a	94249.81	474902.0	20.8	6.07	0.99	<2.1		Unresolved
R138	a	94302.89	475113.0	2.9	2.48	0.13	4.2	12	Unresolved
R139	a	94253.91	465411.5	14.6	4.10	1.02	3.7	158	....
R140	DS	94257.28	464738.2	38.4	11.17	0.99	9.2	125	Unresolved
R141[a]	NS	94257.6	472041	11.2	...	...	...	...	...
R145	1)s	94312.25	462421.6	50.4	15.14	0.97	21.7	51	FR 11
R147	1)s	94314.40	475148.1	72.4	13.45	1.35	18.7	0	FR 11?
R148	1)s	94314.34	473757.0	88.5	30.31	0.86	8.9	5	Unresolved
R151	1)s	94316.68	462606.7	61.1	21.91	0.82	9.0	18	Unresolved
R152	1)s	94318.90	461103.1	40.2	16.57	0.71	9.8	53	Unresolved
R160	NS	94350.45	473537.1	1.5	0.61	0.72	<4.4	...	Unresolved

TABLE 2—*Continued*

Source (1)	Sample (2)	R.A. (3)	Declination (4)	$S_{1.4}$ (5)	$S_{4.86}$ (6)	α (7)	θ (8)	P.A (9)"	Morphology (lo)
R167[a]	NS	94411.4	463406	1.5	...	...	...	...	
R] 69[a]	NS	94415.4	481923	3.8	...	...	...	...	
R171	DS	94427.80	460533.7	54.3	13.51	1.12	37.9	14	FR II
R] 74	1)s	94443.65	462156.0	50.2	29.58	0.42	<0.6	...	Unresolved
R176	DS	94448.85	473211.5	36.5	8.98	1.13	37.7	18	FR II
R] 80	a	94508.32	455815.2	27.5	7.4?	1.05	2.1	125	Unresolved
R] 82A	DS	94502.34	474757.5	84.9	29.71	0.84	<1.0	...	Unresolved
R182B	1)s	94508.60	474632.2	73.0	25.51	0.84	2.6	64	Unresolved
R190[a]	NS	94528.2	473448	2.7	...	...	...	...	...
R191	NS	94529.45	470046.3	13.1	3.27	1.12	23.7	115	FR II?
R192[a]	NS	94537.7	464148	2.6	...	...	...	...	...
R194	1)s	94543.53	463142.6	44.6	17.39	0.76	<0.9	...	Unresolved
R195	a	94545.26	462456.2	27.8	11.82	0.69	4.7	59	Unresolved
R201	DS/NS	94607.26	482643.8	97.8	33.10	0.87	11.8	103	FR I
R202	1)s	94608.09	363722.0	53.0	12.78	1.14	44.2	47	FR 11
R203A	NS	94609.81	481605.7	4.9	2.82	0.44	14.3	93	?
R203B	a	94617.76	481639.4	2.8	1.63	0.44	9.0	177	Unresolved
R212	NS	94644.10	472434.4	11.8	7.16	0.40	12.9	81	FR 1/11
R213[a]	NS	94646.4	463420	7.9	...	...	...	...	...
R216	1)s	94700.54	460721.8	56.2	29.88	0.51	1.7	14	Unresolved
R217[a]	NS	94703.3	461128 .	3.8	..	..	...	...	
R223[a]	NS	94734.3	474747	2.5	...		...	...	...
R226	DS	94747.34	481757.6	41,0	11.06	1.05	36.6	131	FR 11
R228[a]	NS	94751.0	472403	2.3	...	...	...	...	...
R230	NS	94752.4	464310	0.8	<1.70	...	....	...	...
R231	a	94753.32	475812.6	1.4	1.36	0.02	17.2	127	FR I
R233	NS	94804.93	482723.7	22.3	8.28	0.80	<1.4	140	Unresolved
R239	NS	94845.93	461953,3	6.3	1.51	1.15	7.4	21	Unresolved
R247	NS	94904.37	480454.5	12.9	3.55	1.04	<3.3	...	Unresolved
R249	DS	94913.23	472035.1	82.6	25.45	0.95	12.5	66	FR 1/11
R251	1)s	94916.02	464324.3	49.9	15.67	0.93	<1.2	...	Unresolved
R252	NS	94619.66	462728.5	8.6	2.38	1.03	10.8	128	FR 1
R254	a	94922.94	480553.7	19.8	7.37	0.79	1.3	58	Unresolved
R262[a]	DS	94943.3	465202	36.2	...		...		
R263[a]	NS	94944.9	470955	0.8	..		...		...
R272[a]	NS	95016.1	471116	1.3	..	...	...	...	...
R273[a]	NS	95016.9	464212	2.6	...	...	...	...	...
R276	1)s	95023.93	463925.5	134.0	46.59	0.85	14.9	158	FR 11
R277	1)s	95025.02	473820.0	48.2	14.21	0.98	<1.0		Unresolved
R279[a]	NS	95034.9	465826	2.7		...	...		...

TABLE 2– -Continued

source (1)	Sample (2)	R.A. (3)	Declination (4)	$S_{1.4}$ (5)	$S_{4.86}$ (6)	α (7)	θ (8)	P.A. (9)	Morphology (10)
R281	NS	95043.29	480200.7	8.8	2.86	0.90	<2.4	···	Unresolved
R285	a	95048.30	480011.4	9.1	2.83	0.94	<2.5	···	Unresolved
R289[a]	NS	95055.1	464355	2.5	···	·····	·····	·····	
R295	DS	95103.35	460222.4	81.2	22.14	1.04	4.0	93	Unresolved
R297	DS	95107.57	472012.4	47.0	12.80	1.05	5.5	124	Unresolved
R303	DS	95129.53	460013.4	56.5	66.19	-0.13	0.8	132	Unresolved
R304	DS	95130.65	475042.5	168.6	62.04	0.80	5.1	122	Unresolved
R305	1)s	95131.03	462222,1	64.6	23.53	0.81	12.1	7 0	FR II
R307A	a	95139.45	472953.8	7.1	2.40	0.87	<2.7	···	Unresolved
R307B	DS	95141.25	472946.2	76.5	25.96	0.87	7.6	136	Unresolved
R310	DS	95153.35	463517.3	39.5	7.39	1.35	2.5	11	Unresolved
R313	DS	95156.77	455746.6	37.1	9.76	1.07	12.1	7 3	FR II
R319	DS	95207.13	472300.3	189.6	51.16	1.05	12.8	2 7	FR II
R324	DS	95228.43	473608.9	69.5	40.62	0.43	1.2	107	Unresolved
R326	DS	95240.70	470413.4	45.7	24.75	0.49	<1.2	···	Unresolved
R329	DS	95251.97	455946.5	63.1	19.70	0.94	14.2	8 9	FR II
R337	DS	95354.64	470738.6	103.6	35.81	0.85	7.7	···	Unresolved
R338	DS	95355.80	461958.0	47.0	10.10	1.24	<1.1	···	Unresolved
R349	DS	95505.76	462808.8	40.9	9.96	1,13	<1.3	···	Unresolved
R350	Ds	95508.04	462259.6	74.8	24.56	0.89	29.6	129	FRI?
R351	1)s	95508.52	473928.3	740.9	887.70	-0.15	1.0	···	Unresolved
R353[a]	1)s	95515.70	472128	42.0	···	·····	·····	·····	

'Not observed at 4.86GHz.

TABLE 3

RESULTS FROM THE R-BAND CCD IMAGING PHOTOMETRY

	Observations			Astrometry				Offset Star			Photometry				
Source (1)	Date (2)	Seeing (3)	$N_{opt}^{23.5}$ (4)	$a \times b$ (5)	P.A. (6)	δX_r (7)	δY_r (8)	δX_s (9)	δY_s (10)	R_s (11)	Type (12)	R (13)	A_{iso} (14)	2a x 2b (15)	P.A. (16)
R013[a]	2/24/90	2.1	124	4.1x2.8	13	0.47	-5.68	-10.2	-39.1	16.8	*Gal*	19.68	47	4.3x3.5	8
R014	2/24/90	3.6	85	15.5x8.6	162	1.77	-3.76	-50.3	18.9	16.4	Gal	19.55	77	6.4x4.6	132
						-2.55	4.91	-54.6	27.6	16.4	Gal	19.80	34	3.8x3.4	12
R016	1/19/91	1.8	230	1.5X1.5	...	-0.68	1.01	84.3	10.6	<15.8	Gal	24.01	5	3.1x1.0	43
R019	2/24/90	1.8	i20	1.9x1.9	...	.....		.....		...	...	...	...	...	...
R020	2/24/90	1.8	236	2.3x2.3	...	1.34	0.30	-42.3	9.1	...	Gal	24.36	3	1.4x1.1	120
R035	2/24/90	1.5	192	1.5X1.5	...	0.17	1.18	65.7	80.8	16.6	Gal	20.35	35	3.9X3.1	69
R042	1/18/91	1.6	...	1.9X1.9	...	-0.44	0.50	12.7	-62.0	17.0	Gal	23.85	4	2.7x1.1	9
R050[b]	1/19/91	1.5	249	2.1x1.4	5	-0.64	-0.20	-17.8	-45.1	16.4	Gal	19.11	84	5.6x5.2	0
R057	2/24/90	1.5	204	2.4x2.4	...	2.35	0.17	86.5	-1.4	<16.5	Gal	23.21	6	1.5X1.3	42
R071	2/24/90	1.5	169	2.1x2.1	...	0.13	0.97	33.4	29.8	16.8	Gal	16.95	353	13.9x8.3	128
R077[a]	2/24/90	1.5	...	1.4X1.4	...	-0.27	2.30	.....		...	Gal	16.97	427	13.3X11.5	5
R080	2/26/90	1.3	194	5.0x4.0	145	-0.62	-0.43	-22.9	-52.3	<17.2	Gal	22.48	14	2.7x2.O	144
						-1..04	-3.35	-23.3	-55.0	<1.7.2	Gal	23.83	5	2.9x0.8	159
R082[c]	2/24/90	1.6	453	1.5X1.5	...	0.40	-0.54	-44.8	23.3	17.6	Gal	18.28	50	4.8x3.7	14
R084[d]	2/24/90	1.7	221	4.6x3.1	31	.....		.....		...	...	...	...	...	...
R091	2/26/90	1.5	187	7.9x4.8	175	0.67	-2.06	69.7	-49.3	<17.2	Gal	22.51	12	2.5x1.7	108
R093	1/20/91	2.3	153	1.5X1.5	...	-0.07	-0.54	78.2	-35.6	<14.5	QSO?	20.10	38	3.9x3.3	105
R109[e]	2/27/90	1.5	230	2.1X2.1	...	-0.17	3.02	0.0	36.0	<17.5	Gal	20.40	36	4.1x3.2	134
RI1O	2/27/90	1.5	193	1.9x1.9	...	1.26	1.31	-28.5	-39.9	<16.5	QSO	20.02	19	2.8x2.4	41
R118	2/27/90	1.4	156	1.3X1.3	...	.....		.....		...	...	...	...	...	...
R121	2/24/90	1.7	199	7.5x4.5	165	-1.68	5.38	12.3	20.5	<15.8	Gal	20.53	33	4.3x3.4	63
R124	1/20/91	1.7	237	1.7X1.7	...	0.60	-0.24	.....		...	Gal	15.63	729	16.3x14.3	130
R130	2/27/90	1.5	247	1.5X1.5	...	0.27	-0.54	39.7	29.5	Brgt	Gal	20.61	31	3.9x3.0	42
R133	2/27/90	1.4	198	1.5X1.5	...	0.71	0.13	57.1	-83.4	<15.5	Gal	15.98	1091	23.0x16.3	57
R139	4/28/91	2.3	237	1.6X1.6	...	0.50	-1.01	-8.9	-67.9	Brgt	Gal	20.29	29	3.4x2.9	22
R140	2/27/90	1.4	242	2.8x2.4	130	-0.77	-0.03	-24.6	87.5	<16.2	Gal	22.30	9	2.0x1.5	117
R145	2/27/90	1.3	223	4.9X3.1	39	-2.70	-4.00	-19.0	45.7	17.2	Gal	21.69	21	3.1x2.2	57
R147	2/27/90	1.7	254	1.4X1.4	...	.....		.....		...	...	...	...	...	...
R148	2/27/90	1.7	227	2.5x2.5	...	1.38	-0.03	18.2	99.6	<14.5	Gal	23.67	5	2.1X1.1	103

TABLE 3—Continued

	Observations			Astrometry				Offset Star			Photometry				
Source (1)	Date (2)	Seeing (3)	$N_{opt}^{23.5}$ (4)	$a \times b$ (5)	P.A. (6)	δX_r (7)	δY_r (8)	δX_s (9)	δY_s (lo)	R_s (11)	Type (12)	R (13)	A_{iso} (14)	$2a \times 2b$ (15)	P.A. (16)
R151	2/27/90	1.5	239	2.1x1.4	18	-0.1'7	-0.13	71.8	42.7	17.5	Gal?	21.10	2'7	4.7x2.4	128
R160	2/24/90	1.6	178	1.7X1.7	...	0.07	-0.12	86.3	29.9	<14.5	QSO	18.02	50	4.4x3.8	0
R171	1/19/91	1.5	...	9.8x6.0	14	0.37	-1.92	-66.2	-45.1	18.6	Gal	22.90	6	1.9X1,3	116
R174	1/19/91	1.5	225	1.4X1.4	...	0.03	1.24	-17.3	-9.0	17.6	Gal	20.41	36	4.4X3.1	108
R182A	1/19/91	1.4	221	1.4X1.4	...	0.94	0.17	2.2	-15.6	<17.0	Gal	23.03	6	1.6x1.2	113
R182B	1/19/91	1.4	221	1.4X1.4	...	0.94	0.17	5.3	-15.7	17.3	Gal	21.25	16	2.8x2.1	80
R191	2/27/90	1.5	267	1.9X1.9	...	0.77	-1.04	-34.4	1.1	19.4	Gal	18.12	204	9.4x7.5	46
R194	2/27/90	1.7	242	1.5x1.5	...	0.47	-0.34	44.5	19.9	18.2	Gal	21.73	27	6.4x3.7	70
R195	1/19/91	1.8	244	2.2x2.2	...	-0.54	2.05	-'78.8	-73.2	16.4	Gal	19.58	79	6.0x4.7	130
R201	2/27/90	1.4	211	1.5X1.5	...	0.10	1.38	52.2	17.7	<16.0	Gal	17.06	378	14.0x9.0	7
R203A	1/18/91	2.8	226	2.2x2.2	...	1.34	-0.87	67.6	-85.4	Brgt	Gal	17.99	219	9.7x7.7	12
R203B	1/18/91	2.8	226	2.2x2.2	...	...	...	...	...	...	...	...	...	...	...
R212	1/18/91	2.3	245	3.3x2.5	81	-1.44	-0.84	-2.5	10.6	<15.8	Gai	18.45	114	6.8x5.4	5i
R216	2/27/90	1.3	190	1.8X1.8	...	0.31	0.14	-85.2	109.3	<15.0	QSO	18.09	54	4.6x3.9	124
R226	1/18/91	3.0	111	2.1X2.1	...	-1.75	-0.17	1.3	-22.1	17.3	Gal	22.91	12	3.3x1.9	43
R230[f]	4/27/90	1.3	215	15.0x15.0	...	4.60	-9.00	...	...	..	Gal	16.49	198	9.1X7.3	110
						6.70	+3.65	2.1	12.7	...	*QSO?*	18.11	39	4.8x2.9	20
R231	1/19/91	1.8	235	2.2x2.2	...	0.13	-0.47	-20.5	-19.8	17.7	Gal	18.72	108	7.4x4.9	132
R233	4/28/90	2.5	...	1.5X1.5	...	-0.37	0.44	..	...		Gal	16.97	332	13.8x8.3	110
R239[a]	~-/~[a]/~-	2.9	167	2.0x2.0	...	-0.74	2.49	67.2	58.2	15.4	Gal	17.45	264	9.7x9.0	9
R247[a]	4/28/90	2.3	186	1.4X1.4	...	-5.21	4.33	25.1	-35.8	16.9	Gal	16.98	420	12.5x11. 0	37
R249	1/18/91	2.2	231	2.5x2.1	66	-0.67	0.97	-14.5	48.6	<16.0	Gal	23.67	5	1.8x1.3	57
R251	1/18/91	2.1	172	1.6X1.6	...	...	...	...	...	...	...	...	...	...	...
R252	1/18/91	1.9	186	2.1x1.3	127	-0.91	-0.97	61.6	24.7	18.3	Gal	18.16	215	9.4X7.3	82
R276	1/18/91	2.3	151	4.7x3.2	158	-1.27	0.92	-33.6	67.4	16.6	Gal	21.38	35	4.3X3.3	134
						2.28	-1.98	-29.7	64.6	16.6	Gal	23.30	7	2.5x1.5	2
R277	1/18/91	2.4	136	1.5X1.5	...	...	...	...	...	...	...	...	...	...	...
R281	4/28/90	1.6	249	1 .4X1.4	...	0.17	-0.27	...	...	...	Gal	16.87	274	10.6X8.8	99
R297	1/19/91	1.4	229	2.5x2.5	...	1.61	1.78	-11.9	76.0	<13.5	Gal	22.76	9	3.5X1.5	20
R303	1/18/91	2.0	248	1.9X1.9	...	-0.42	0.66	-45.3	11.8	<15.0	QSO?	17.22	173	9.4x6.4	157

TABLE *3—Continued*

	Observations			Astrometry				Offset Star			Photometry				
Source (1)	Date (2)	Seeing (3)	$N_{opt}^{23.5}$ (4)	a × b (5)	P.A. (6)	δX_r (7)	δY_r (8)	δX_s (9)	δY_s (10)	R_s (11)	Type (12)	R (13)	A_{iso} (14)	$2a \times 2b$ (15)	P.A. (16)
R304	1/18/91	1.9	222	1.9X1.5	122	0.03	0.03	31.3	-63.8	15.1	Gal	18.76	122	7.1X5.7	105
R305	1/18/91	1.8	221	4.4x3.2	70	-2.27	2.30	-.52.4	16.4	17.1	Gal	19.05	82	7.5x4.0	98
R307A	1/18/91	1.6	246	3.1X3.1	. . .	-0.57	-0.03	-117.0	106.8	17.0	Gal	22.'75	11	2.1x1.7	30
R307B	1/18/91	1.6	246	3.5X3.1	136	-1.38	-0.24	-99.9	99.5	17.0	Gal	22.68	9	2.1x1.5	134
R319	1/19/91	1.9	106	3.1X3.1	. . .	-0.40	-1.14	38.0	69.0	17.4	QSO	20.98	18	2.7x2.3	69
R337	1/19/91	1.5	*246*	*2.1X1.4*	**10**	**0.81**	-0.74	-28.3	-49.9	<15.5	Gal	20.56	33	3.8x3.1	0

[a]The optical counterpart lies slightly outside the error ellipse. It was accepted for either it is optically bright with a radius *much* larger than its apparent angular distance to the radio source position or it is well between the two radio lobes.

[b]The integration time for the R-band CCD image is only 300 seconds.

[c]R082 is in a very dense galaxy cluster at z = 0.407 (Dressier & Gunn 1992). The magnitude may be slightly contaminated.

[d]There is an optical object near one of the radio components.

[e]This optical identification is slightly outside the error ellipse. It was accepted because the central position of this weak radio source is somewhat uncertain.

[f]Radio map at 4.86GHz is not available. The offsets [i.e., cols. (7) and (8)] for the second probable optical counterpart are with respect to the optics! position of the first one.

TABLE 4

ANALYSIS OF CLUSTERING AROUND THE DS RADIO SOURCES

Sample (1)	Sou rccs (2)	R (mag) (3)	$S_{1.4}$ (mJy) (4)	log $P_{1.4}$ (W Hz^{-1}) (5)	< A N > (6)
DS1	RO35,R1O9,RI 10,R121, R130,R145,R151 ,)1174, R194,R282B,R337	median=20.6 (20.1 to 21.7)	median=62 (37 to 470)	median=26.1 (25.9 to 27.0)	$\sim 0 \pm 2.4$
DS2	R050,R216,R304,R305	mean=18.7 (18.1 to 19.1)	mean = 114 (56 to 169)	mean=25.7 (25.5 to 25.9)	$\lesssim 3 \pm 2.4$
NSal	R082,R191,R195,R231, R252	mean= 18.6 (18.1 to 19,6)	mean :: 10 (1.4 to 28)	mean = 24.6 (23.9 to 25.1)	8 ± 2.9

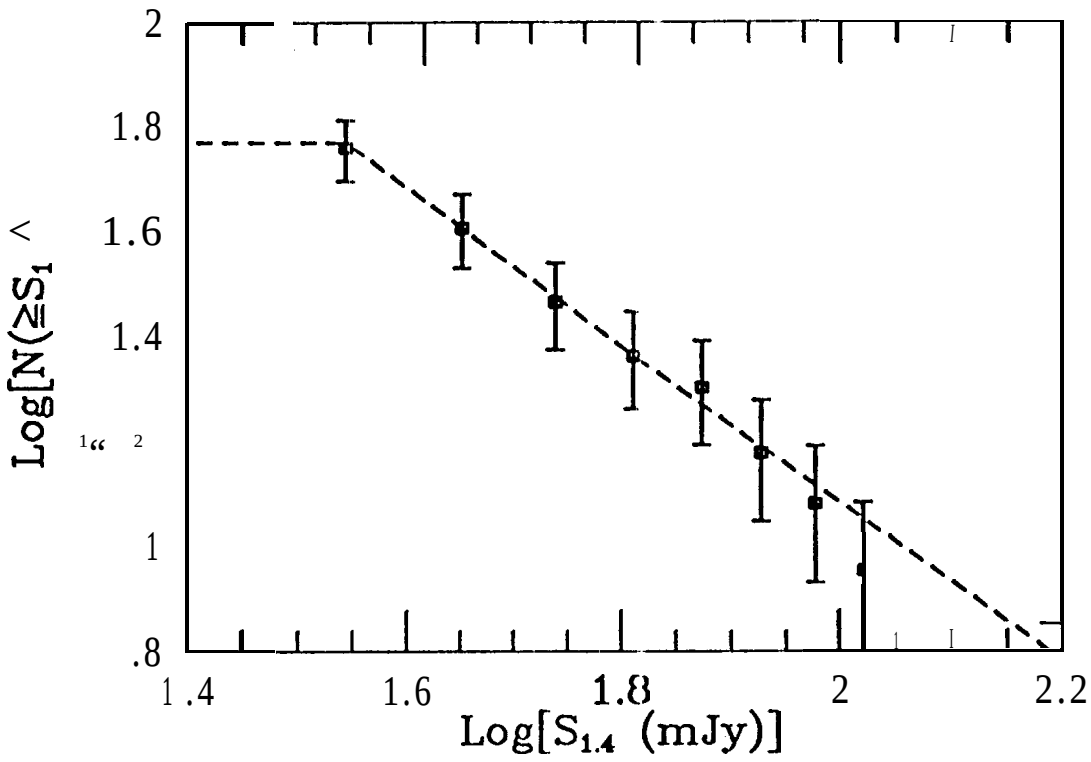

Figure 1

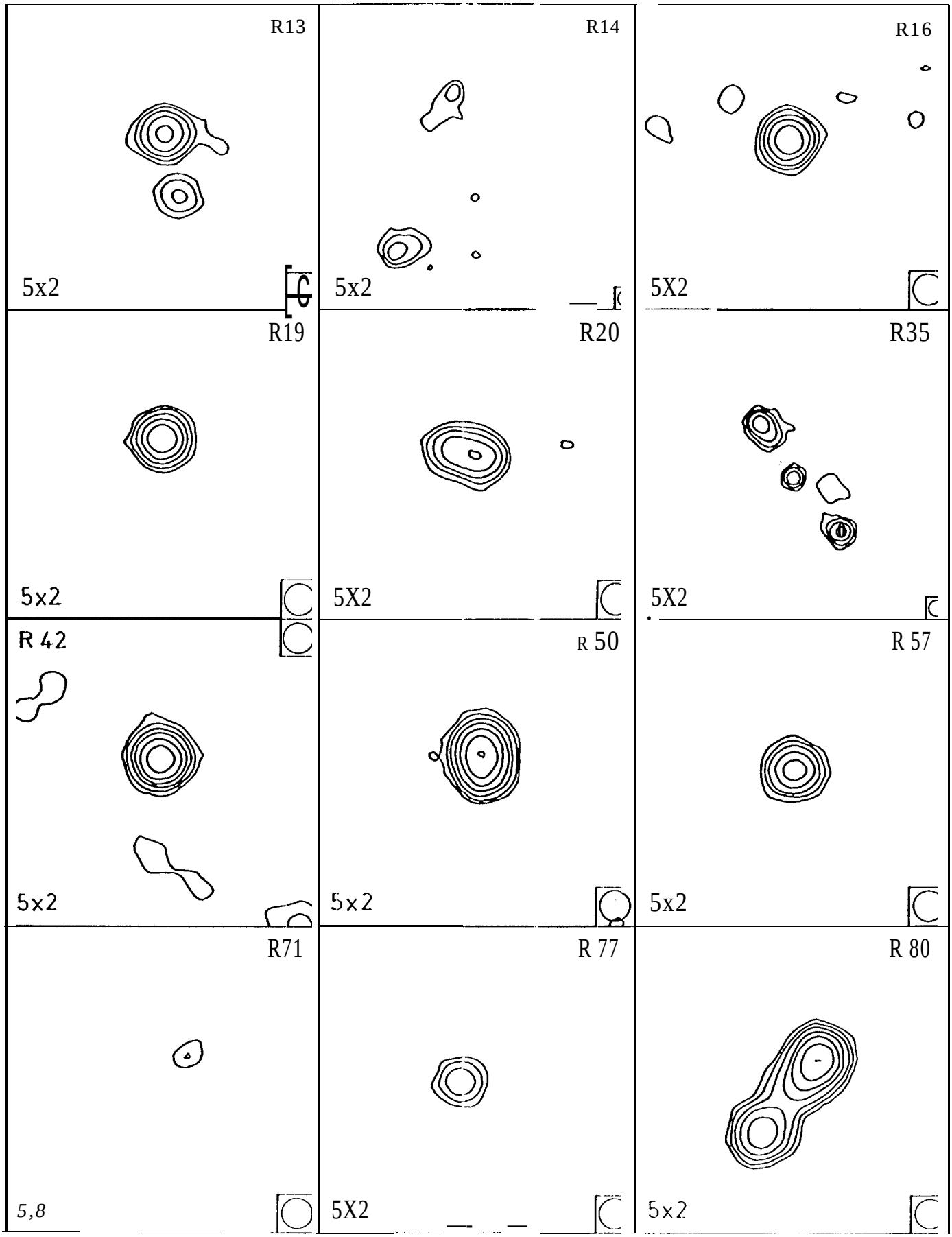
R13
5x2
R14
5x2
R16
5X2
R19
5x2
R20
5X2
R35
5X2
R 42
5x2
R 50
5x2
R 57
5x2
R71
5,8
R 77
5X2
R 80
5x2

Fig. 2a

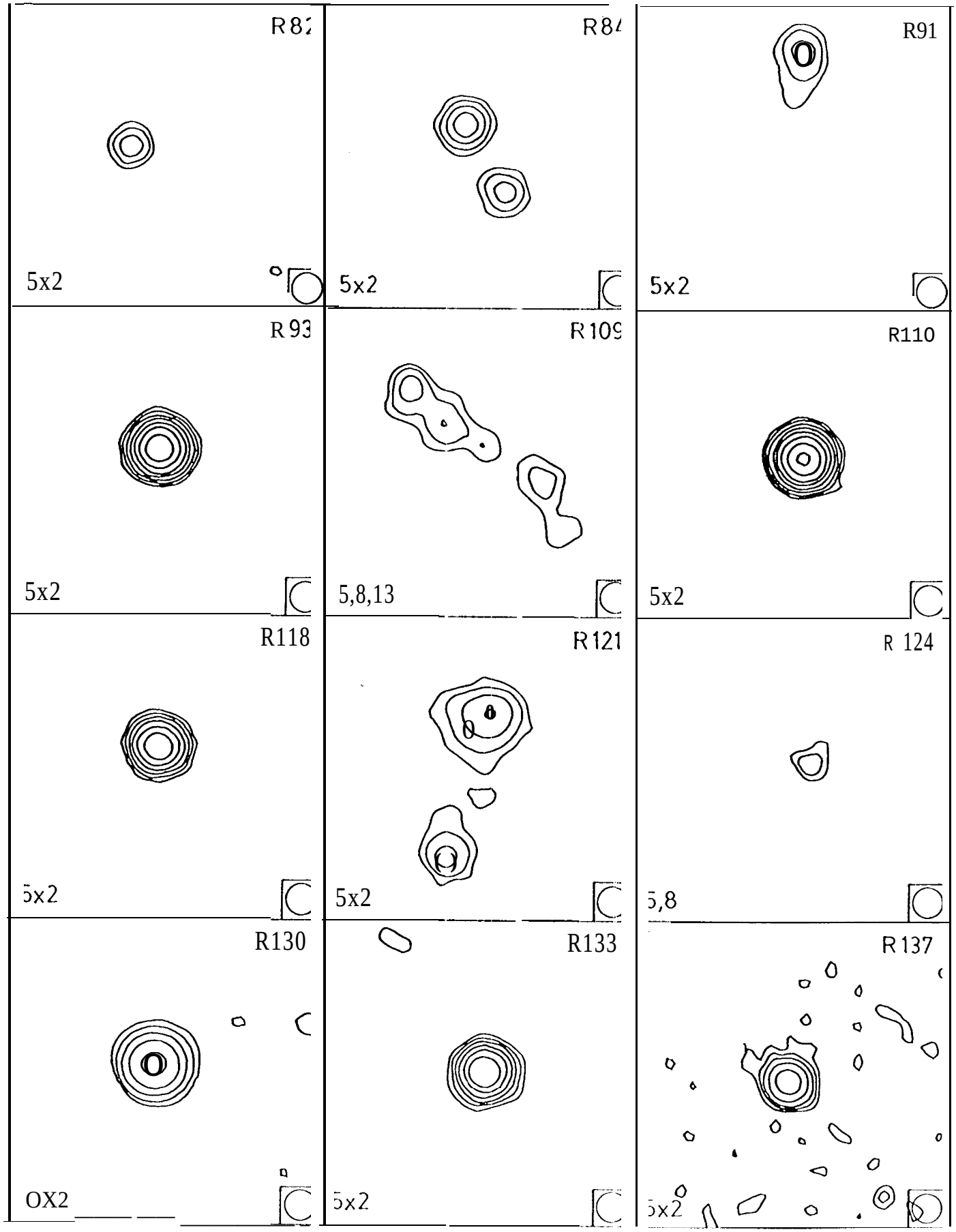
R82
5x2
R84
5x2
R91
5x2
R93
5x2
R109
5,8,13
R110
5x2
R118
5x2
R121
5x2
R 124
5,8
R130
OX2
R133
5x2
R137
5x2

Fig. 26

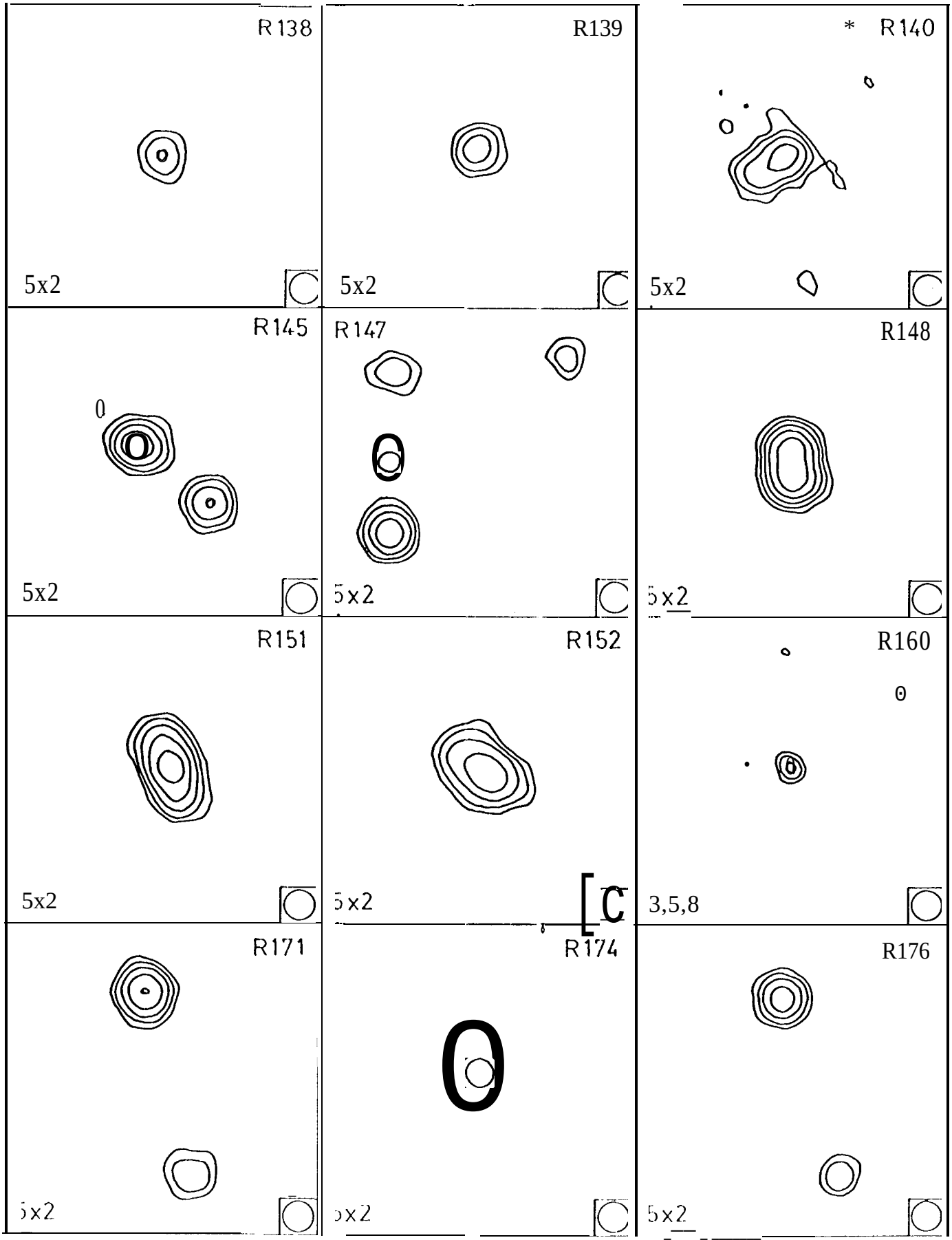
R138
5x2
R139
5x2
* R140
5x2
R145
5x2
R147
5x2
R148
5x2
R151
5x2
R152
5x2
R160
3,5,8
R171
R174
R176
5x2

Fig. 2C

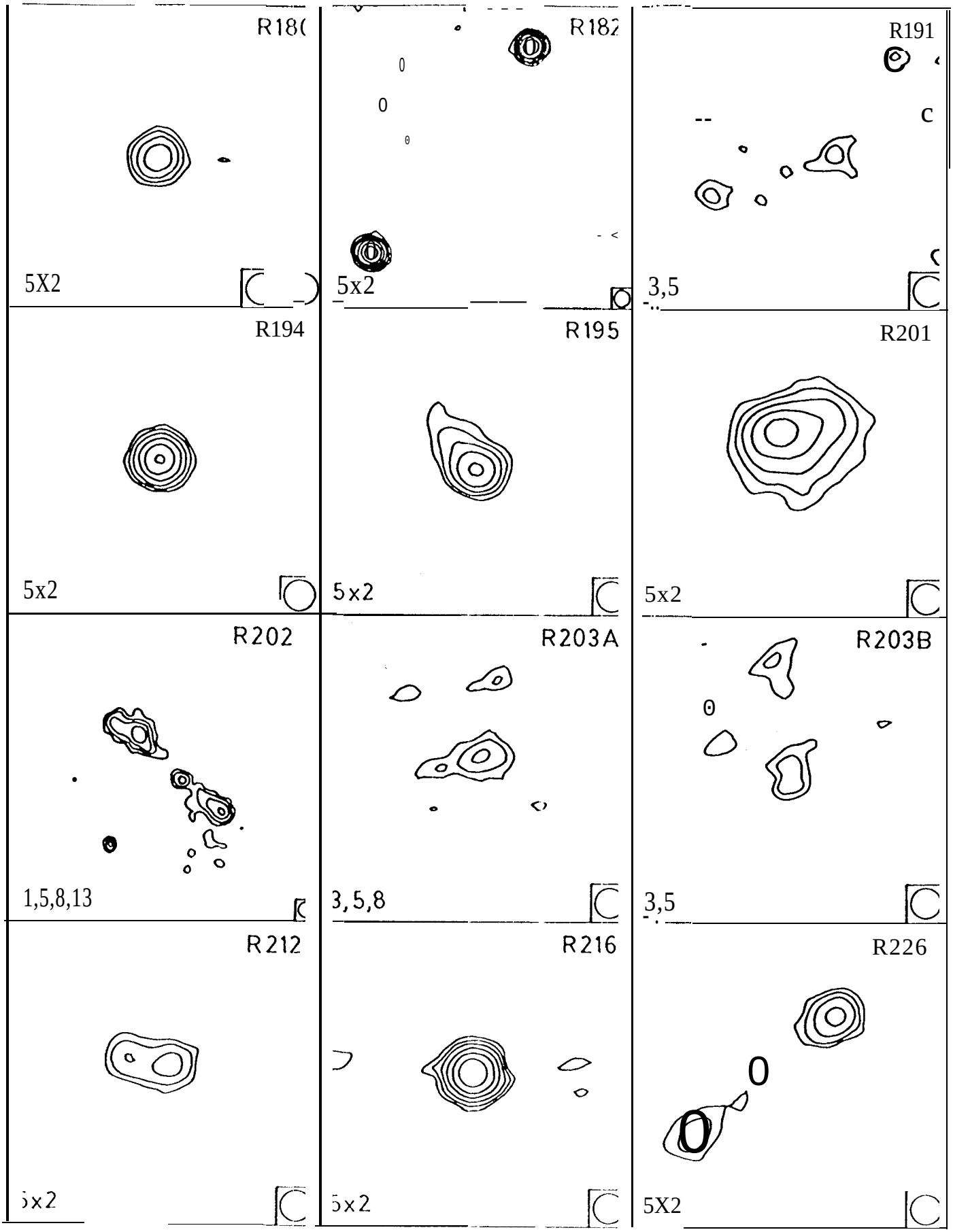
R180
5X2
R182
5x2
R191
3,5
R194
5x2
R195
5x2
R201
5x2
R202
1,5,8,13
R203A
3,5,8
R203B
3,5
R212
5x2
R216
5x2
R226
5X2

Fig. 2d

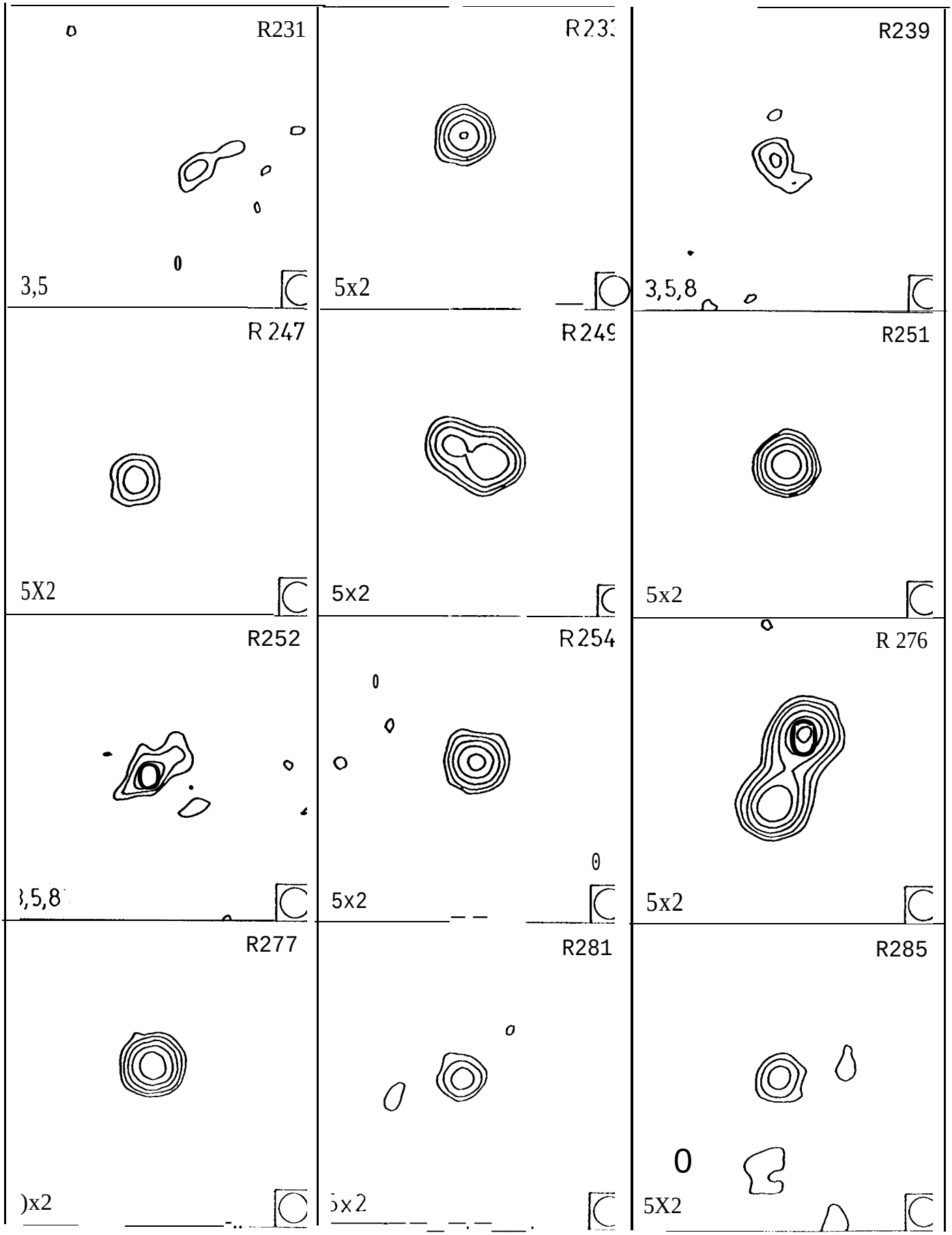
R231
3,5
R23
5x2
R239
3,5,8
R 247
5X2
R249
5x2
R251
5x2
R252
3,5,8
R254
5x2
R 276
5x2
R277
)x2
R281
5x2
R285
5X2

Fig. 2e

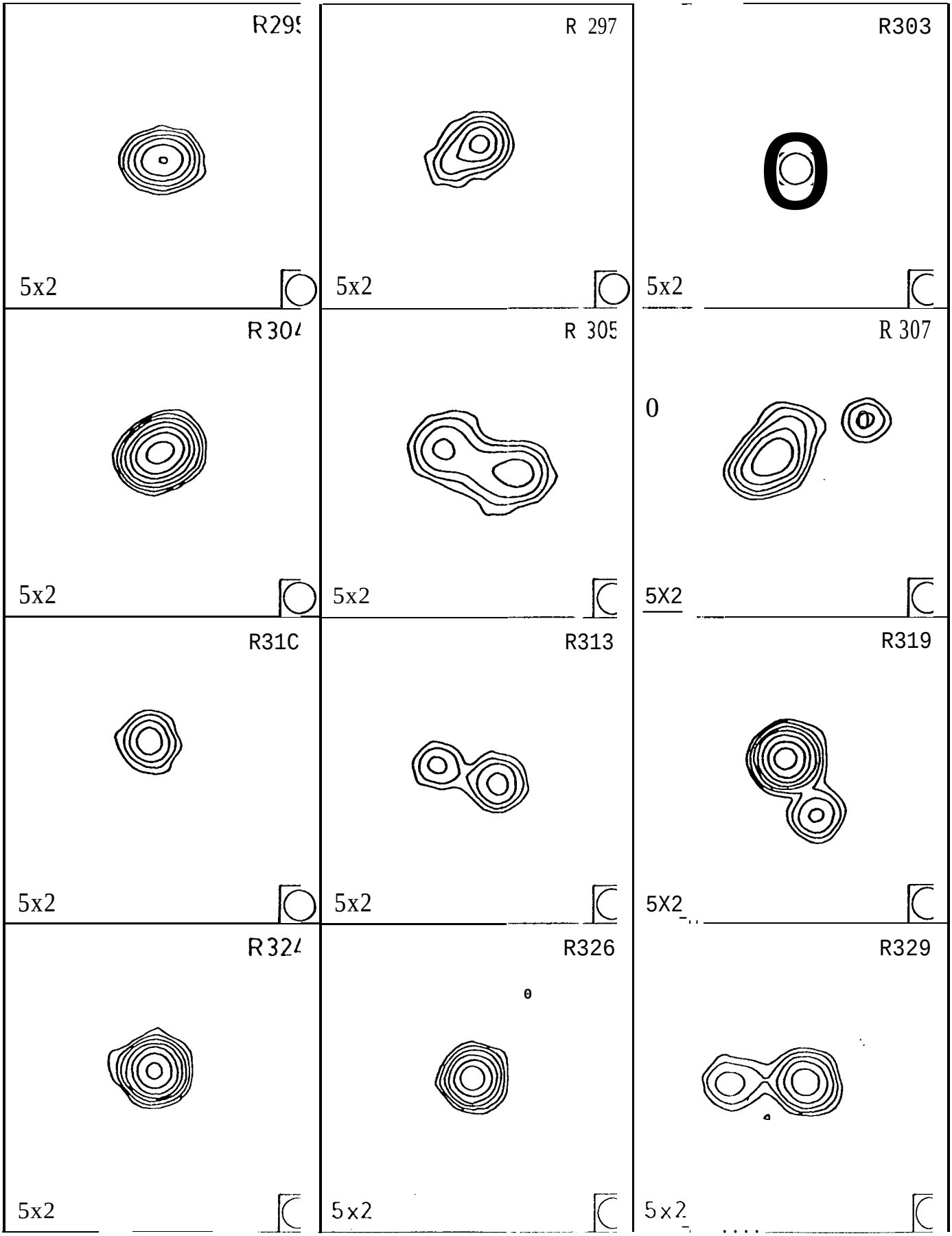
R29
5x2
R 297
5x2
R303
5x2
R 30
5x2
R 305
5x2
R 307
5X2
R31C
5x2
R313
5x2
R319
5X2
R32
5x2
R326
5x2
R329
5x2

Fig. 2f

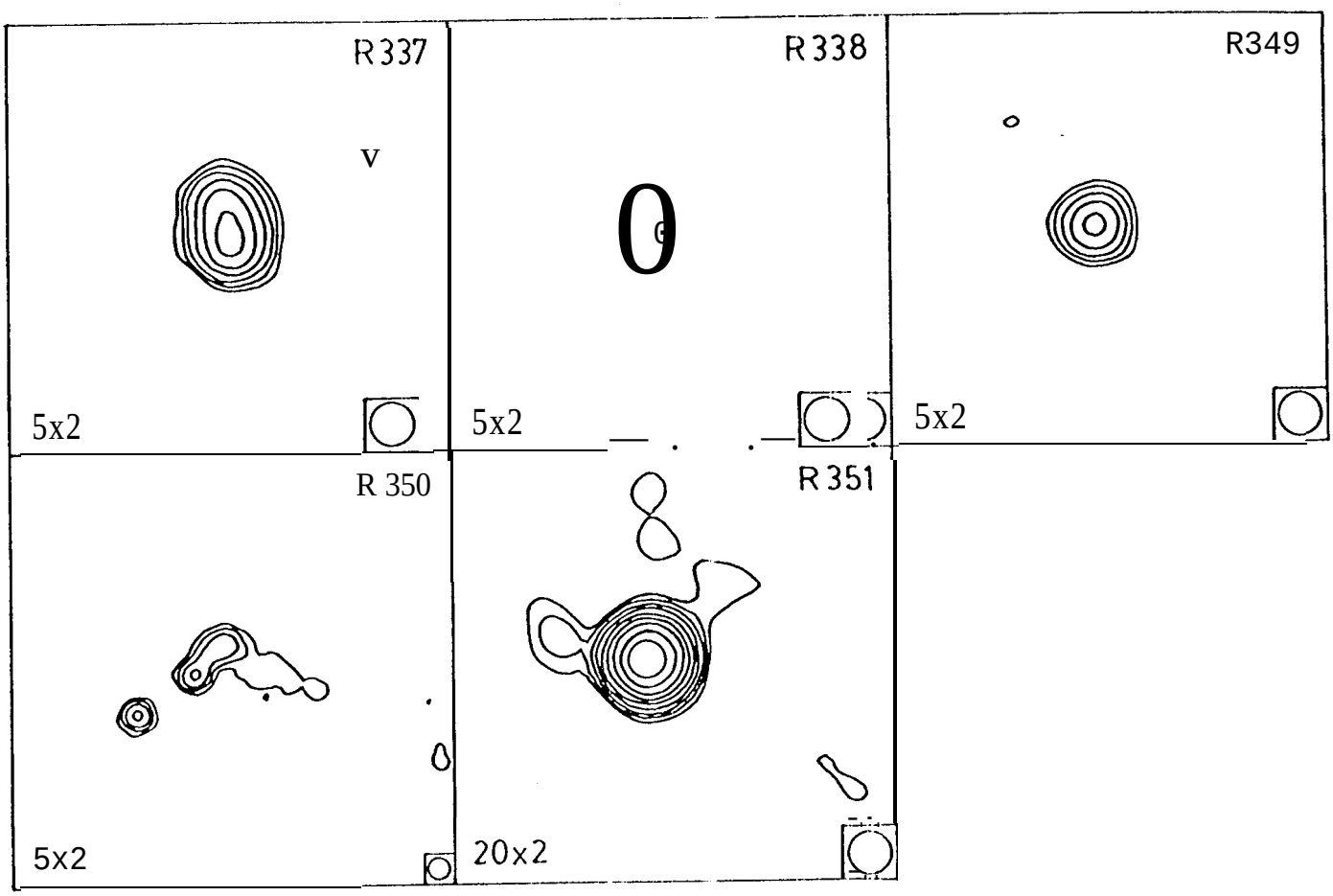

Fig. 29

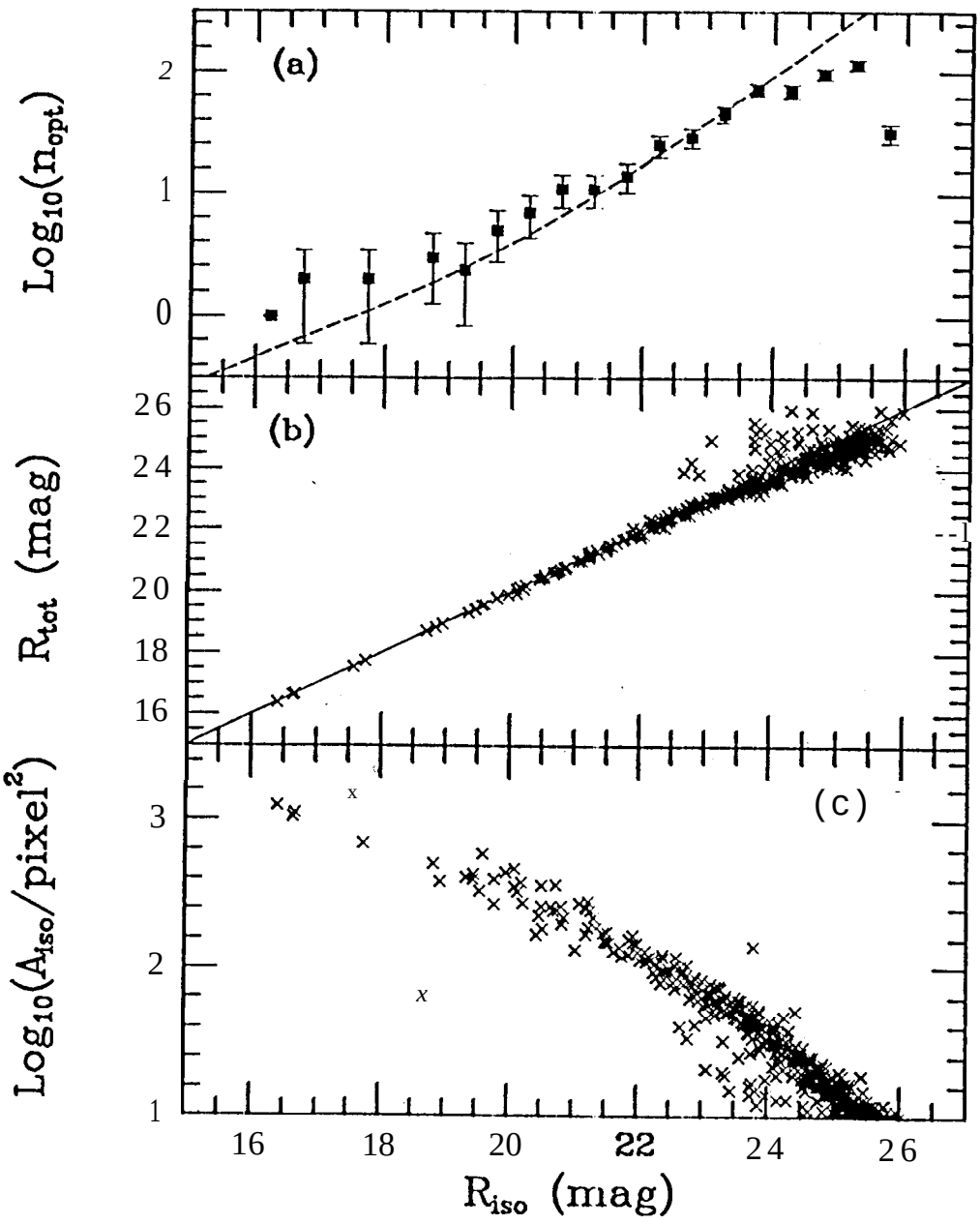
(a)
(b)
(c)
$Log_{10}(n_{opt})$
R_{tot} (mag)
$Log_{10}(A_{iso}/pixel^2)$
R_{iso} (mag)
2
1
0
26
24
22
20
18
16
3
2
1
16
18
20
22
24
26

Figure 3

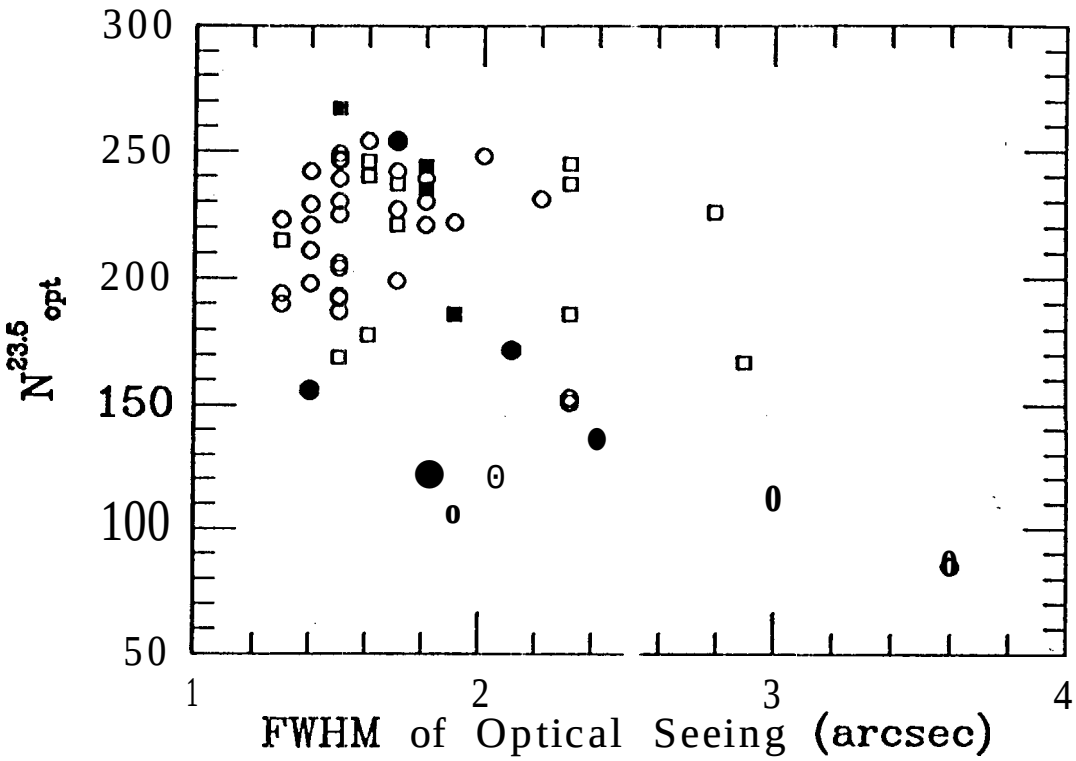
300
250
200
150
100
50
$N^{23.5}_{opt}$
1
2
3
4
FWHM of Optical Seeing (arcsec)

Figure 4

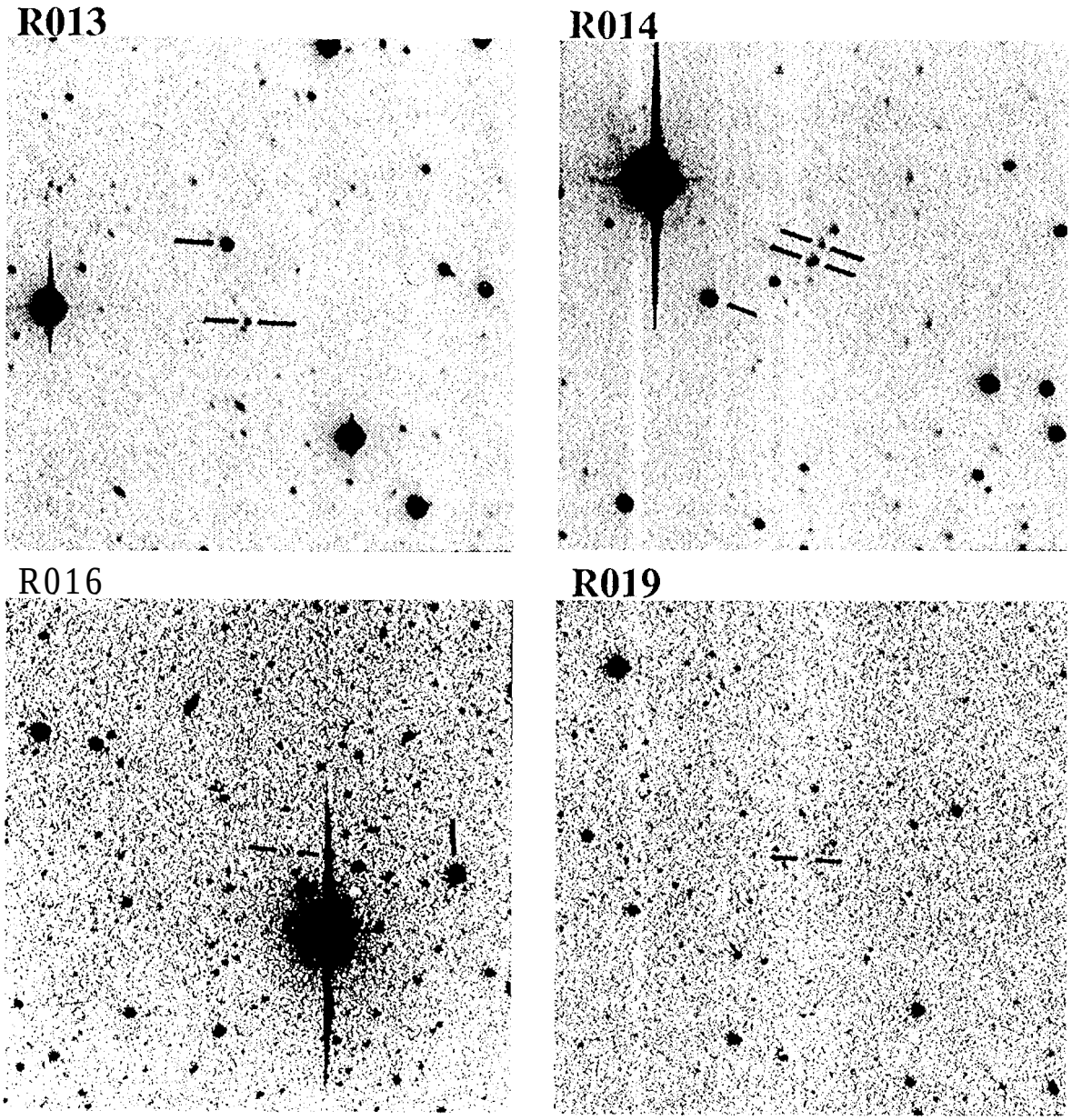

Fig. 5

R020

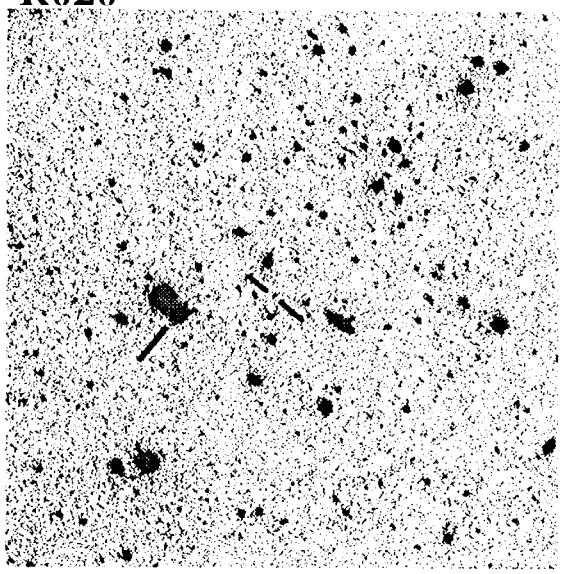

R035

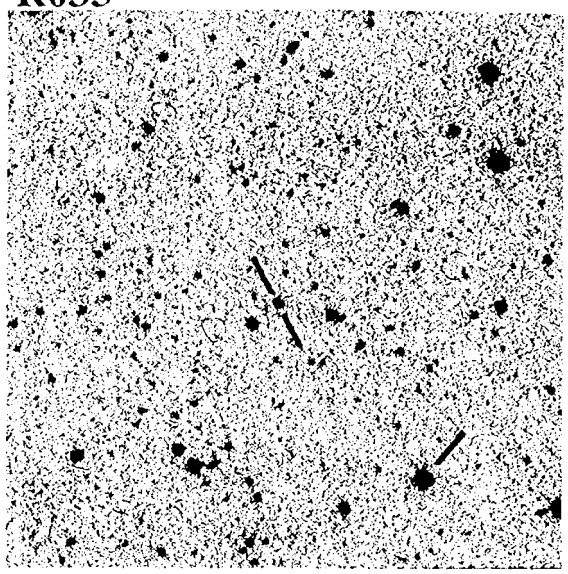

R042

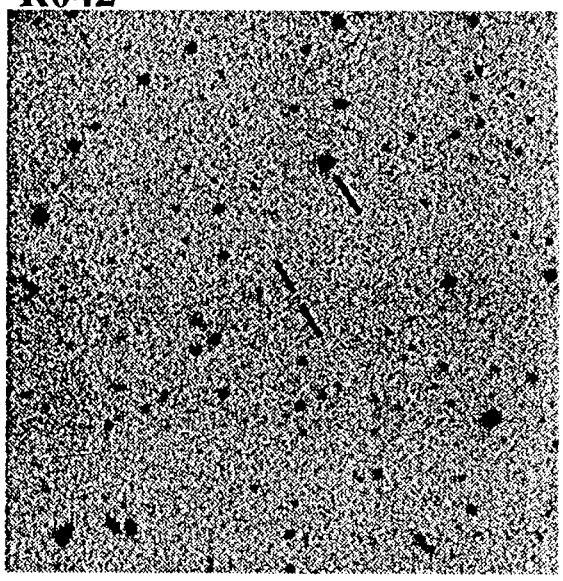

R050

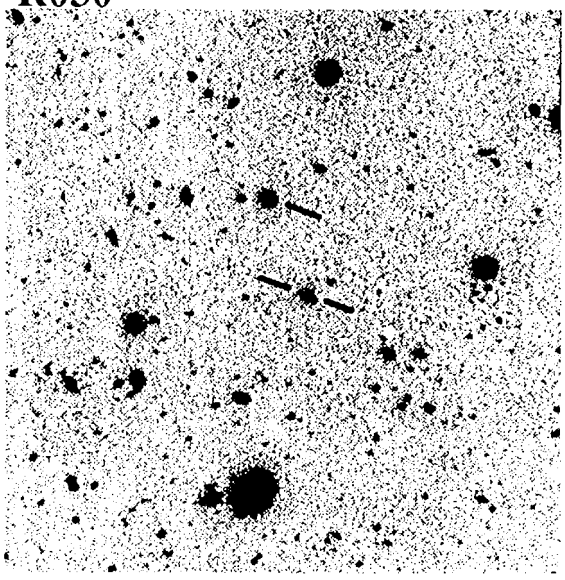

R057

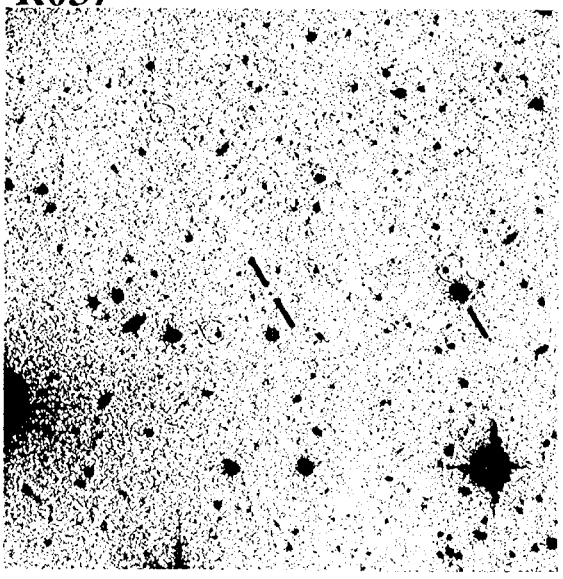

R071

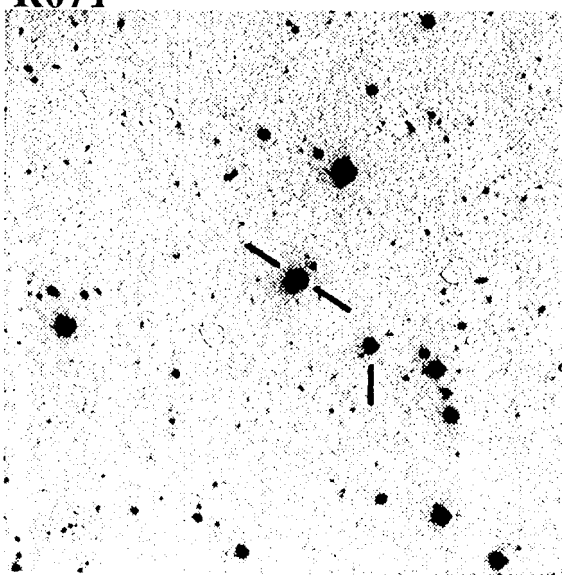

R077

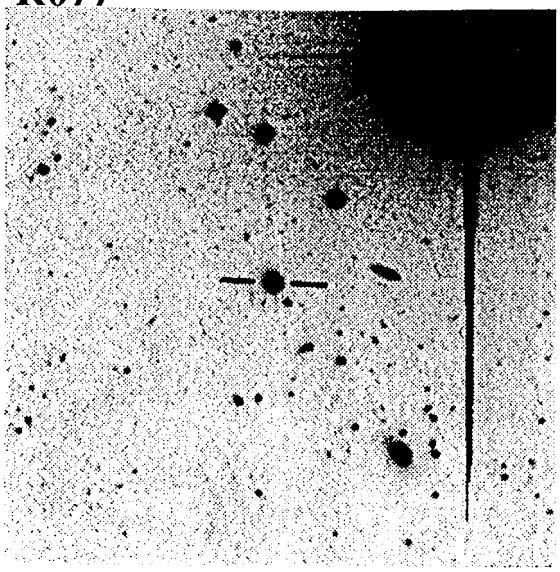

R080

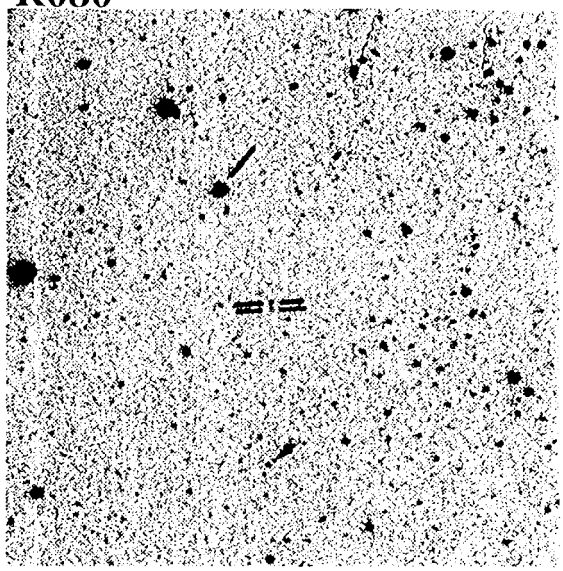

R082

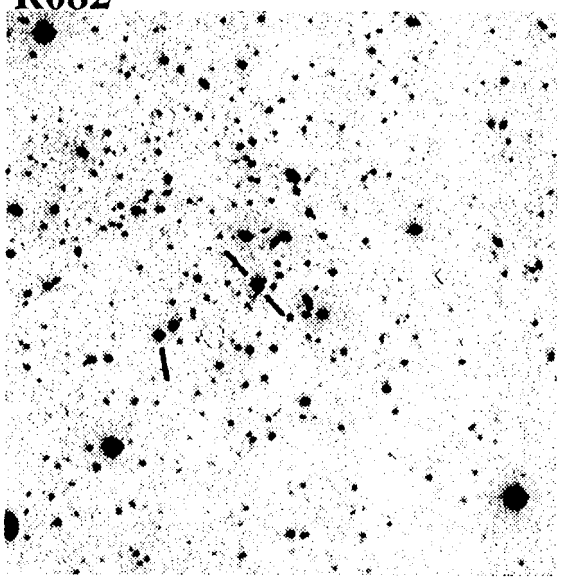

R084

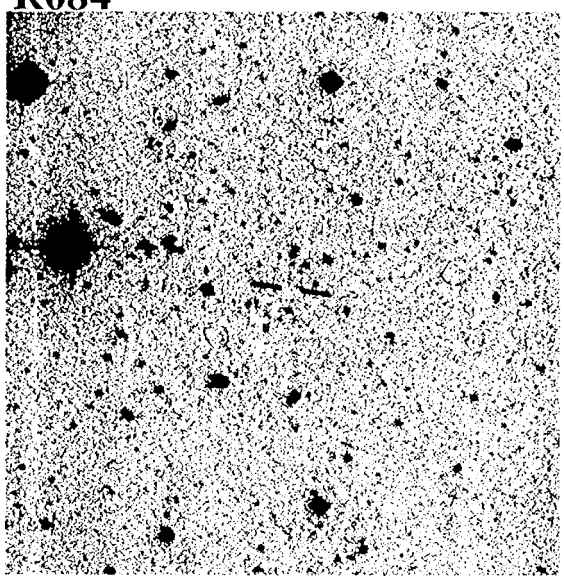

R091

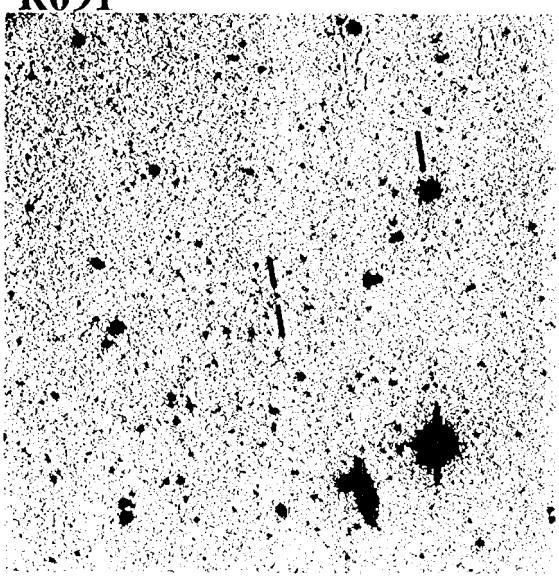

R093

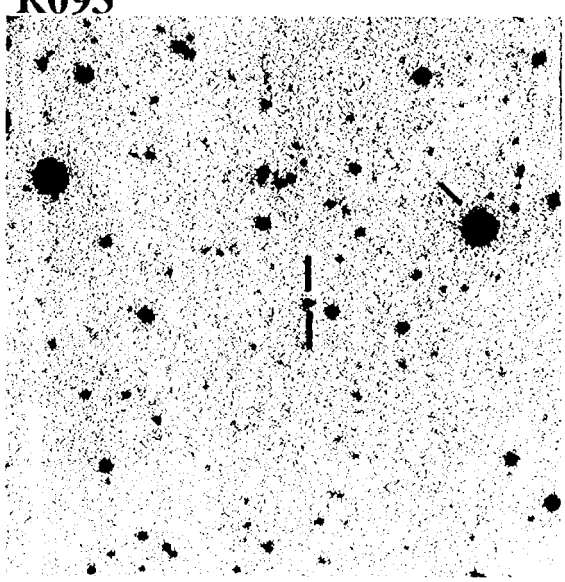

R109

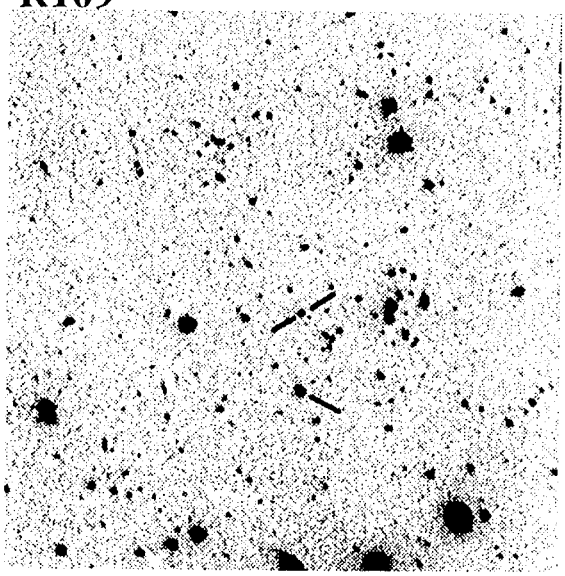

R110

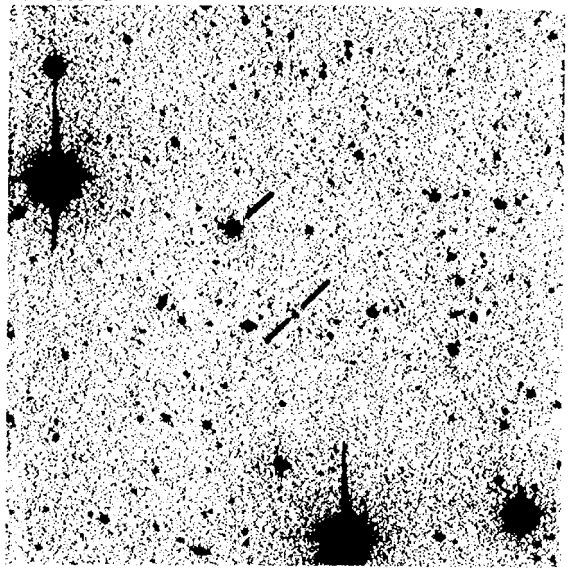

R118

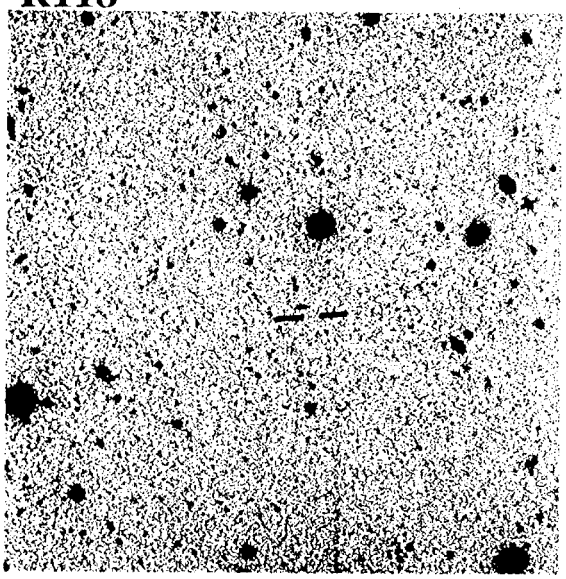

R121

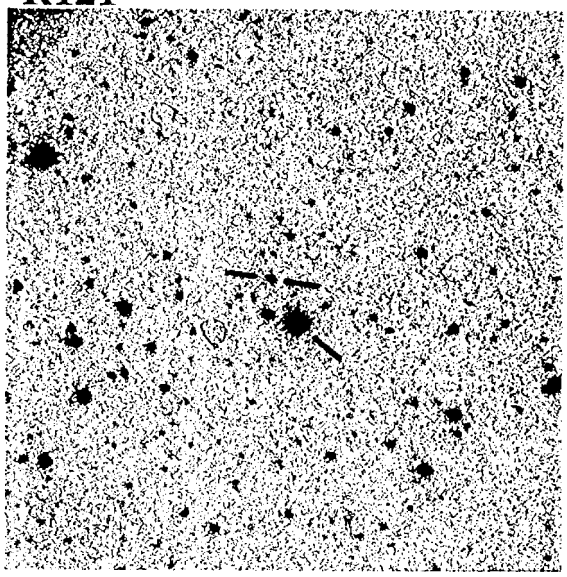

R124

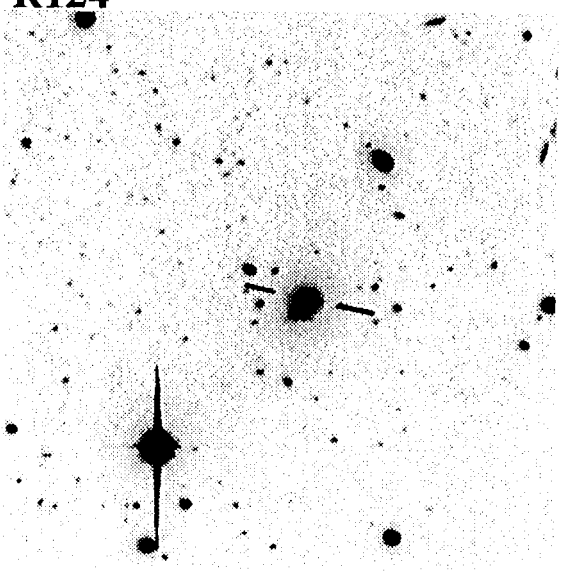

R124(zoom)

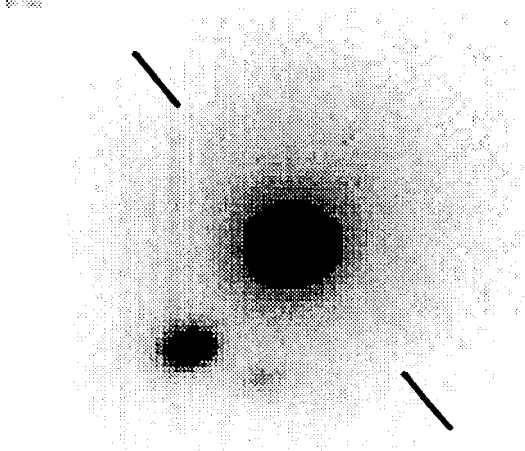

R130

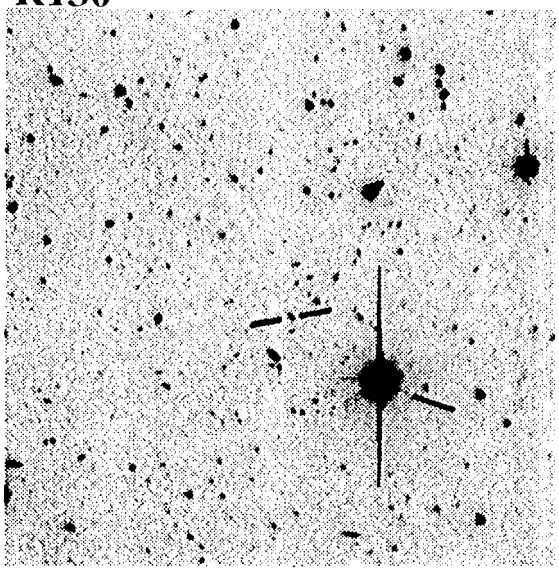

R133

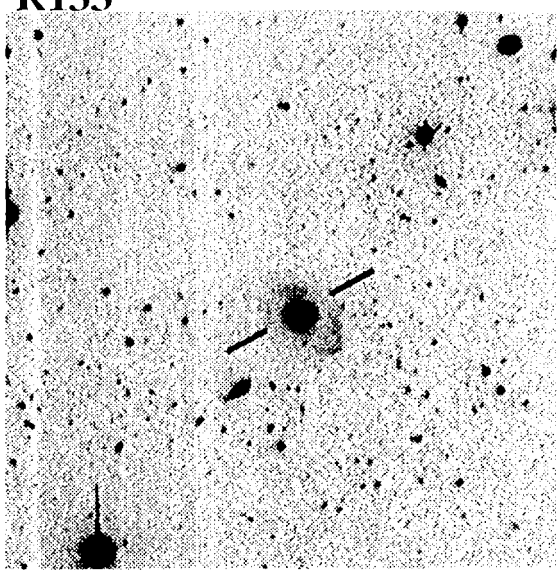

R139

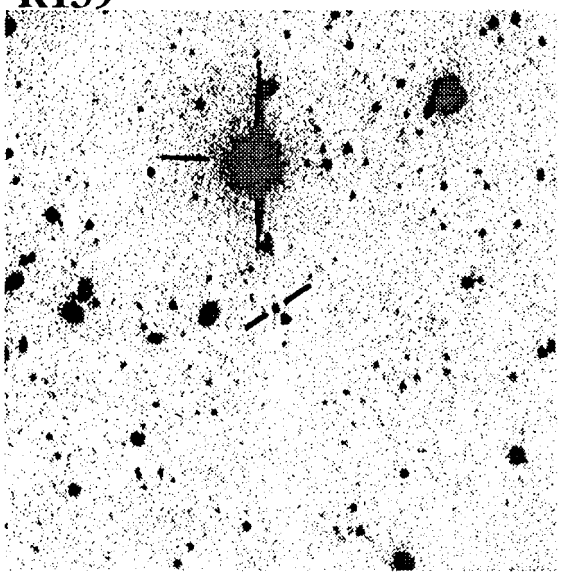

R140

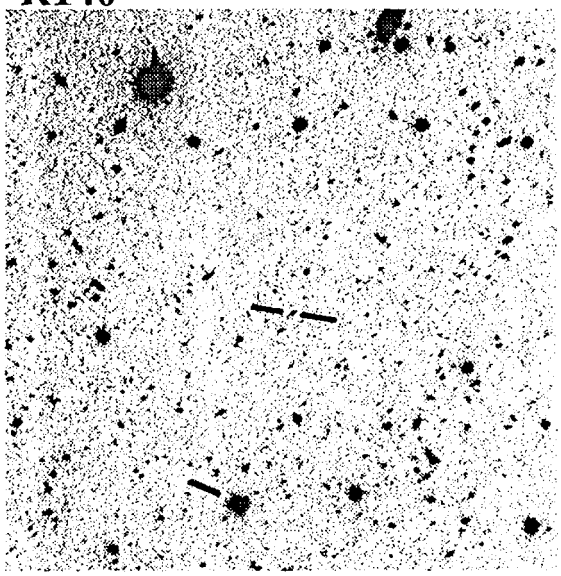

R145

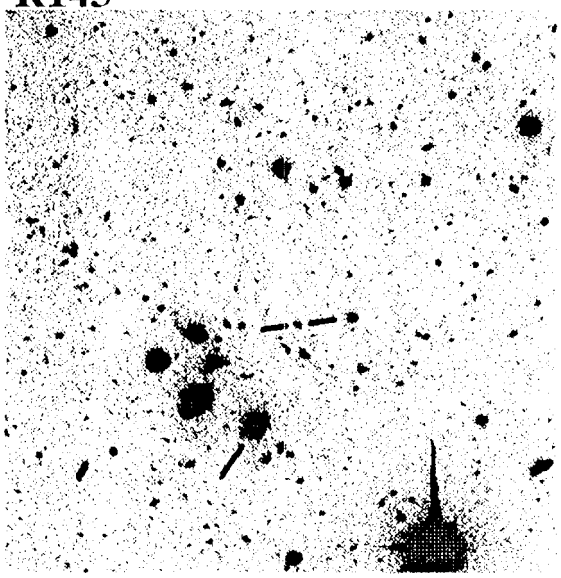

R147

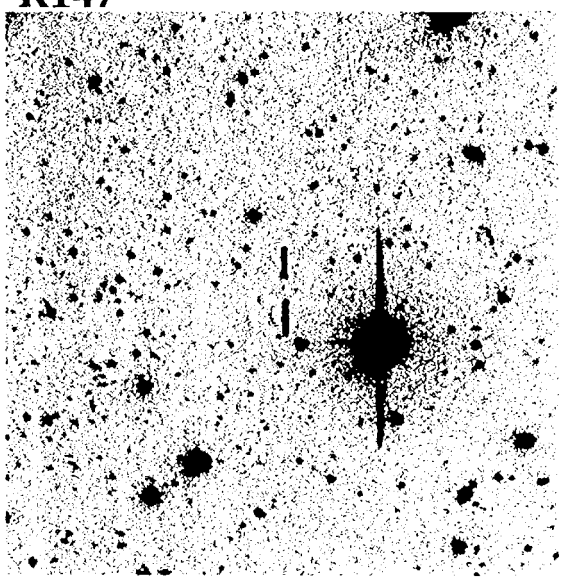

R148

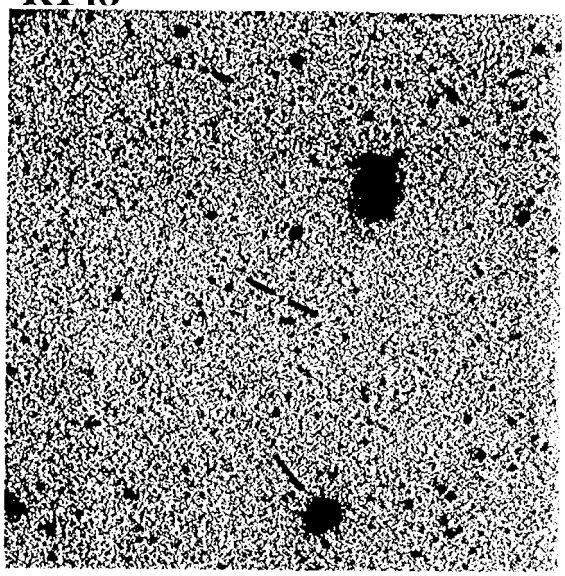

R151

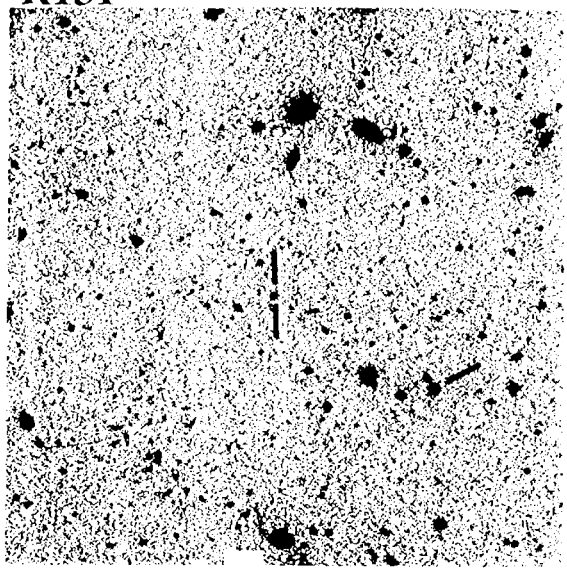

R160

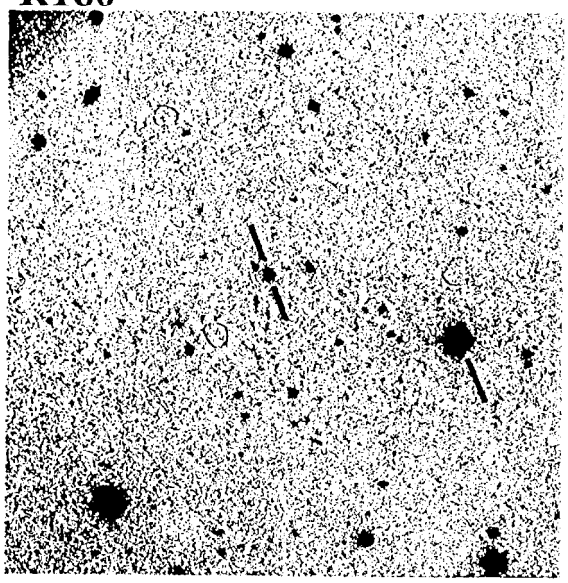

R171

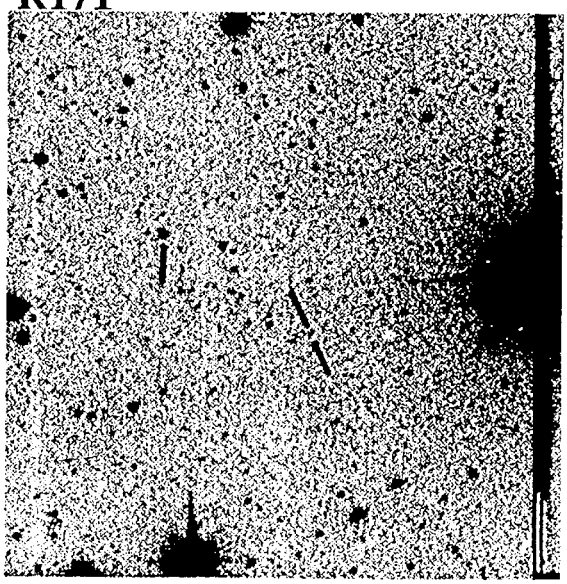

R174

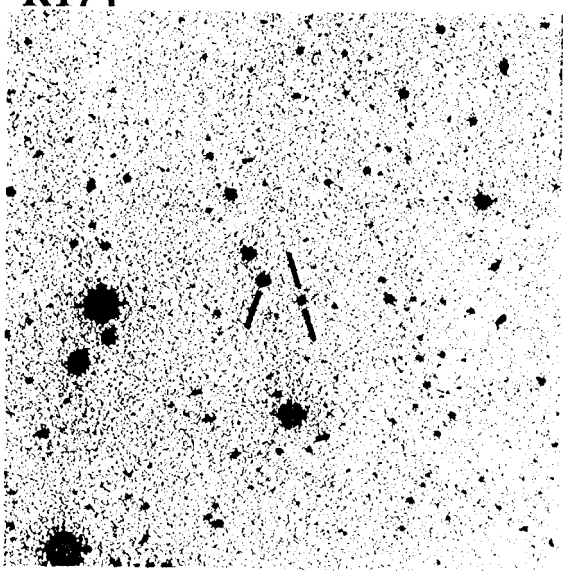

R182(A+B)

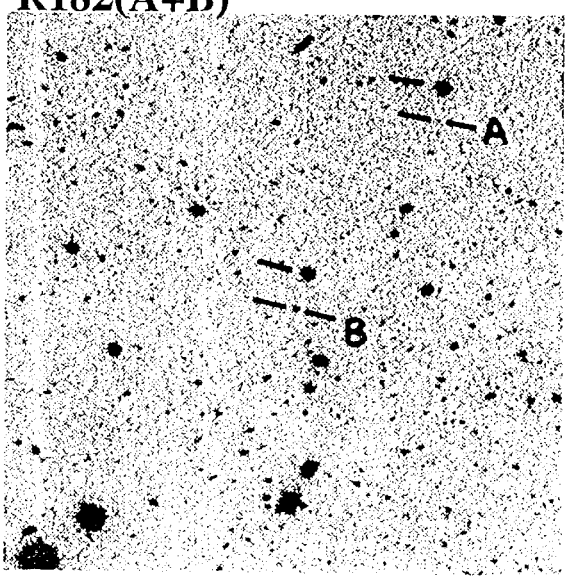

R191

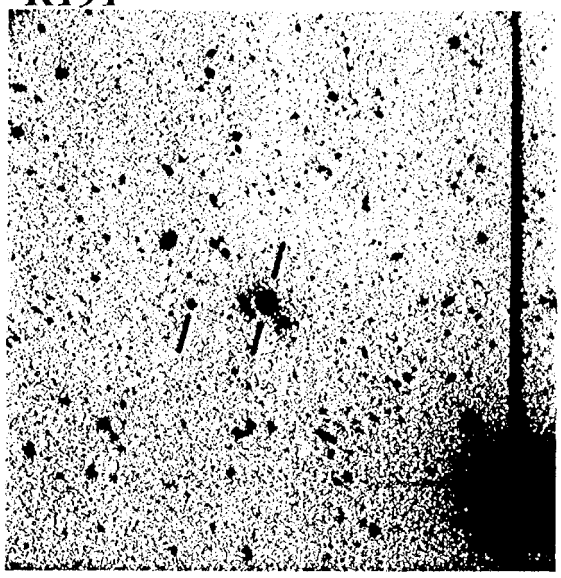

R194

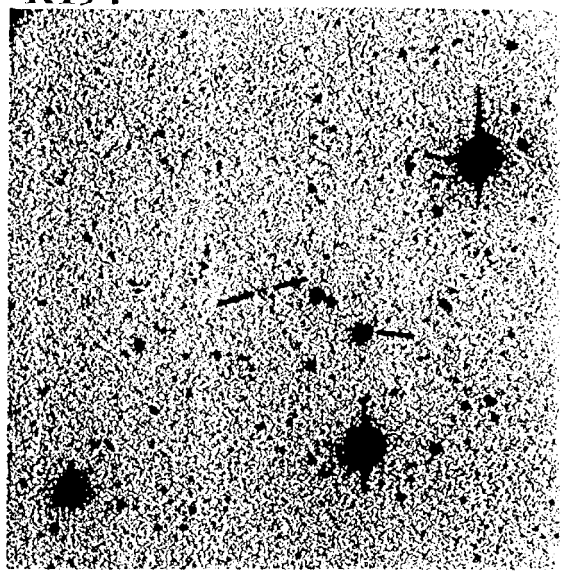

R195

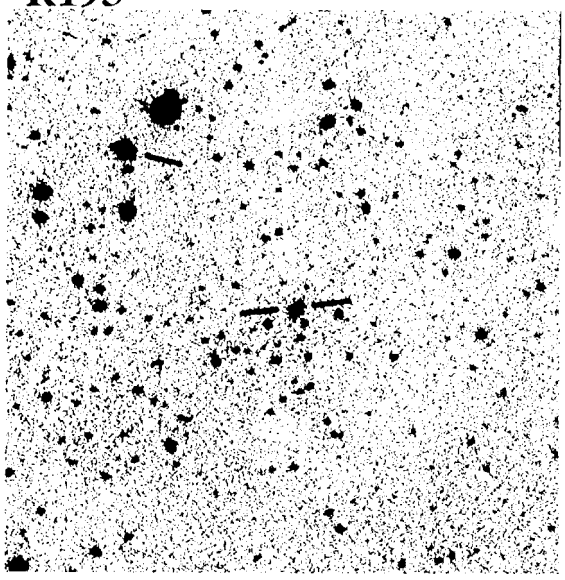

R201

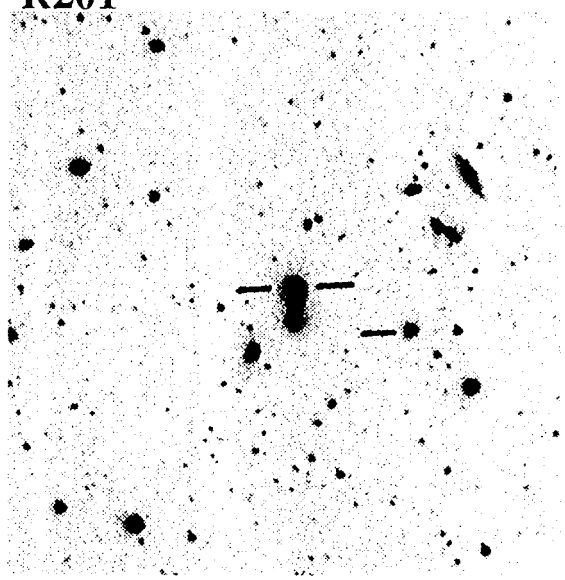

R203(A+B)

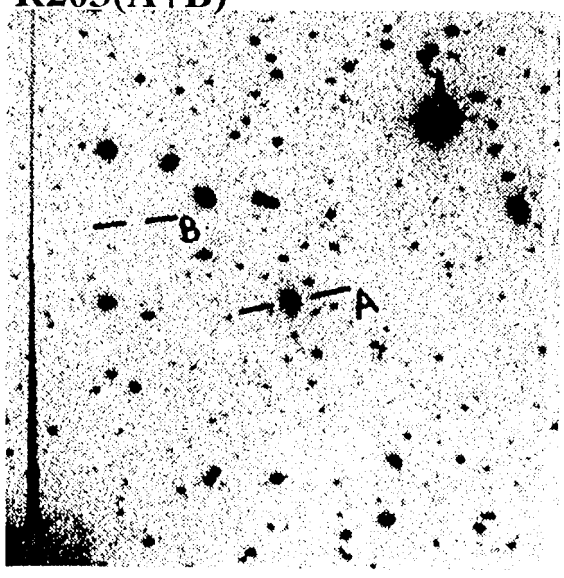

R212

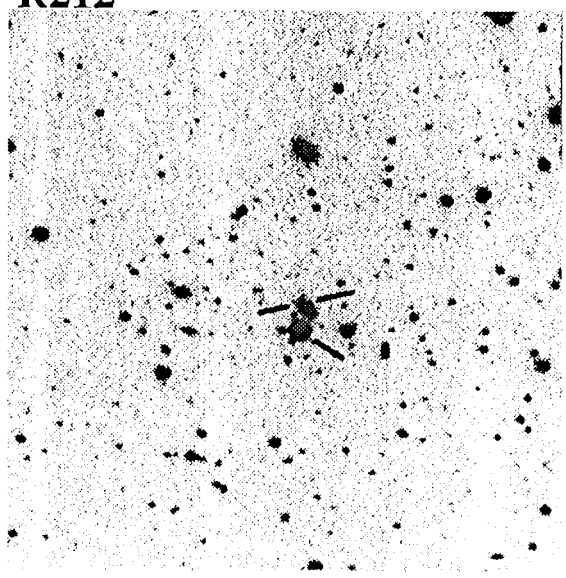

R212(zoom)

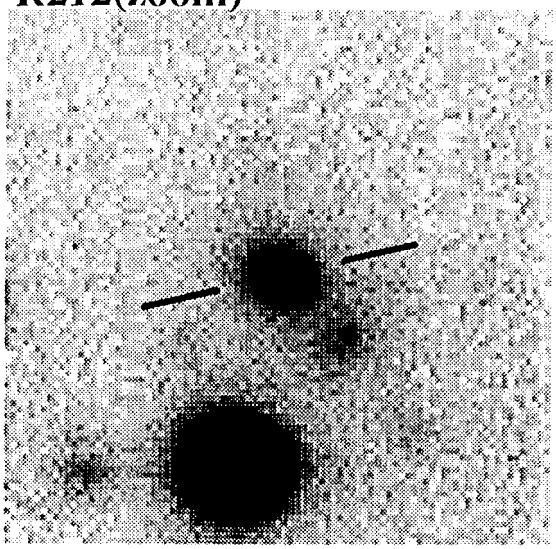

R216

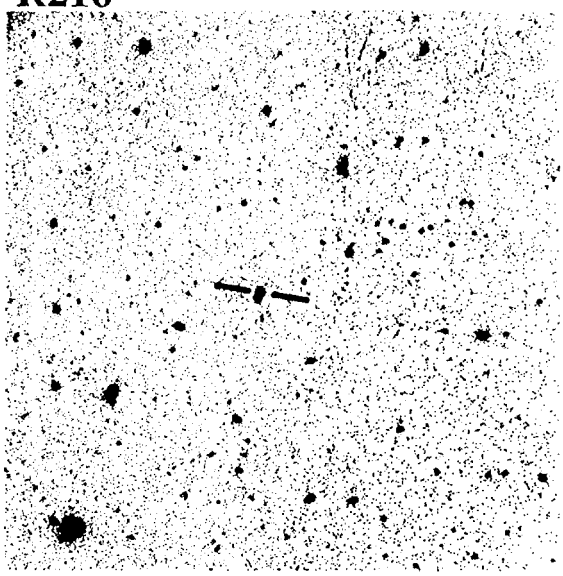

R216(zoom)

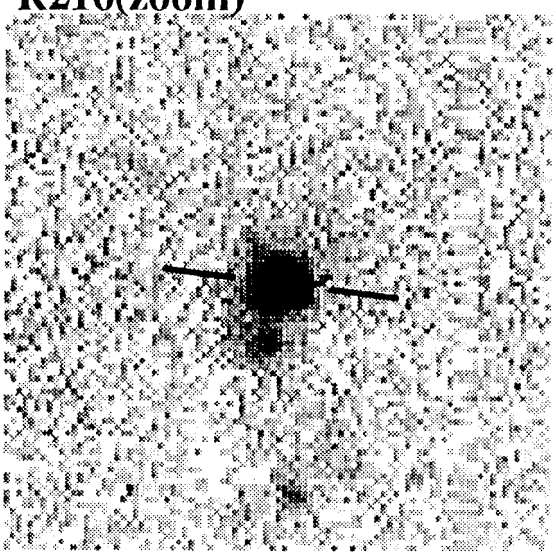

R226

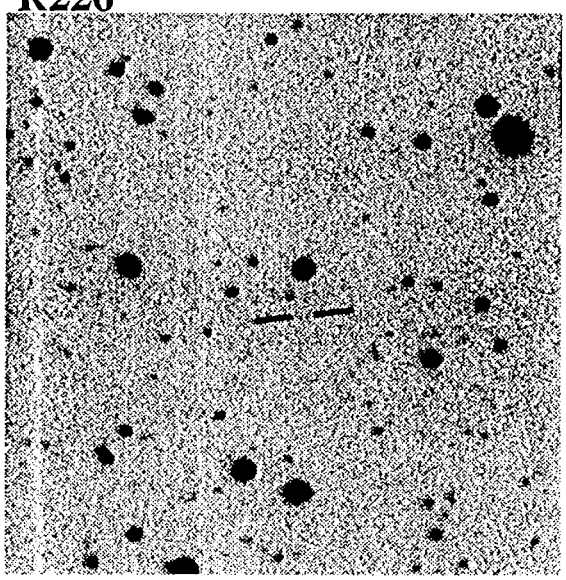

R230

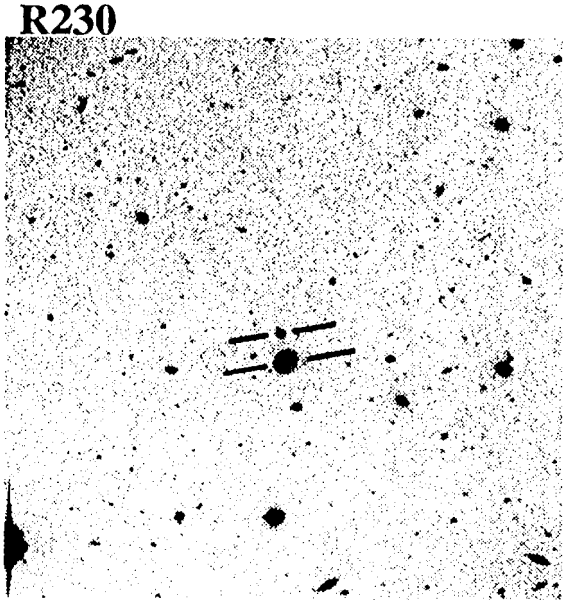

R231

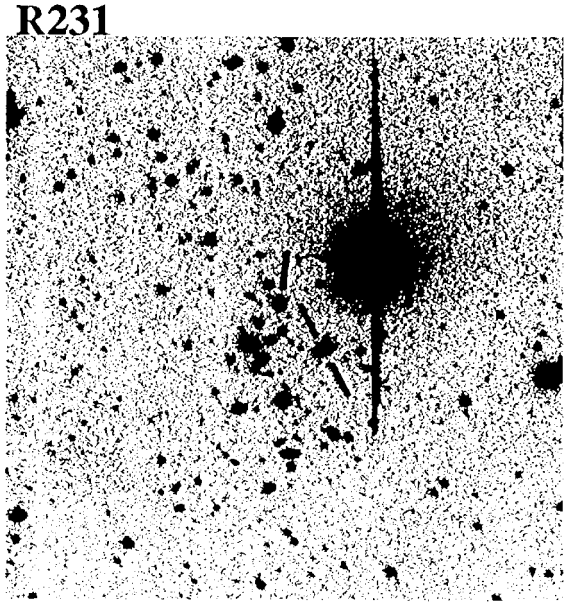

R233

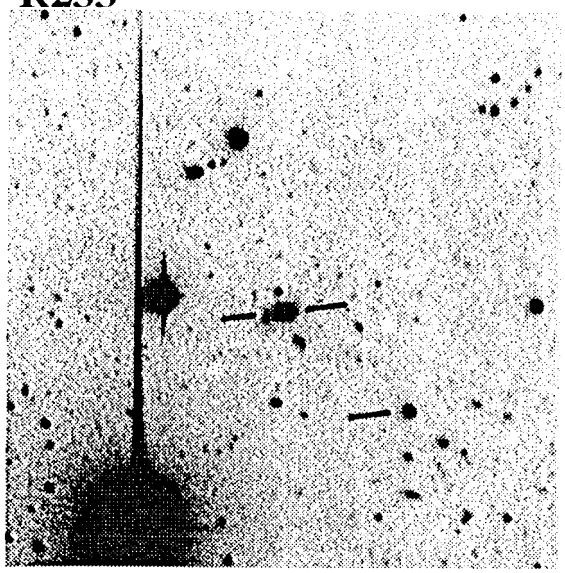

R239

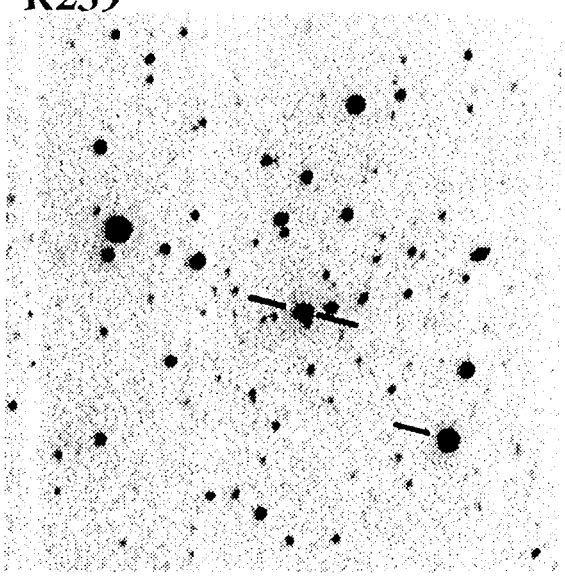

R239(zoom)

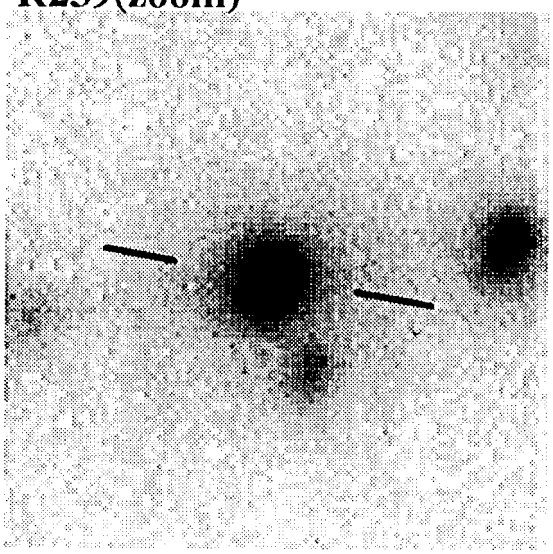

R247

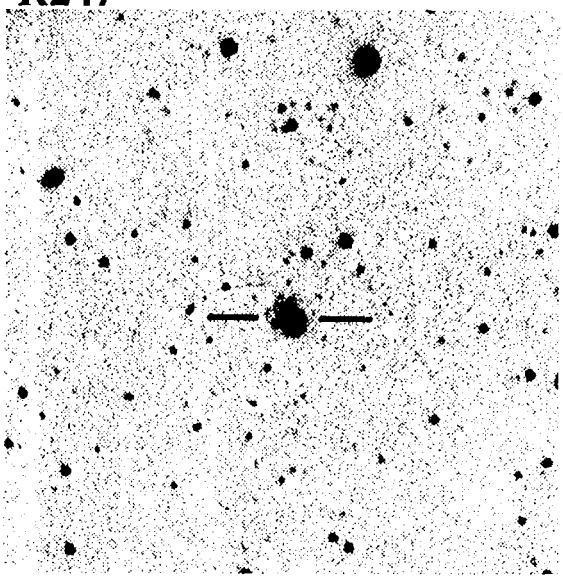

R249

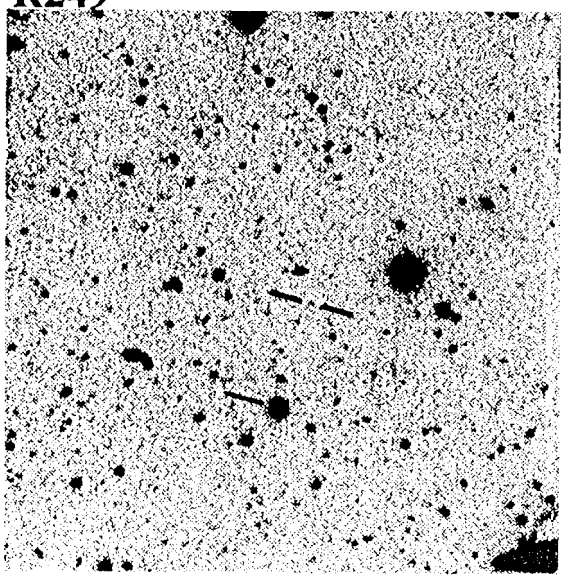

R251

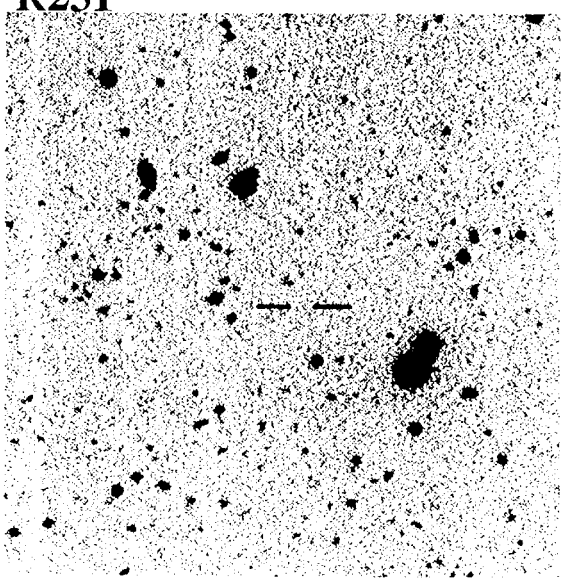

R252

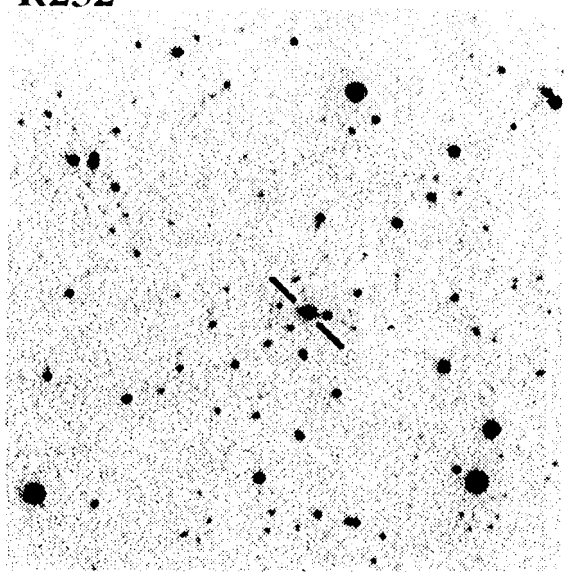

R276

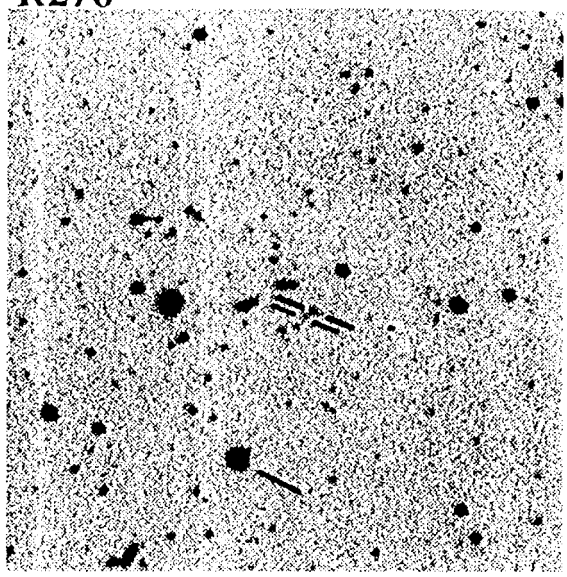

R277

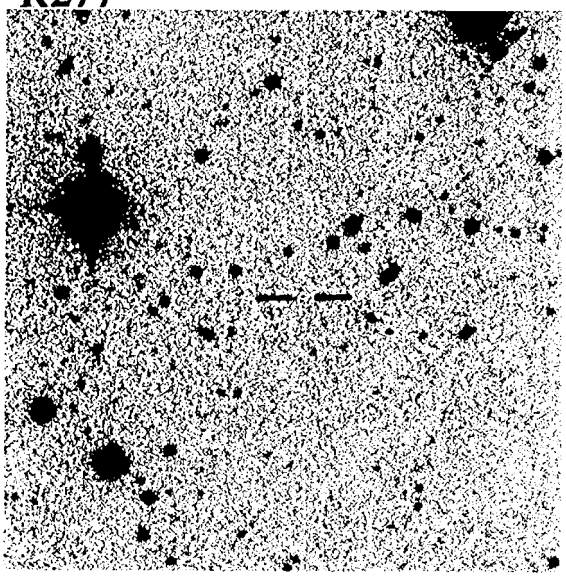

R281

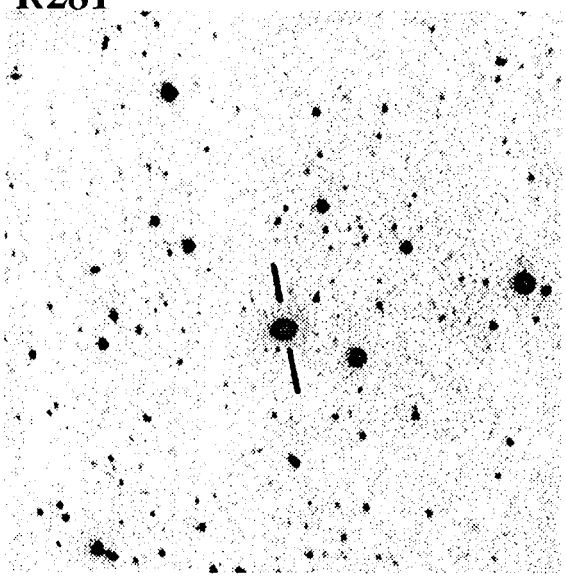

R297

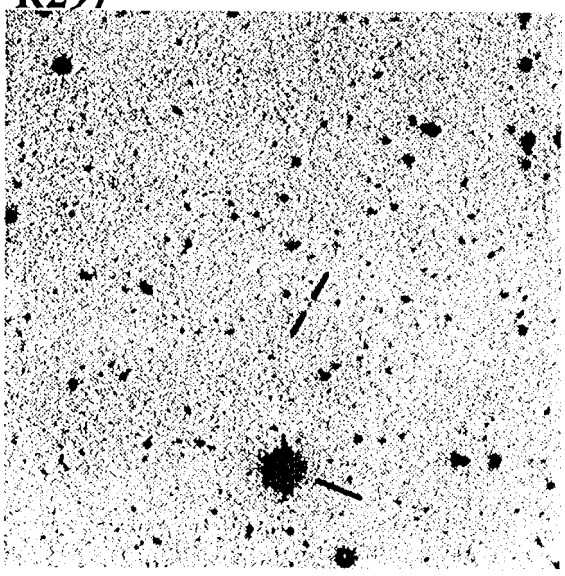

R303

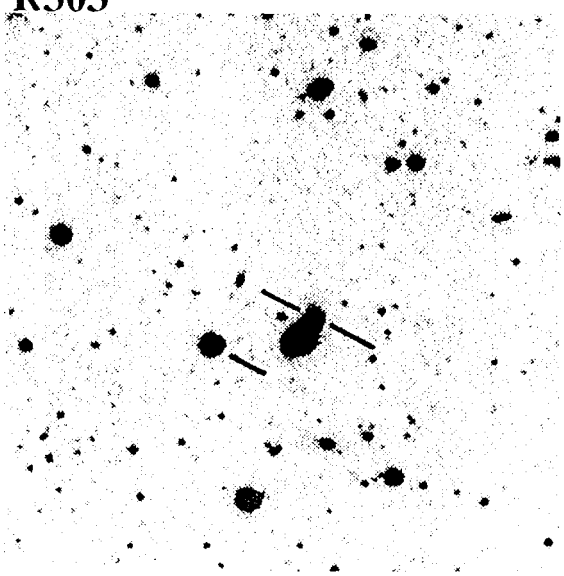

R304

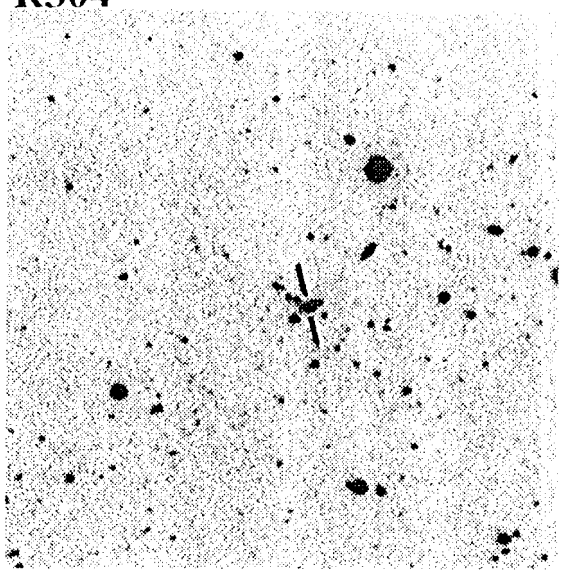

R304(zoom)

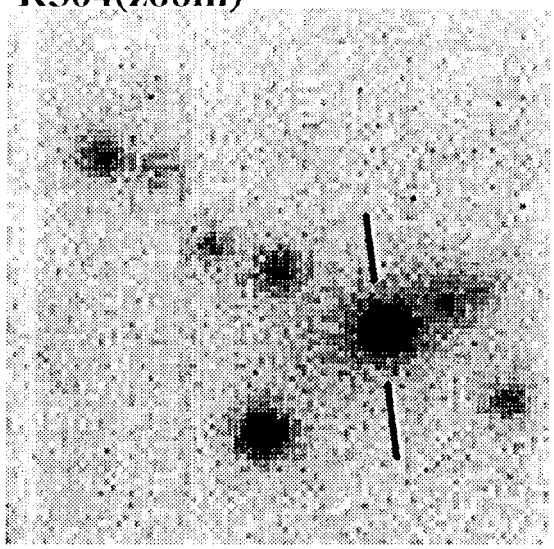

R305

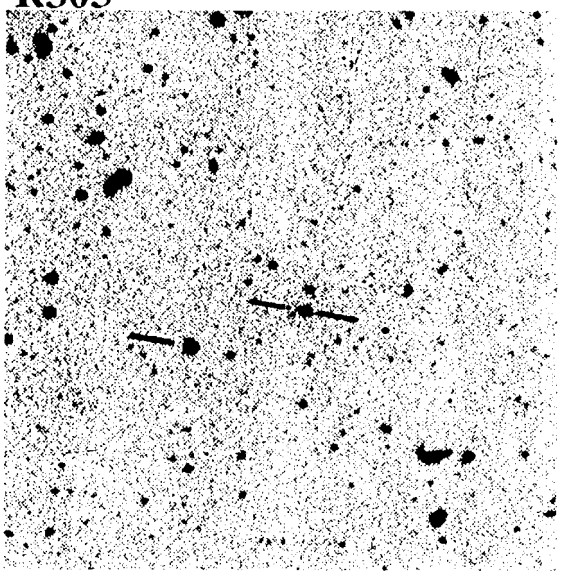

R307(A+B)

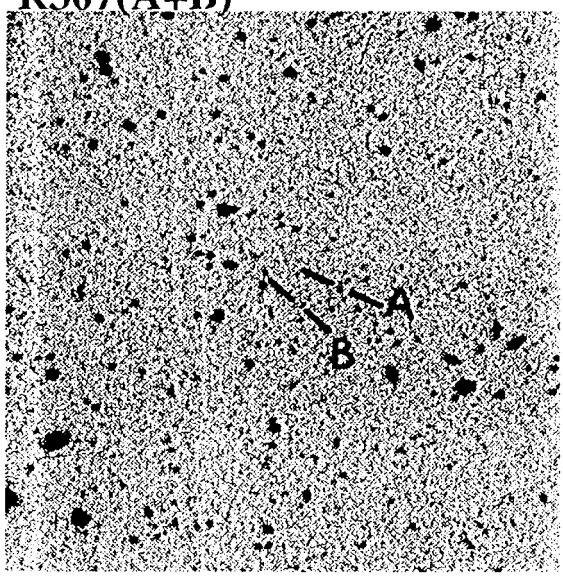

R319

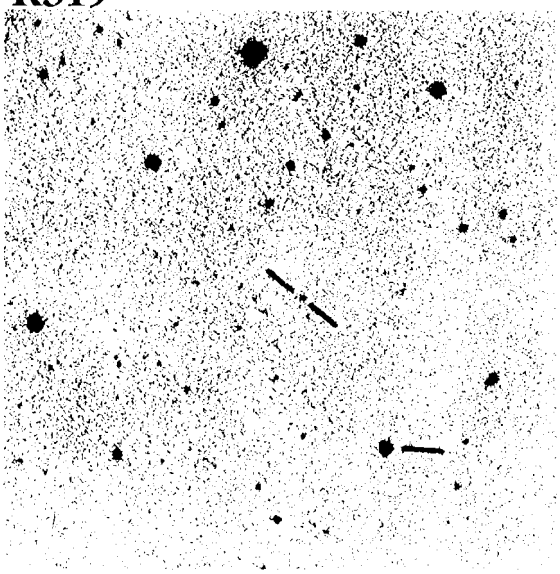

R337

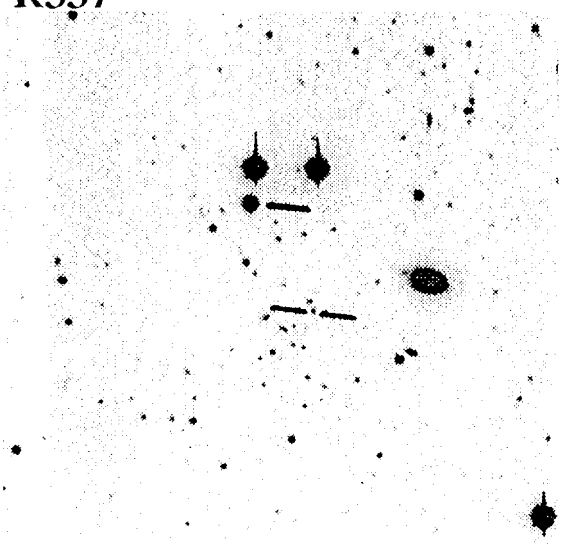

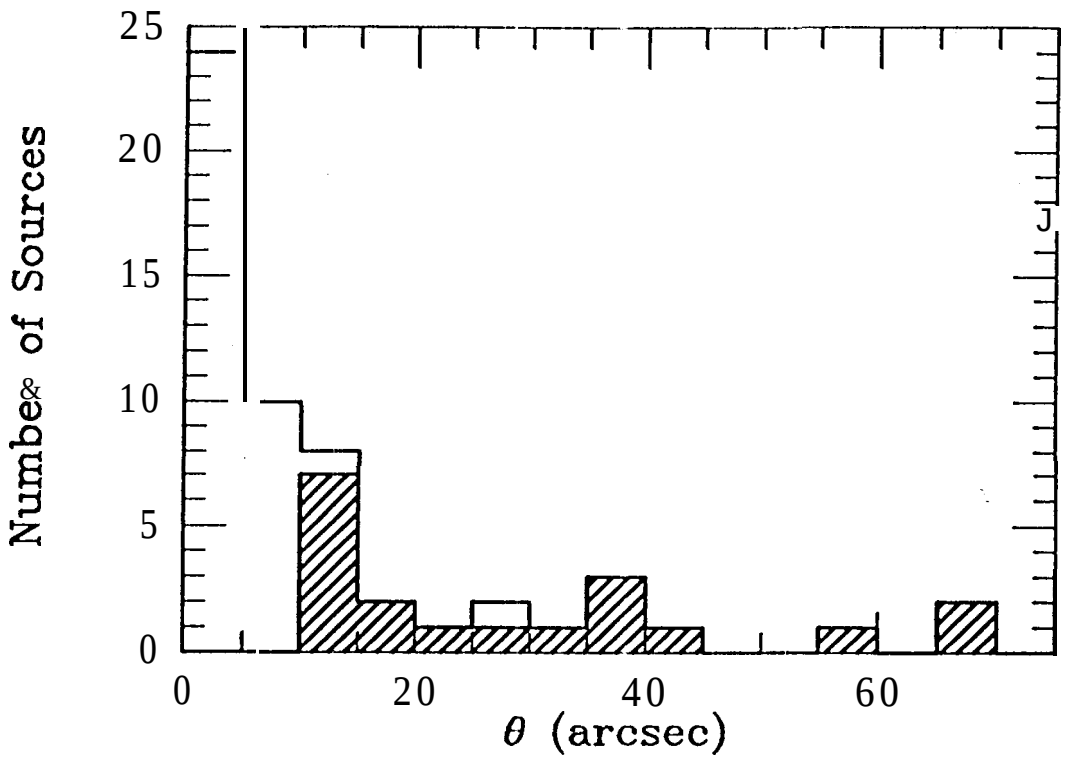

Figure 6

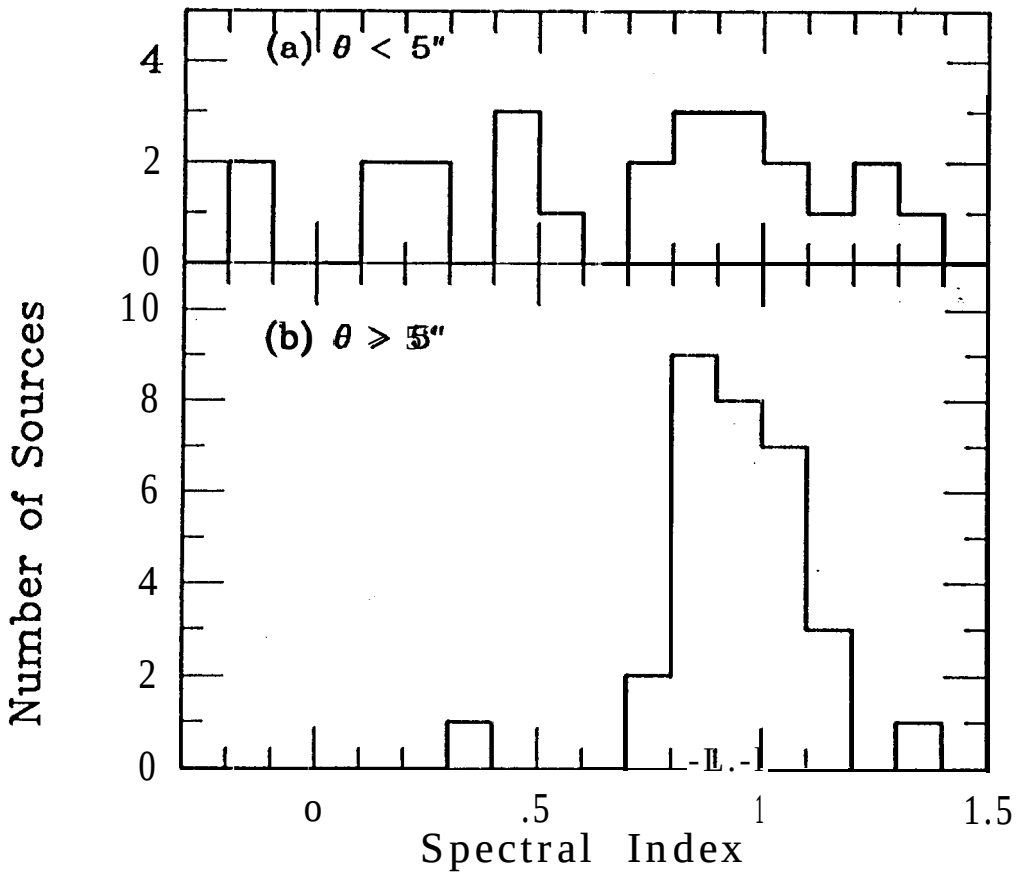

Figure 7

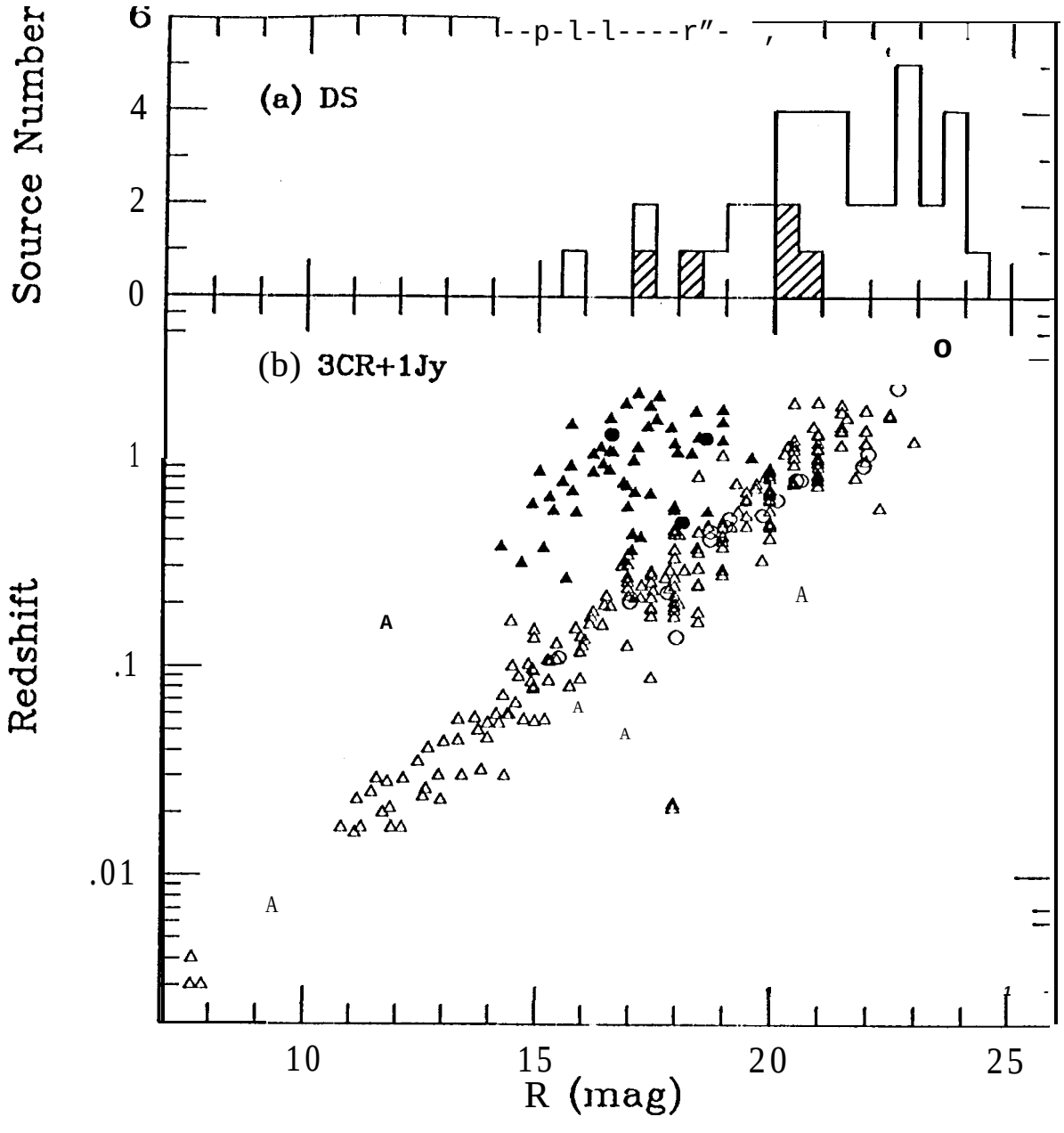
Source Number
6
4
2
0
(a) DS
(b) 3CR+1Jy
Redshift
1
.1
.01
10
15
20
25
R (mag)

Figure 8

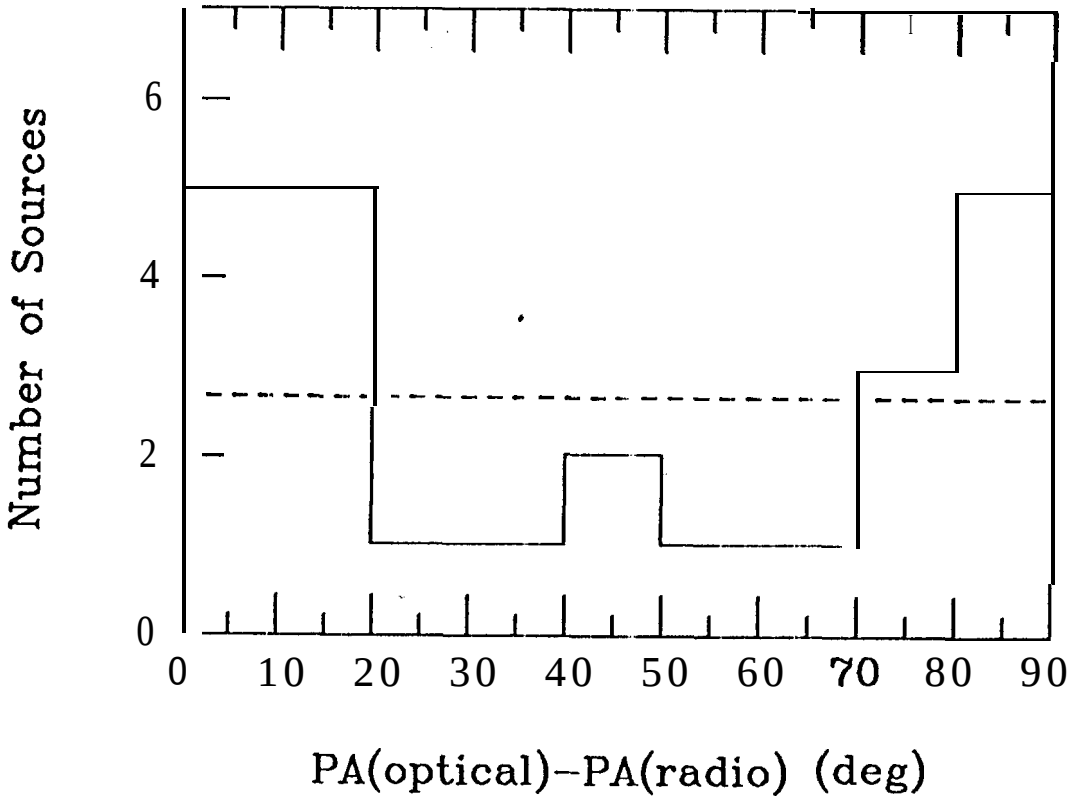
Number of Sources
6
4
2
0
0
10
20
30
40
50
60
70
80
90
PA(optical)–PA(radio) (deg)

Figure 9

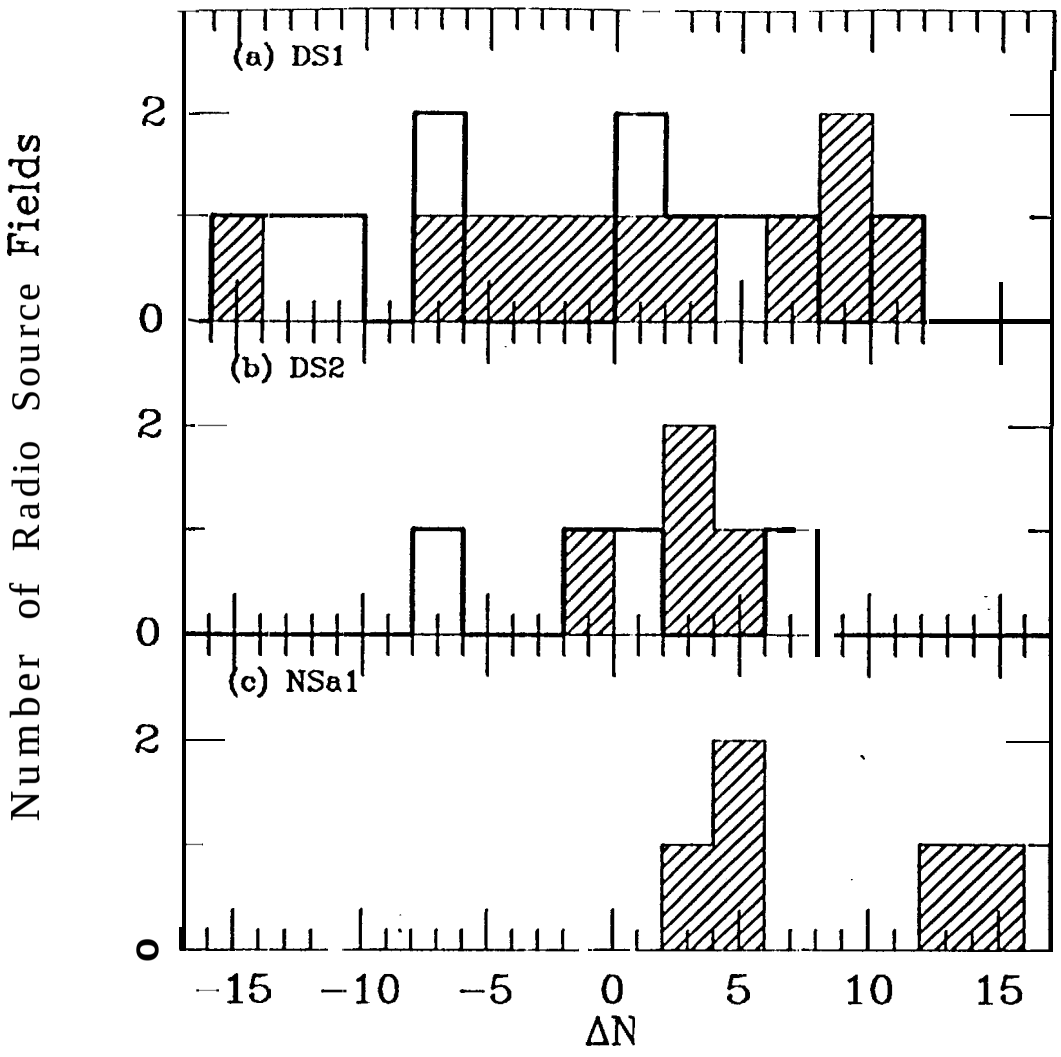
(a) DS1
(b) DS2
(c) NSa1
Number of Radio Source Fields
2
0
2
0
2
0
−15
−10
−5
0
5
10
15
ΔN

Figure 10

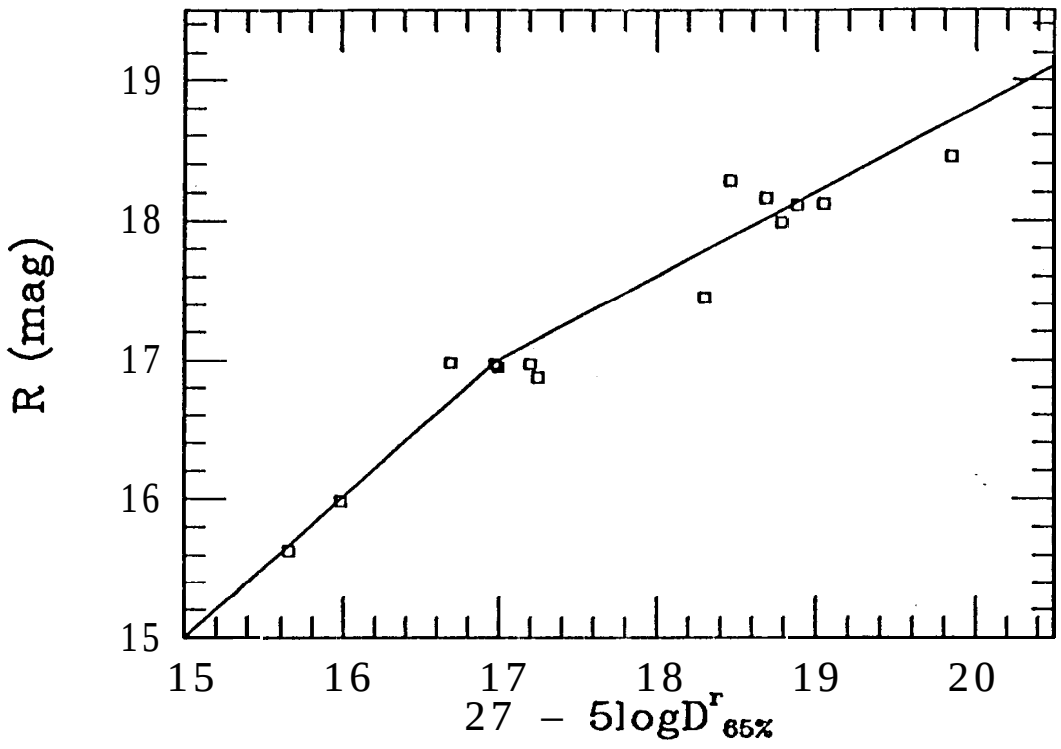

Figure 11

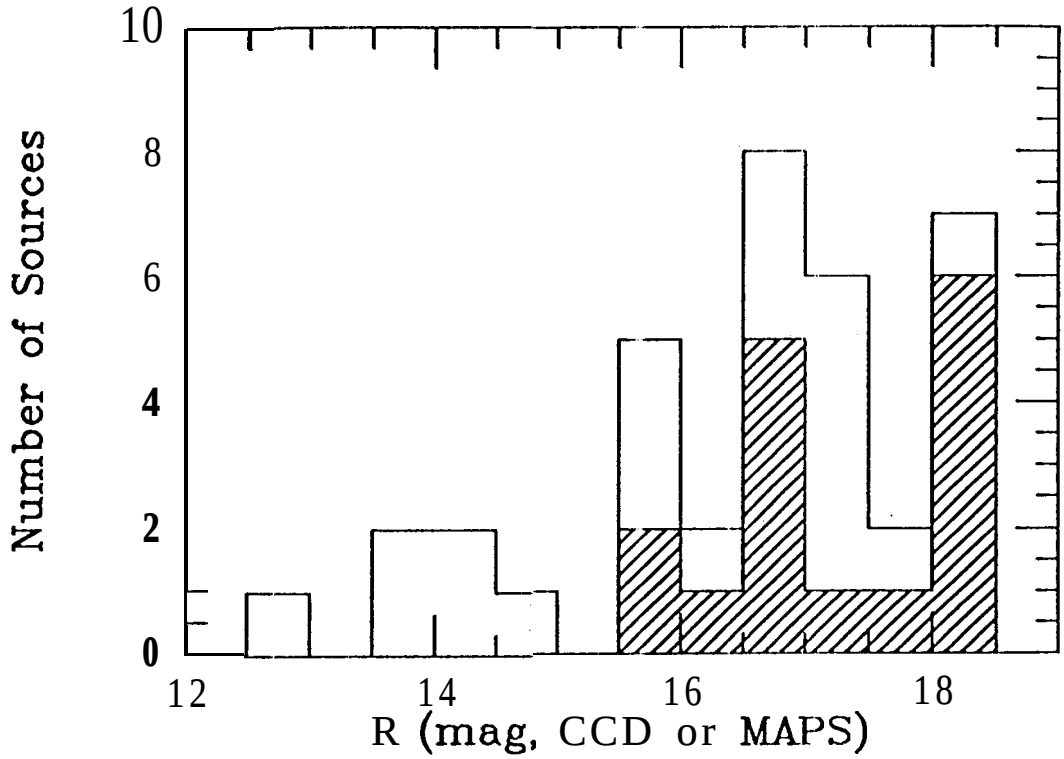

Figure 12

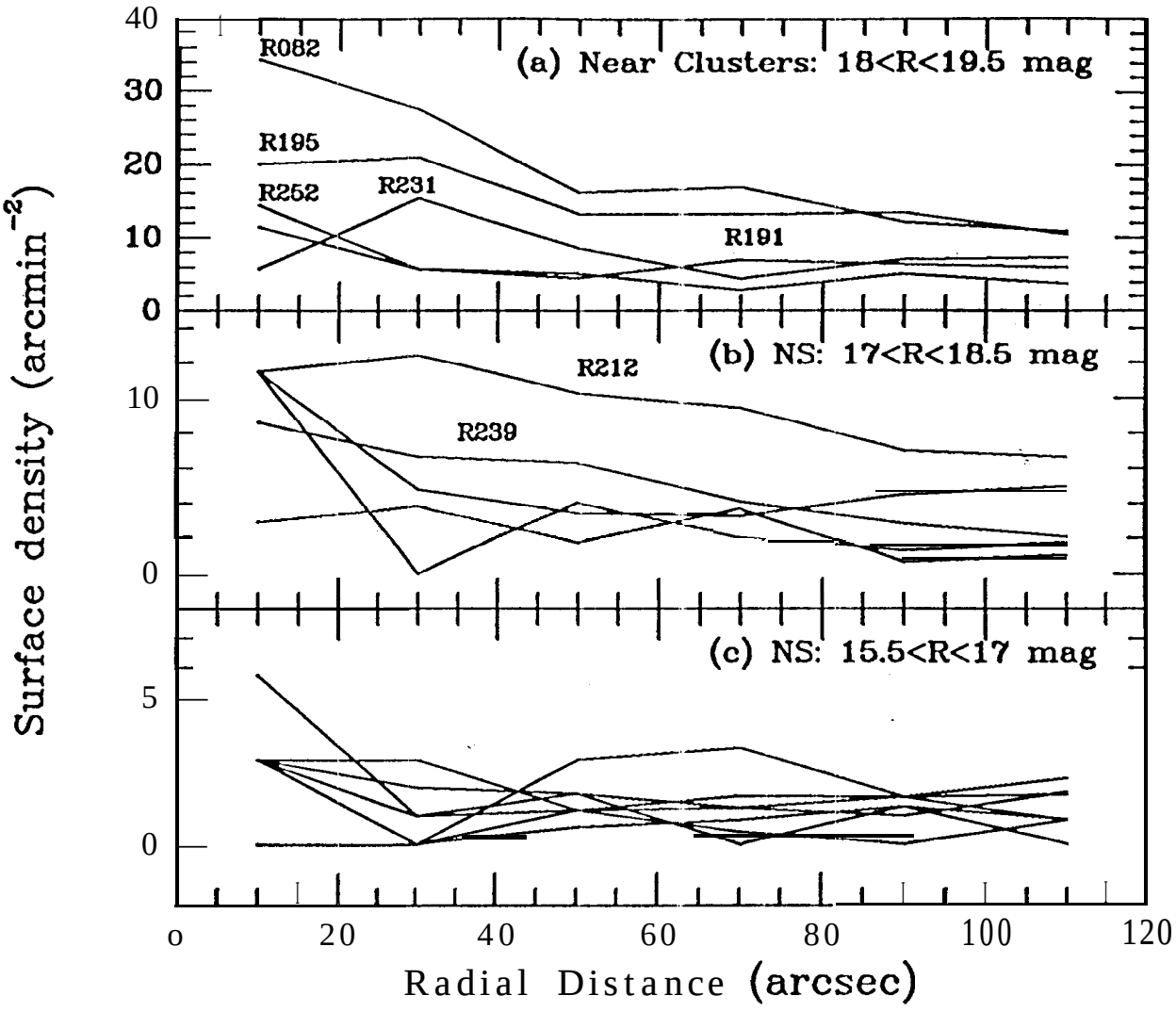
(a) Near Clusters: 18<R<19.5 mag
R082
R195
R252
R231
R191
(b) NS: 17<R<18.5 mag
R212
R239
(c) NS: 15.5<R<17 mag
Surface density (arcmin^{-2})
Radial Distance (arcsec)
40
30
20
10
0
10
0
5
0
0
20
40
60
80
100
120

Figure 13

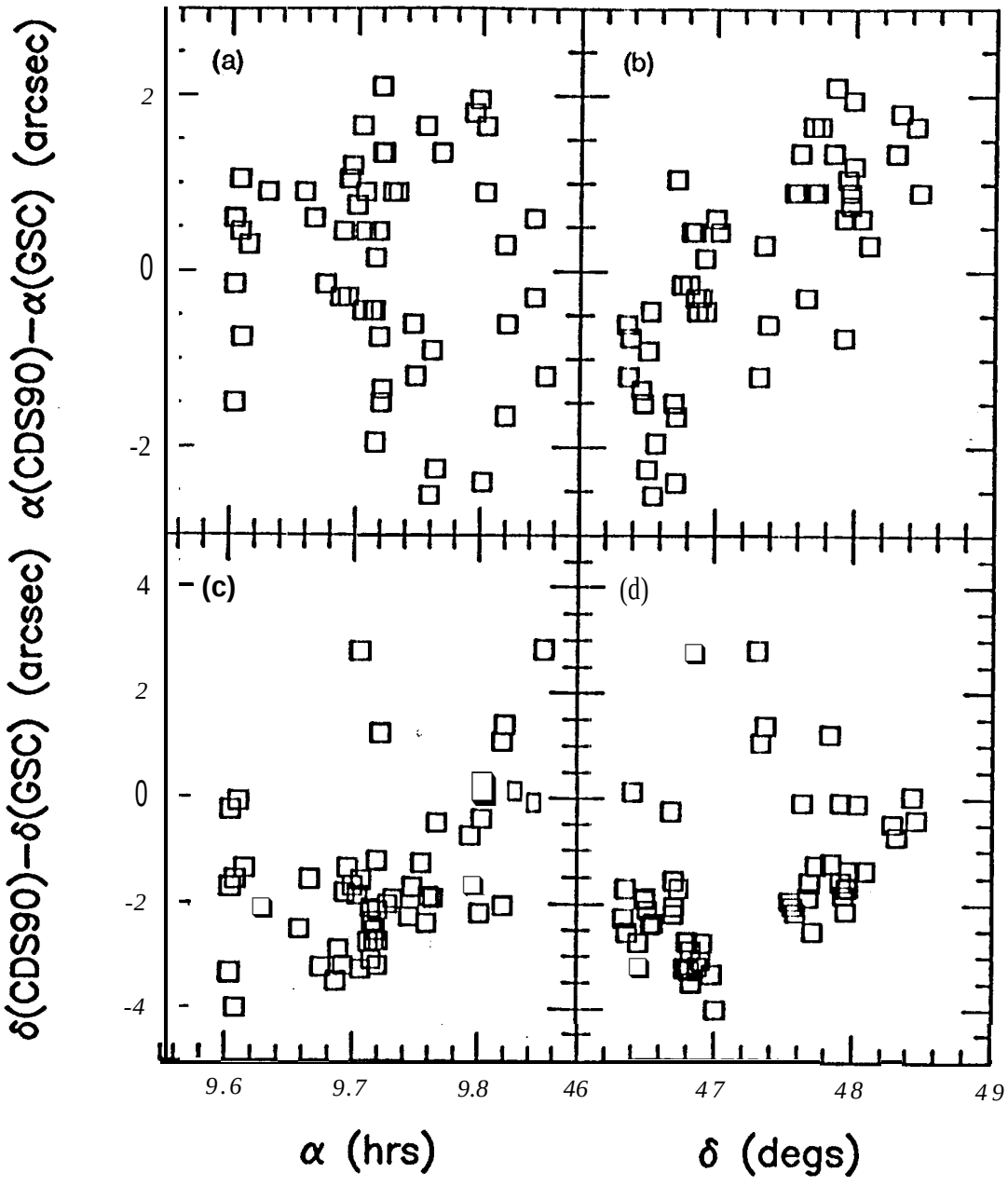
δ(CDS90)−δ(GSC) (arcsec) α(CDS90)−α(GSC) (arcsec)
(a)
(b)
(c)
(d)
2
0
-2
4
2
0
-2
-4
9.6
9.7
9.8
46
47
48
49
α (hrs)
δ (degs)

Figure 14